

MCR-76-564

Contract NAS2-9381

(NASA-CR-152123-Task-1-Final) INFRARED  
IMAGERY OF SHUTTLE (IRIS). TASK 1 Final  
Report (Martin Marietta Corp.) 151 P  
HC A08/MF A01 CSCI 22B

CR 152123

N81-25132

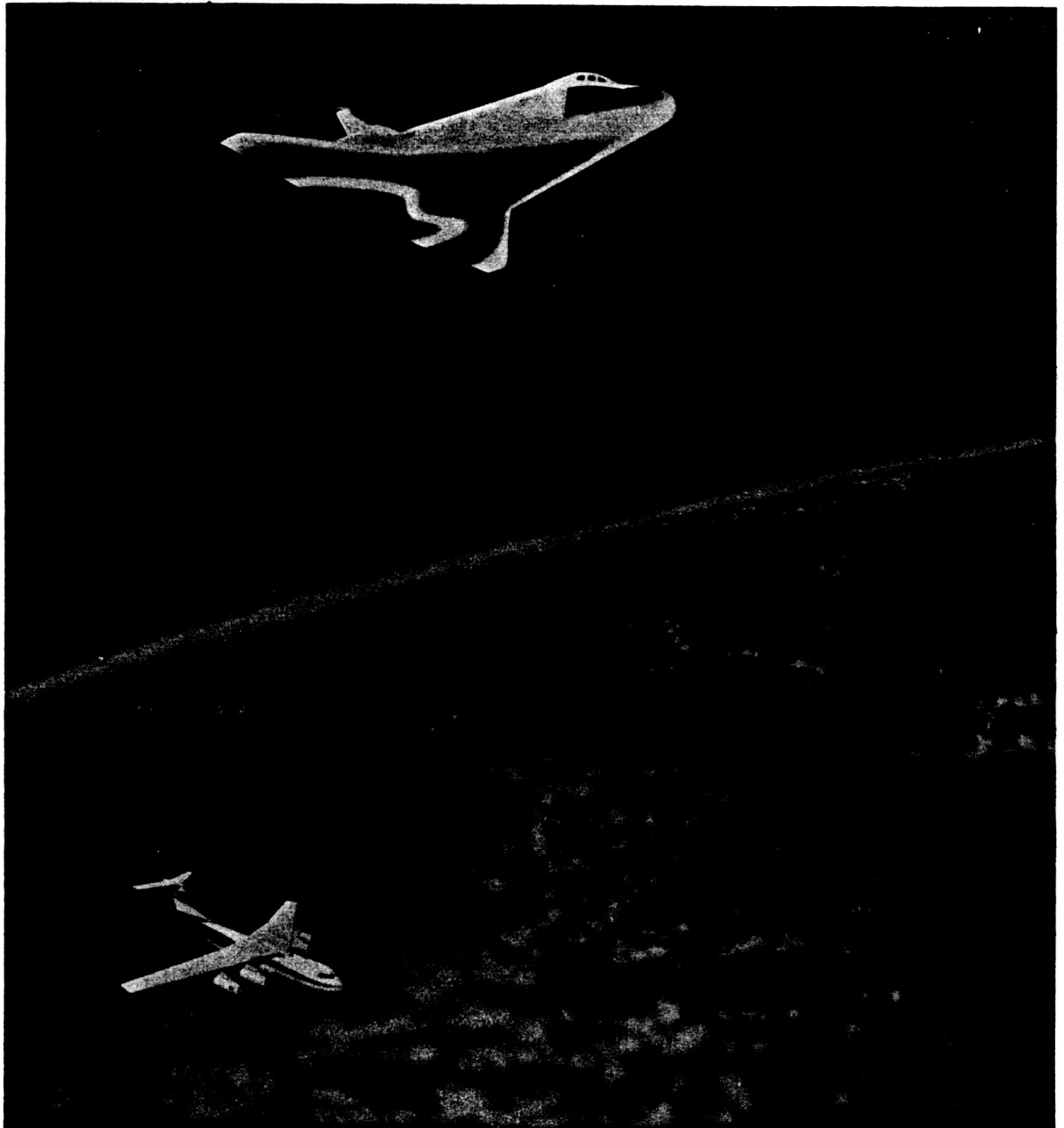
G3/16 Unclas  
26038

Task 1

Final  
Report

August 1977

# Infrared Imagery of Shuttle (IRIS)



**MARTIN MARIETTA**

1 ■  
  
MCR-76-564

Contract NAS2-9381

Final  
Report


August 1977

---

Task 1

**INFRARED IMAGERY  
OF SHUTTLE  
(IRIS)**

Approved

A handwritten signature in black ink, appearing to read "Clifford J. Choccol". The signature is fluid and cursive, with the first and last names being more prominent.

Clifford J. Choccol  
Program Manager

**MARTIN MARIETTA CORPORATION**  
**P. O. Box 179**  
Denver, Colorado 80201

## SUMMARY

---

The feasibility of remote high resolution infrared imagery of the Shuttle Orbiter lower surface during entry to obtain accurate measurements of aerodynamic heat transfer has been demonstrated. Such images can be taken from an existing aircraft/telescope system (the C141 AIRO) with minimum modification or addition of systems using available technology. These images will have a spatial resolution of 1 meter or better and a temperature resolution of 2.5% for temperatures between 800 and 1900 K. Data reconstruction techniques will provide a geometrically and radiometrically corrected array on addressable magnetic tape ready for display by NASA.

Schedule considerations dictate a timely start on FY1978 to mesh with the first Shuttle Orbiter test flights in late 1979 and early 1980 and additional work in the form of subsystem breadboards is recommended to prove principle before system construction.

## CONTENTS

---

	<u>Page</u>
INTRODUCTION . . . . .	1
EXPERIMENT . . . . .	3
OBSERVING PLATFORM OPTIONS . . . . .	11
ACQUISITION SYSTEM . . . . .	19
IMAGE PLANE SYSTEM . . . . .	51
DATA HANDLING SYSTEM . . . . .	61
IMAGING SYSTEM PERFORMANCE . . . . .	73
DATA RECONSTRUCTION . . . . .	99
COST AND SCHEDULE . . . . .	113
RECOMMENDATIONS FOR FUTURE WORK . . . . .	131
CONCLUSIONS . . . . .	135
REFERENCES . . . . .	137
APPENDIX . . . . .	139

## Figure

---

1.	Shuttle Orbiter Maximum Temperature Contours . . . . .	4
2.	Shuttle Orbiter Centerline Temperature Distributions . . . . .	5
3.	Shuttle Orbiter Body Flap Juncture Temperature Distribution . . . . .	6
4.	Shuttle Orbiter Centerline Transition Location . . . . .	7
5.	Shuttle Orbiter Nominal Entry Trajectory Characteristics (Orbit 14414) . . . . .	8
6.	Atmospheric Transission - AMOS Ground Station . . . . .	12
7.	Convair 990 Acquisition & Data System . . . . .	13
8.	Convair 990 MTF (Expected) of 45 cm Telescope . . . . .	14
9.	Acquisition and Imaging Geometry - Lear Jet . . . . .	16
10.	Airborne Observatory . . . . .	17
11.	Acquisition Geometry - C141 . . . . .	20
12.	Acquisition System . . . . .	21
13.	Acquisition System . . . . .	22
14.	Tracking Scope Rotating Recticle . . . . .	24
15.	Acquisition System - Filter . . . . .	26

16.	Acquisition System and Tracking System Parameters . .	27
17.	Acquisition System and Stabilizing System Cl41 . . . .	28
18.	AZ Servoloop (91.5 cm Telescope) . . . . .	29
19.	LOS Servoloop (91.5 cm Telescope) . . . . .	30
20.	AZ Tracker Servoloop (New Acquisition Tracker) . . . .	31
21.	Elevation Servo (91.5 cm Telescope) . . . . .	32
22.	Acceleration and Rate Capabilities . . . . .	33
23.	Acquisition, Track & Settle Timing vs Max Slew Rates . . . . .	35
24.	Simulation of EL and AZ Control . . . . .	36
25.	Simulation of EL and AZ Control . . . . .	37
26.	Simulation of EL and AZ Control . . . . .	38
27.	Simulation of EL and AZ Control . . . . .	39
28.	Simulation of EL and AZ Control . . . . .	40
29.	Simulation of EL and AZ Control . . . . .	41
30.	Simulation of EL and AZ Control . . . . .	42
31.	Simulation of EL and AZ Control . . . . .	43
32.	Simulation of EL and AZ Control . . . . .	44
33.	Initial Pointing Angle Calculations To Be Done in HP2100 . . . . .	46
34.	Tracking Scope Elevation Errors . . . . .	47
35.	Tracker Demod & Interface . . . . .	48
36.	ADAMS Interface Servo (HP2100) . . . . .	49
37.	Primary Telescope Image Plane . . . . .	53
38.	Cl41 Imaging System . . . . .	54
39.	Dewar Assembly . . . . .	56
40.	Detector Calibration . . . . .	57
41.	Data Handling Schematic . . . . .	63
42.	Temperature Information Flow . . . . .	65
43.	Temperature Versus Counts . . . . .	67
44.	Orbiter Nose Region Models . . . . .	74
45.	Orbiter Shock Layer Models . . . . .	75
46.	Trajectory Conditions & Shock Layer Properties . . . .	76
47.	Orbiter Windward $\odot$ Radiative Equil Temperatures . . .	77
48.	Orbiter Windward $\odot$ Radiative Heat Flux . . . . .	78
49.	Effect of Shock Layer Properties on $\odot$ Radiative Heat Flux . . . . .	79
50.	MTF - Bow Shock . . . . .	80
51.	Atmospheric Transmittance (Cl41) . . . . .	81
52.	MTF - Atmospheric Turbulence . . . . .	82
53.	MTF - Boundary Layer . . . . .	84
54.	MTF - Optics . . . . .	85
55.	91.5 cm Telescope Point Spread Function . . . . .	86
56.	91.5 cm Telescope MTF . . . . .	87
57.	MTF - Image Motion . . . . .	88
58.	MTF - Detector . . . . .	89
59.	Electrical Bandwidth . . . . .	90
60.	Background Irradiance at Entrance Aperture . . . . .	91
61.	$\Sigma$ MTF . . . . .	93

62.	Imaging System Parameters . . . . .	94
63.	Minimum Resolvable Temperature . . . . .	95
64.	Spatial Resolution . . . . .	96
65.	Imaging System Performance (12 Bit Digital Conversion) . . . . .	97
66.	Imaging System Performance (12 Bit Conversion) . . . .	98
67.	Image Processing/Unscramble and Intensity Correction . . . . .	101
68.	Image Processing/Reconstruction and Geometric Correction . . . . .	103
69.	Image Processing/Calibration . . . . .	108
70.	Image Processing/Display - Graphic and Tabular . . . .	110
71.	Image Processing/Display - Gray Scale and Color Images . . . . .	111
72.	Hardware - Processing and Display Capability . . . . .	112
73.	Preliminary Program Cost Breakdown . . . . .	114
74.	Acquisition System - Estimating Input Sheets . . . . .	115
75.	Image Plane System - Estimating Input Sheets . . . . .	116
76.	Data Systems - Estimating Input Sheets . . . . .	117
77.	System Support - Estimating Input Sheets . . . . .	118
78.	Program Support - Estimating Input Sheets . . . . .	119
79.	Schedule: Infrared Imagery of Shuttle - Black Box #1 - Acquisition System . . . . .	120
80.	Schedule: Infrared Imagery of Shuttle - Black Box #2 - Image Plane System . . . . .	121
81.	Schedule: Infrared Imagery of Shuttle - Black Box #3 - Data System . . . . .	122
82.	Schedule: Infrared Imagery of Shuttle - System Support . . . . .	123
83.	Schedule: Infrared Imagery of Shuttle - Software . .	124
84.	Work Breakdown Structure for Shuttle Infrared Imaging System . . . . .	125
85.	Acquisition System - WBS Dictionary . . . . .	126
86.	Image Plane System - WBS Dictionary . . . . .	127
87.	Data System - WBS Dictionary . . . . .	128
88.	System Support - WBS Dictionary . . . . .	129
89.	Program Support - WBS Dictionary . . . . .	130
90.	Follow-on Task Estimate . . . . .	132
91.	Infrared Imagery of Shuttle - Preliminary Follow-on Contract Schedule NAS2-9381 . . . . .	133
92.	C141 Data and Acquisition Geometry - 282 sec Case . .	141
93.	C141 Data and Acquisition Geometry - 544 sec Case . .	142
94.	C141 Data and Acquisition Geometry - 791 sec Case . .	143
95.	C141 Data & Acquisition Geometry - 922 sec Case . . .	144
96.	Streak Camera Configuration . . . . .	145

## INTRODUCTION

---

Early in 1976 NASA-Ames Research Center expressed an interest in the Infrared Imagery of heated surfaces such as the Shuttle Orbiter during reentry. Necessary information to substantially reduce the weight and cost of thermal protection systems of future space transportation systems could result from accurate flight data on: (1) the lower surface heating rate distribution, (2) the location of boundary-layer transition, and (3) location and extent of flow separation in front of control surfaces. This imaging would be obtained by an appropriate telescopic sensor system mounted in one or more chase aircraft stationed appropriately along the Shuttle reentry ground track.

Initially, an approach was taken to fly the chase aircraft perpendicular to the Shuttle flight direction to maximize the viewing time (cross track approach). It became apparent that within the maximum viewing time (10 to 20 sec), no significant surface temperature changes would occur precluding the desire for multiple images. In addition, the angular rates between the Shuttle and chase aircraft became complex and were excessive, requiring major redesign of any telescope stabilization system.

At this point, NASA-Ames Research Center undertook an in-house study and generated an approach where the chase aircraft flew parallel to the Shuttle ground track (along-track approach). Since multiple images or integration times in excess of a few microseconds were unnecessary, the streak camera idea was introduced. (See Ref. 1 and Fig. 96). The streak camera, as it applies here, is a linear array of detectors at the image plane of a telescope. The detectors are sampled at a rate compatible with image motion to obtain a desired resolution. Tracking of the object is unnecessary as long as the object passes through the field-of-view of the telescope. One image is obtained for each linear array of detectors.

The feasibility study contract was then awarded. NASA directed the contractor to undertake the study based on the in-house findings. These tasks included: (1) An IR technology survey to investigate the current state of sensor technology; (2) a preliminary design of all subsystems with regard to environment, power, and support requirements; (3) a system performance describing the end-to-end capabilities of the design including error sources; and (4) a cost and schedule assessment for the design, fabrication, assembly, installation, and support during the first six Shuttle development flights. The purpose of this report is to summarize the results of the above analysis.





## EXPERIMENT OBJECTIVE

---

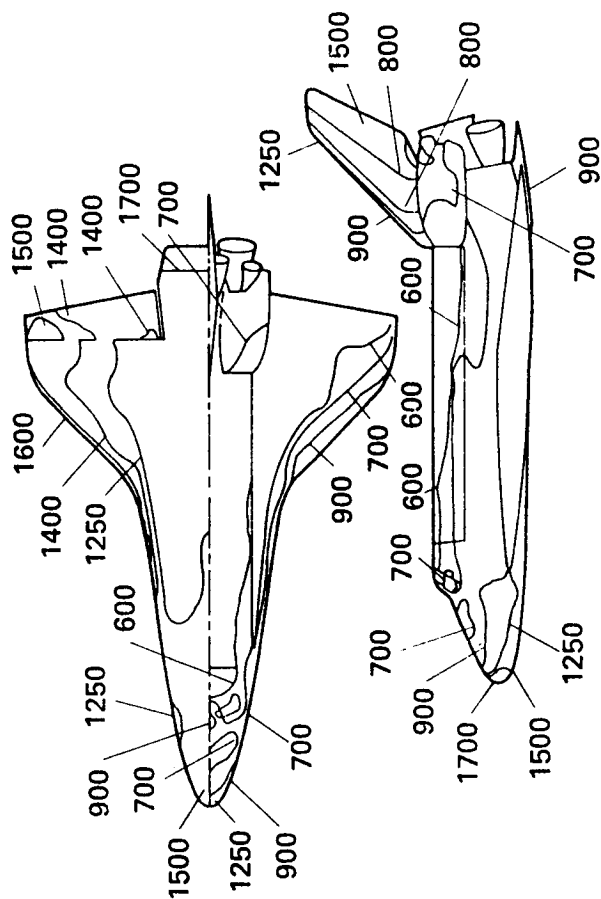
The objective of the experiment is to obtain high resolution (1 meter or better) surface maps of the Shuttle Orbiter lower and side surfaces with a temperature accuracy of at least 2.5% during peak heating, flap deflection, and transitional heating periods of the reentry profile. This information is required to verify computational predictions and experimental extrapolations to provide data for possible TPS block changes.

Predicted temperature distribution and transition points for the Shuttle Orbiter reentry profile 14414 are shown in Figures 1 through 4. All six Orbital Flight Test (OFT) reentry profiles are expected to have similar temperature distributions, However, the time from entry when these events occur will be different. Maximum temperatures on the windward and side surfaces are not expected to exceed 1900 K and are generally above 600 K during the time period of interest.

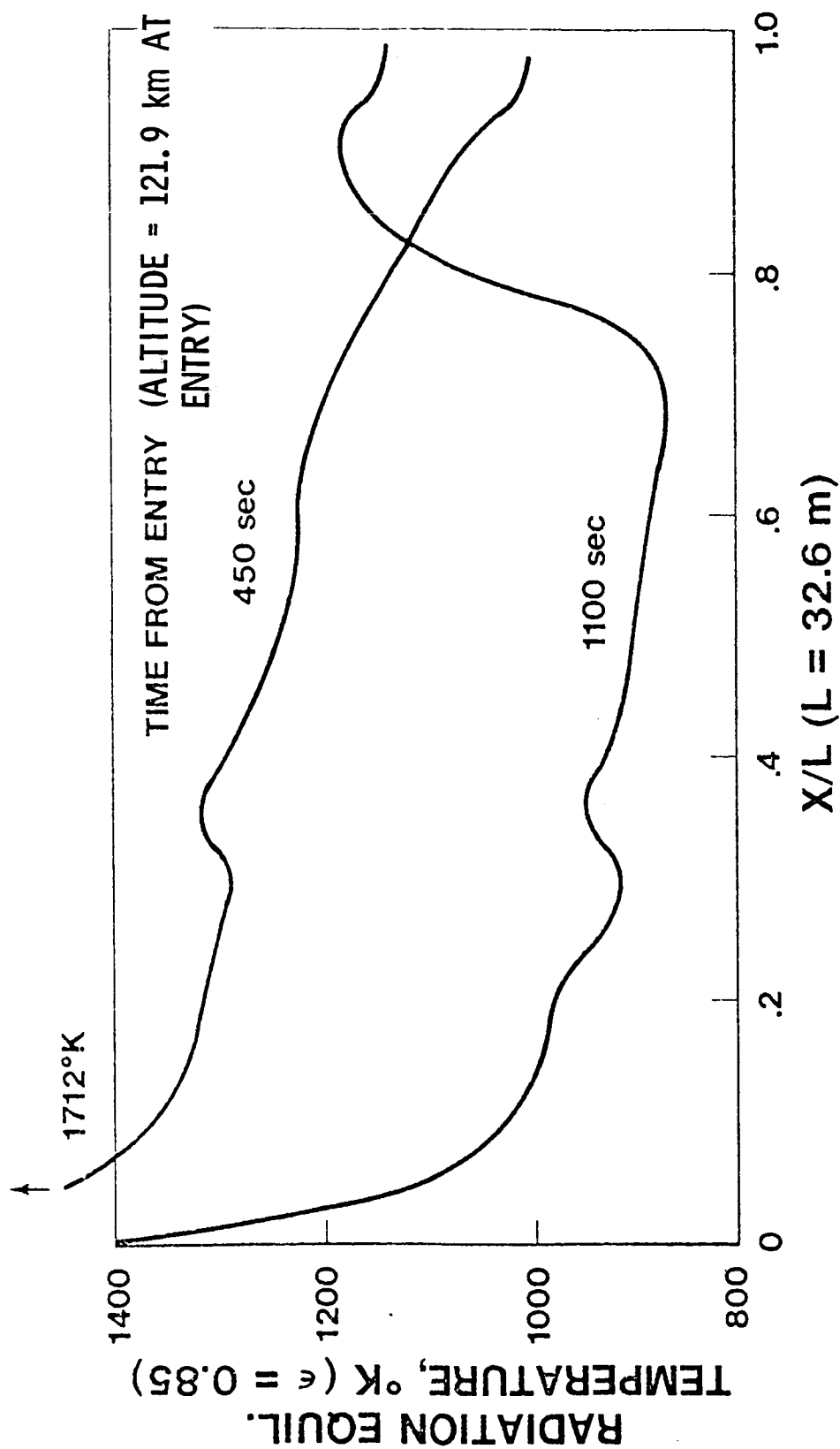
Implications associated with the experiment cover many facets. First, as shown in Figure 5, are the variations in Shuttle Orbiter altitude, velocity, angle-of-attack and bank angle which must be accommodated (Ref. 2). The key points of interest during the reentry (peak heating, flap deflection, and transitional heating) correspond to a given time from entry for a given reentry profile. Figure 5 data are for reentry profile 14414. OFT 1, 2 and 3 profiles are slightly different (Ref. 3). As an example, peak heating occurs at  $T = 400$  sec for orbit reentry 14414 and at  $T = 282$  sec for OFT 1. (Refer to the appendix for OFT 1 reentry trajectory data.) This corresponds to a Shuttle Orbiter altitude of 74.3 km, a velocity of 7.16 km/sec, an angle-of-attack of  $40^\circ$  and a bank angle of  $74^\circ$ . To obtain accurate, high-resolution data with one system for these varying conditions requires a versatile observing platform and data system.

The second consideration is associated with the expected radiation from the Shuttle Orbiter. At temperatures ranging from 600 to 1900 K, a black body will have its radiation peak between 1.5 and 4.8 micrometers. For these temperatures, the wavelengths for which the first derivative of radiant energy with temperature is a maximum occur between approximately 1.3 and 2.7 micrometers. This suggests that the optimum detector/filter response should be about 2 micrometers with a limited spectral bandwidth.

Thirdly, the requirement for at least 1 meter resolution at a maximum range of 75 km implies an angular resolution of 1.7 arcsec with foreshortening from the nonnormal aspect of the surface to the line-of-sight of  $40^\circ$  maximum. At a wavelength of 2.0 micrometers, a diffraction-limited telescope would require an aperture

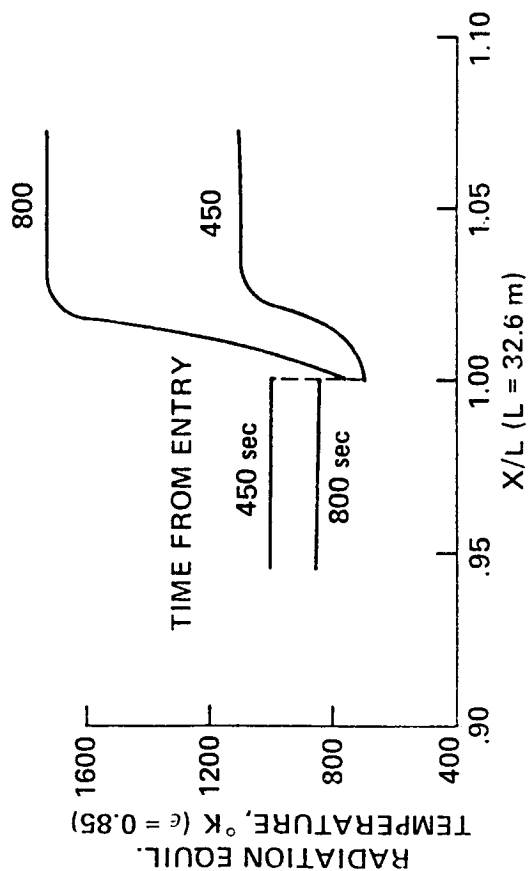


**NOTE: ALL TEMPERATURES IN K**

REENTRY PROFILE  
14414**MARTIN MARIETTA**

# SHUTTLE ORBITER BODY FLAP JUNCTURE TEMPERATURE DISTRIBUTION FIG. 3

REENTRY PROFILE  
14414

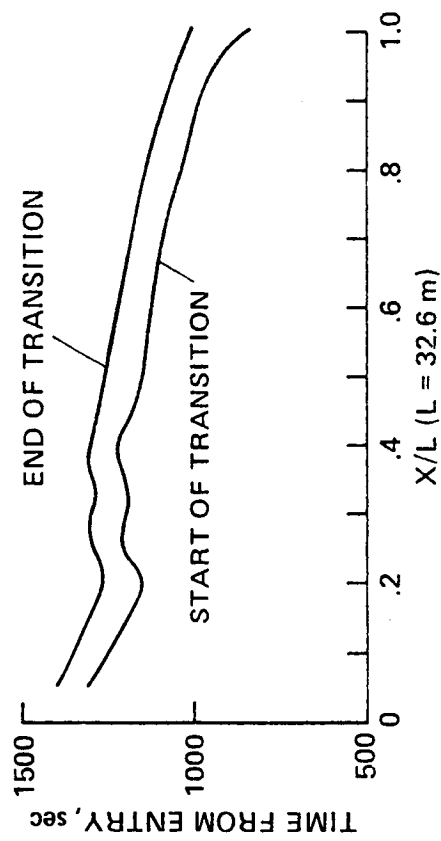


MARTIN MARIETTA

SHUTTLE ORBITER CENTERLINE TRANSITION LOCATION

FIG. 4

REENTRY PROFILE  
14414

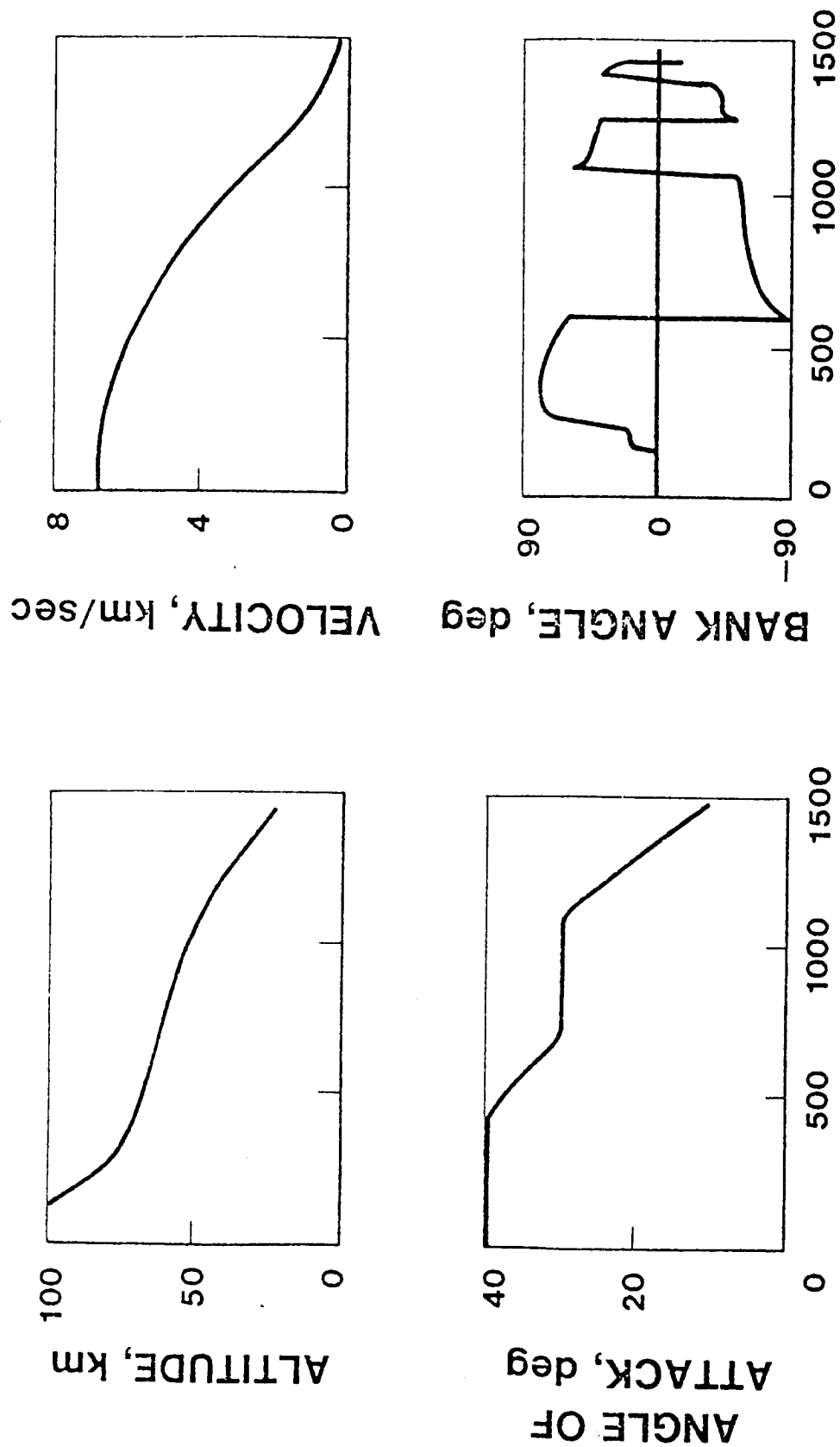


MARTIN MARIETTA

# SHUTTLE ORBITER NOMINAL ENTRY TRAJECTORY CHARACTERISTICS (ORBIT 14414) FIG. 5

REF. 2

8



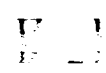
TIME FROM ENTRY, sec

MARTIN MARIETTA

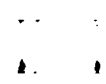
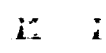
of at least 30 cm. Considering other degrading factors such as atmospheric effects, finite detector elements, image motion and the unavailability of a perfect diffraction limited telescope, an aperture of 60 to 100 cm is suggested.

In addition to the desirability of observing each OFT at a unique position along the reentry path, a verification of system performance before OFT 1 is necessary. A test flight using an aircraft that can simulate expected angular rates, temperatures, and angular size will provide the verification. The only candidate aircraft found that approaches these requirements is the YF-12 flying at an altitude of 24.4 km at 1.03 km/sec.

Finally the aircraft should be capable of a cruising altitude of 14 km (above most atmospheric water). This is arrived at by considering the wavelength requirements for maximum sensitivity to the expected temperature range of 1.5 to 2.5 micrometers. The versatility required of the observing platform is to ensure proper position with respect to the Shuttle Orbiter for a variety of reentry conditions. In addition, this aircraft must have the capacity for a telescope with an aperture of 60 to 100.



Platform Options





## OBSERVING PLATFORM OPTIONS

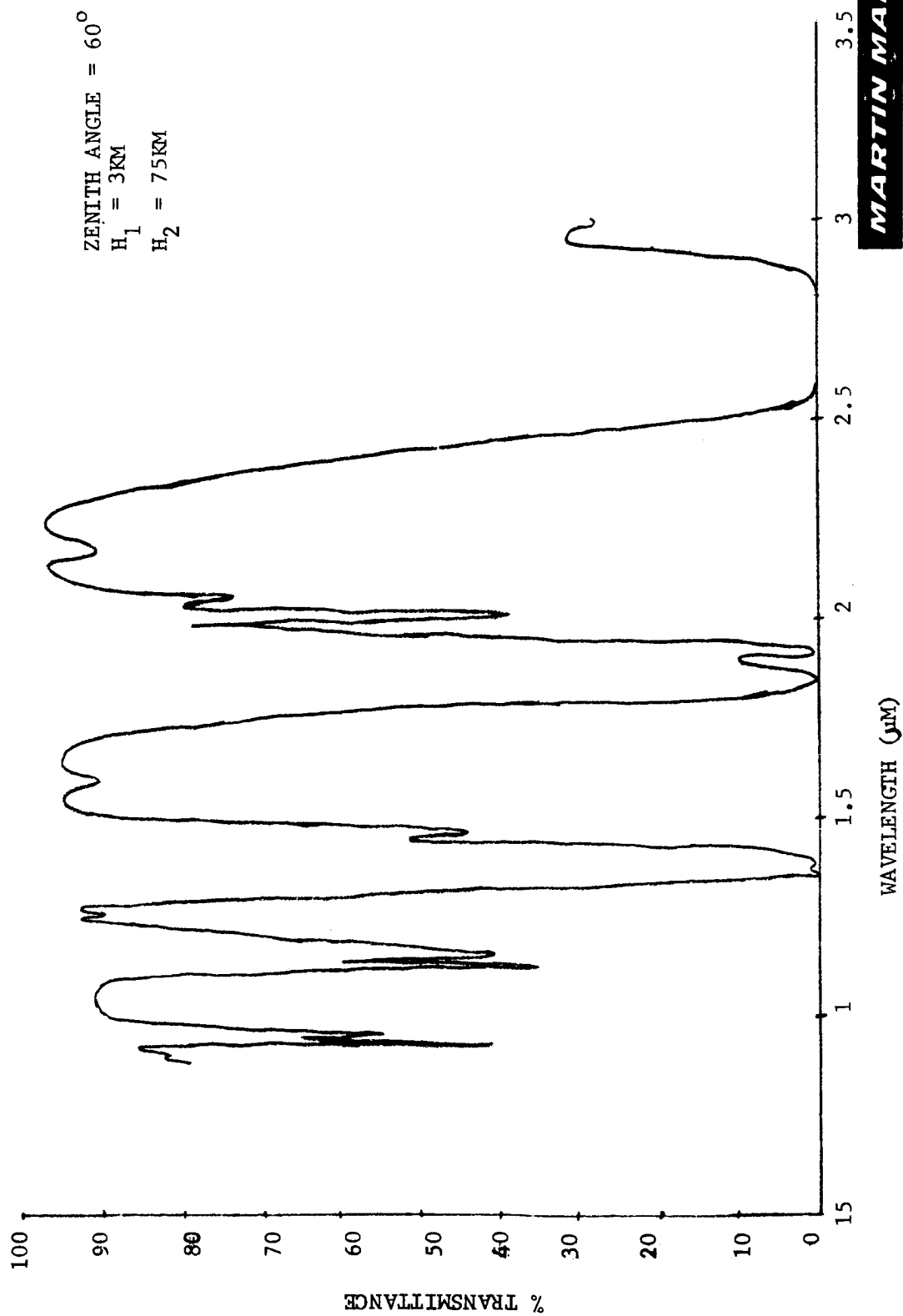
---

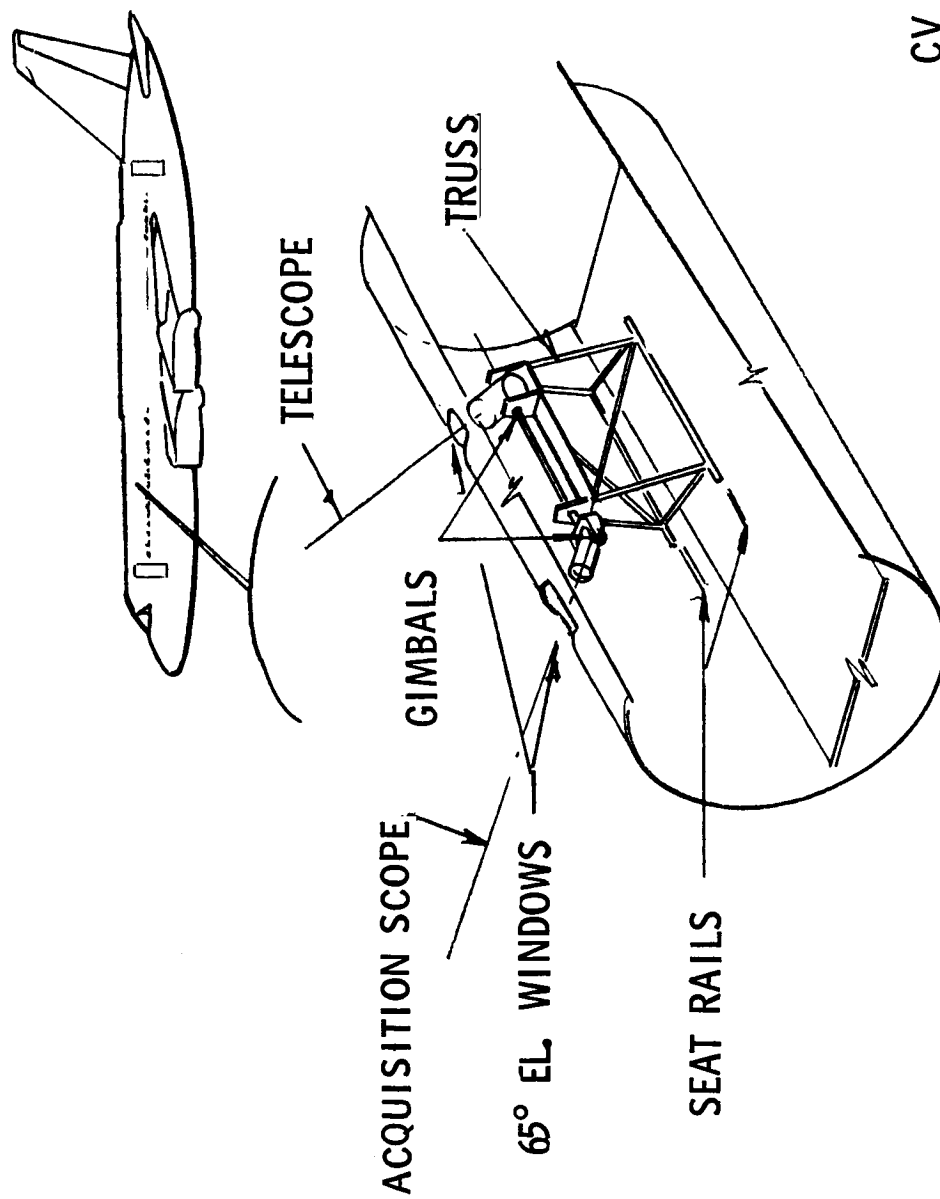
Four candidate observing platforms were considered, including one ground-based station.

ARPA Maui Optical Station - The ground-based station studied was the ARPA Maui Optical Station (AMOS), MT Haleakala, Hawaii. This facility has a 1.6-meter aperture telescope capable of tracking up to  $6.6^\circ/\text{sec}$  (Ref. 4). This feature would allow either formatted data or the streak camera approach to be used. The aperture available provides excessive signal to the point that image integration is not an advantage (the main reason for formatted data). The streak camera technique is quite suitable and would provide excellent data on the Shuttle Orbiter when it is within 200 to 300 km of the station. Beyond this range, the resolution required cannot be met. This is the major disadvantage of the ground-based platform because it cannot accommodate the variety of geographical positions necessary to observe the Shuttle at prescribed points in its reentry profile. Finally, the temperature data taken at an altitude of 3 km will not be accurate due to fluctuations in the water content of the atmosphere. Figure 6 represents the atmospheric transmission from AMOS and shows strong water absorption bands in the 1.5 to 2.5 micrometer region of the spectrum. The AMOS facility does not appear to be a viable candidate observing platform for this experiment.

Convair 990 - The NASA Convair 990 meets many of the basic requirements of this experiment (Ref. 5). It can be positioned optimally. A telescope that might be placed on board (see Fig. 7) is compatible with the streak camera but cannot be of sufficient aperture. The available window size (45 cm) and location ( $65^\circ$  above water line) limit the resolution on the Shuttle Orbiter to between 2 and 5 meters. Figure 8 represents the expected MTF of a redesigned, 45-cm aperture telescope that could be used on the C990. This candidate observing platform is marginal at best and would require substantial internal modifications including a completely new gimbal platform within the aircraft.

Lear Jet - The NASA Lear Jet also meets many of the general requirements of an observing platform (Ref. 6). Its altitude and geographical range are adequate. As in the Convair 990, the resolution obtained by the Lear Jet is limited by the size and position of observing windows. The maximum aperture telescope that could be used is 30 cm at an elevation of  $25^\circ$  above waterline resulting in a maximum Shuttle surface resolution of 1.5 to 2 meters. The Lear Jet is more favorable than the Convair 990 for lower surface viewing even though the available telescope aperture is less because the window elevation allows viewing of the Shuttle at an angle closer to the Shuttle lower surface normal. For





CV 900 ACQUISITION  
SYSTEM

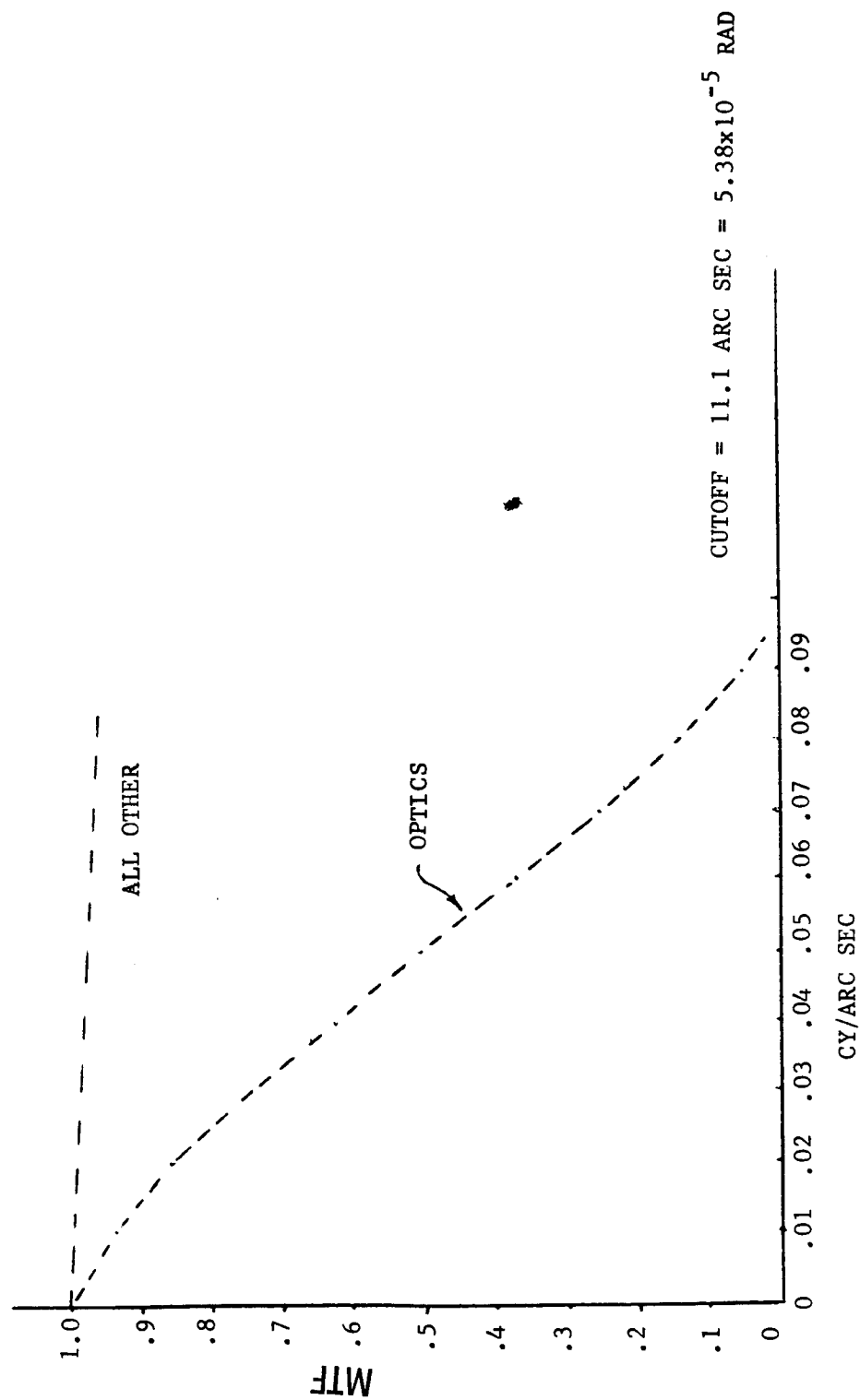
# CONVAIR 990. MTF (EXPECTED) OF 45 cm TELESCOPE

FIG. 8

REDESIGN 45.7 cm APERTURE TELESCOPE TO f/25

FL = 11500 mm

$\beta = 9 \times 10^{-5}$  RAD = .054 CY/ARC SEC



viewing of the side surfaces, the Convair 990 may be the preferred of these two aircraft. The telescope stabilization system on-board the Lear Jet is unique because it can provide elevation rates up to  $50^\circ/\text{sec}$ . This allows the acquisition system to be part of the main telescope since the response to an error signal can be corrected within the field-of-view of the guide telescope (see Fig. 9). Other candidate platforms require a complete separate acquisition system. This candidate then is also marginal; however, it would require fewer modifications because a 30-cm telescope and stabilization system are currently installed in the Lear Jet.

C141 - The NASA C141 Airborne Infrared Observatory (AIRO) meets all the requirements of locatability and altitude. The 91.5-cm telescope on-board will provide a Shuttle surface resolution of 1 meter or better (see Fig. 10). In most high temperature regions, the resolution will approach 0.7 meters for the longest range condition (peak heating) and approach 0.5 meters for shorter range conditions (Ref. 7). In addition, the telescope elevation is adjustable between  $+35^\circ$  and  $+75^\circ$  above waterline and can be optimized for each Shuttle Orbiter reentry condition. The on-board stabilization and telescope drive systems are adequate. No modifications are required other than gain adjustments on some servoloops. This aircraft is the only candidate with an on-board system control and data handling computer (HP2100). The streak camera technique is directly adaptable to the telescope similar to current IR experiments. The only modifications required are to mount an acquisition system on the telescope head ring. It will not interfere with any operation of the telescope and does not have to be removed for other experiments. The aircraft and telescope facilities are best suited for this experiment.

In the remainder of this report it is assumed that the NASA C141 AIRO is the observing platform.

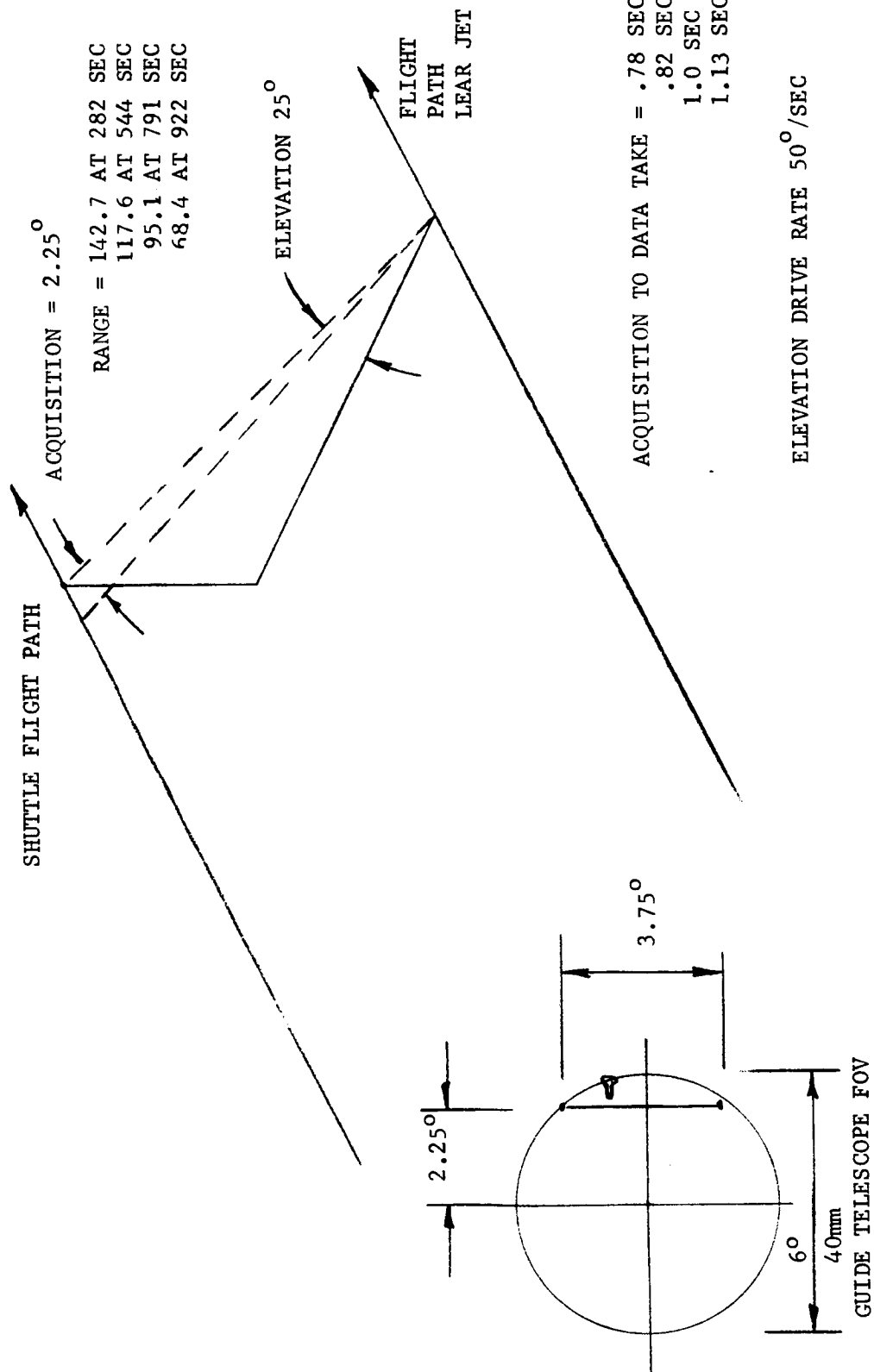
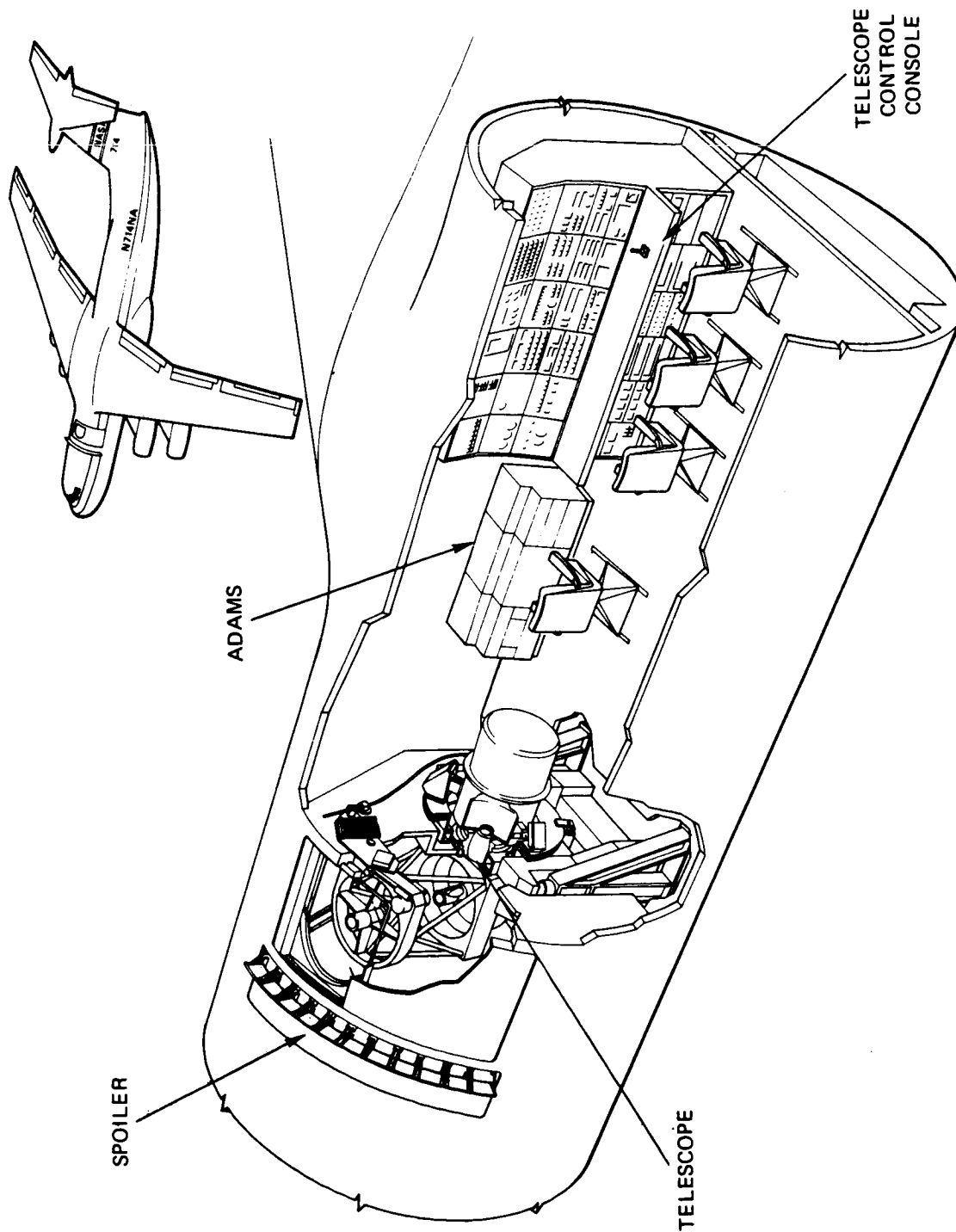
**MARTIN MARIETTA**

FIG. 10

AIRBORNE OBSERVATORY







## ACQUISITION SYSTEM

---

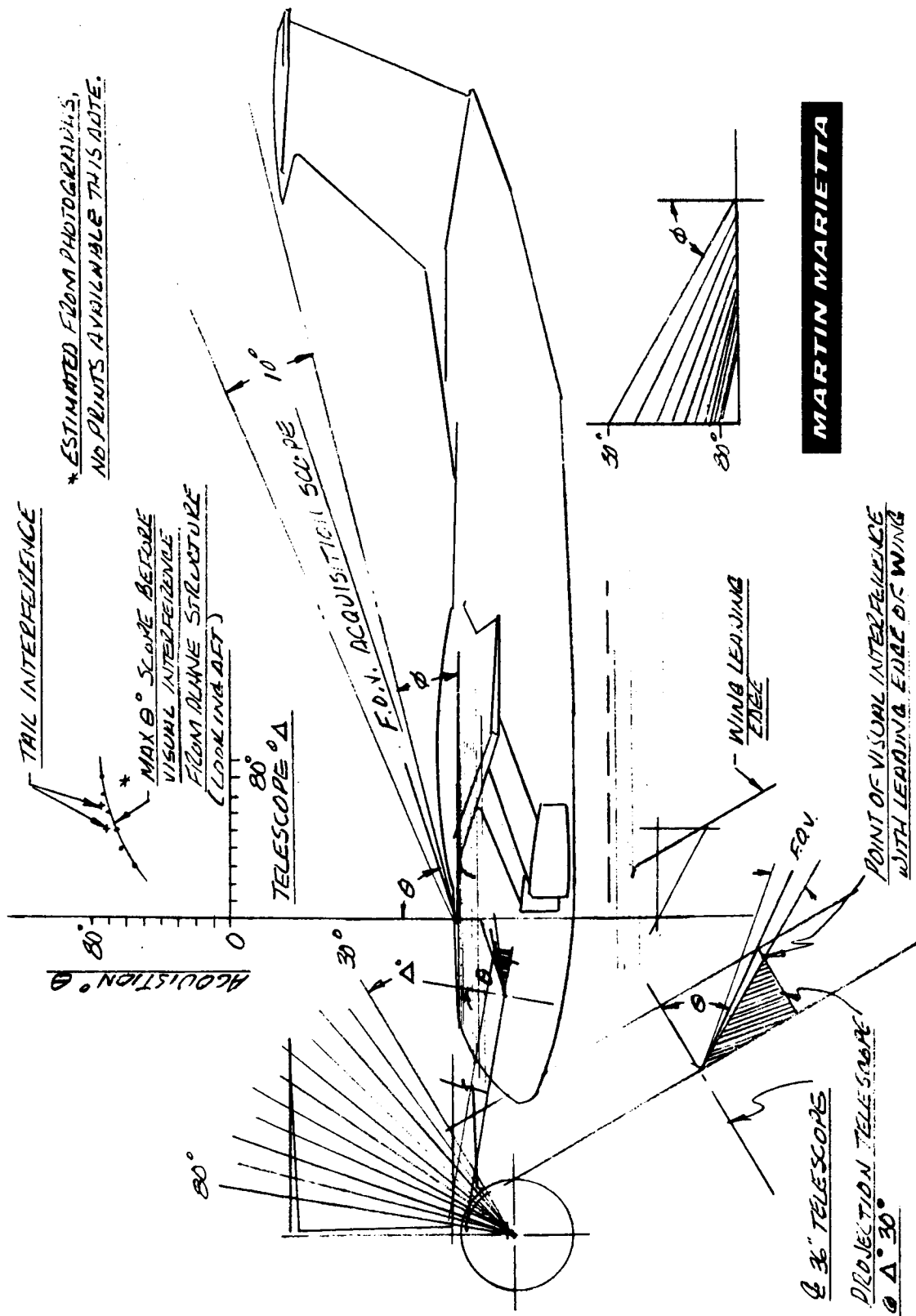
As discussed previously, the basis for the streak camera is: the object must fly through the telescope field-of-view (FOV), preferably the center of the field, within some reasonable tolerance. The FOV of the AIRO is 14 arcmin. To minimize the number of detectors required, it was stipulated that the Shuttle image pass within the center 5 arcmin of the telescope FOV.

The design requirements of the acquisition system are: (1) find the Shuttle while accounting for its uncertainty in position with respect to the aircraft, (2) lock-on the Shuttle and track it thereby providing an elevation error to the main telescope drive system, and (3) maintain this lock until the Shuttle image passes within  $\pm 2.5$  arcmin of the telescope line-of-sight. This can be accomplished by mounting the acquisition system on the main telescope with the gimbal axis  $90^\circ$  to both the telescope elevation axis and line-of-sight. As the telescope is driven in elevation based on the error signal received from the acquisition system, both move in elevation reducing the error signal.

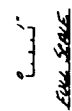
The uncertainty of the Shuttle position with respect to aircraft position and the maximum range of elevation adjustment dictates the FOV of the acquisition system to be  $9^\circ$ . The cross track error of the Shuttle can be 15 km and the altitude error 3 km when the acquisition range is at least 90 km. The along-track error of the Shuttle is of no concern when flying parallel to the Shuttle.

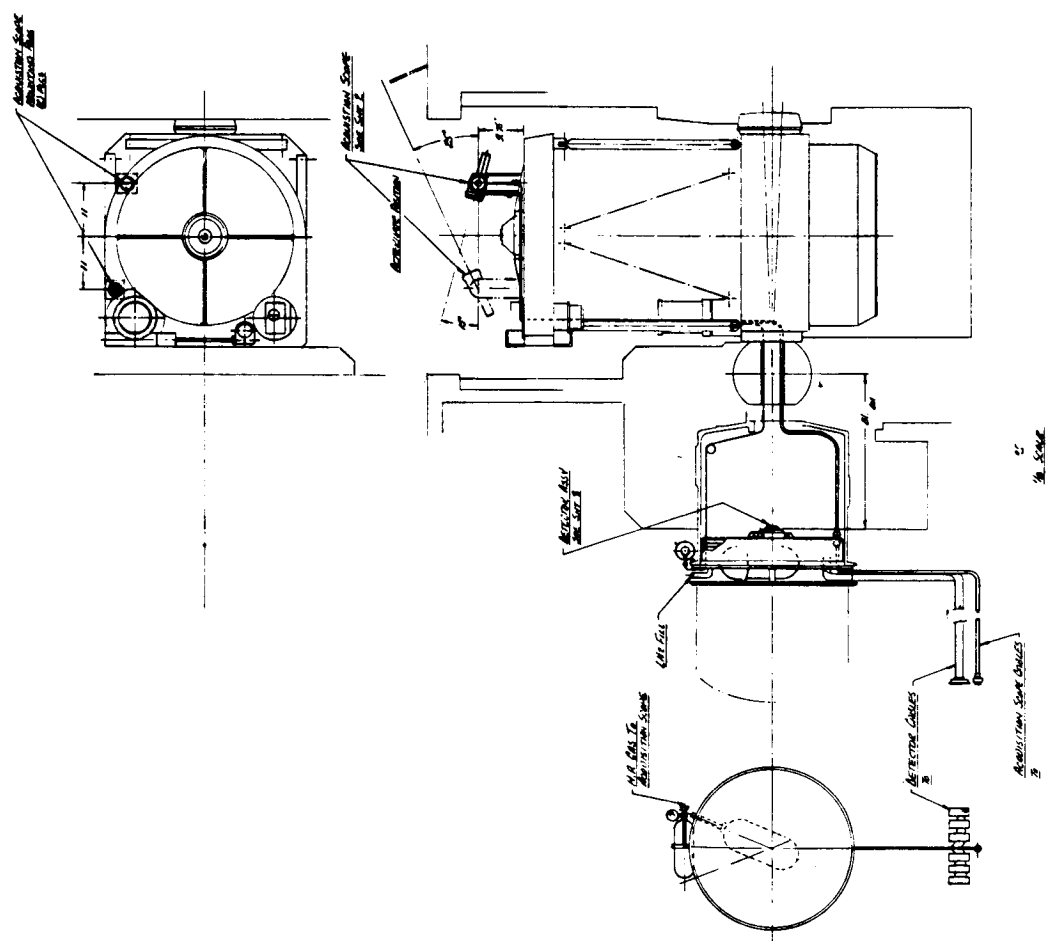
The design chosen for the acquisition system is an infrared refracting lens that provides an image of the  $9^\circ$  field on a rotating reticle. Behind the reticle is a condensing lens and a cryostat-cooled indium antimonide detector. The whole system is mounted on a gimbal axis that is  $90^\circ$  to both the telescope elevation axis and the telescope line-of-sight. The rotation around this axis by the acquisition system is called acquisition angle.

The acquisition angle required is governed both by: (1) the first point the Shuttle can be detected at based on signal-to-noise, and (2) the time required to move the telescope through the maximum elevation change required. Figure 11 depicts the maximum acquisition angle available before interfering with aircraft structure. Based on the  $9^\circ$  FOV of the acquisition system, the maximum motion allowed in elevation is  $4.5^\circ$ . The maximum elevation rate for the existing elevation drive with electrical modification is  $0.33^\circ/\text{sec}$ . This provides 13.5 sec plus a 6 sec contingency or 20 sec of acquisition time. The maximum acquisition angle that can be accommodated based on the highest angular rates is  $62^\circ$  (see Appendix). This is compatible with the available acquisition angle of  $65^\circ$  at a telescope elevation angle of  $55^\circ$ . Figures 12 and 13 show the acquisition system design.



## FIG. 12

[illegible]

[illegible]

Telescope - The major components of the telescope are the collector lens system, a reticle that modulates the energy received from the target and acts as a spatial filter, a condenser lens that images the aperture on an Indium Antimonide (InSb) detector, and an optical filter. Other significant components are a nitrogen gas Joule-Thompson cryostat, optical switches, tachometer, and a brushless motor.

The telescope drive components include a motor, tachometer, and a resolver.

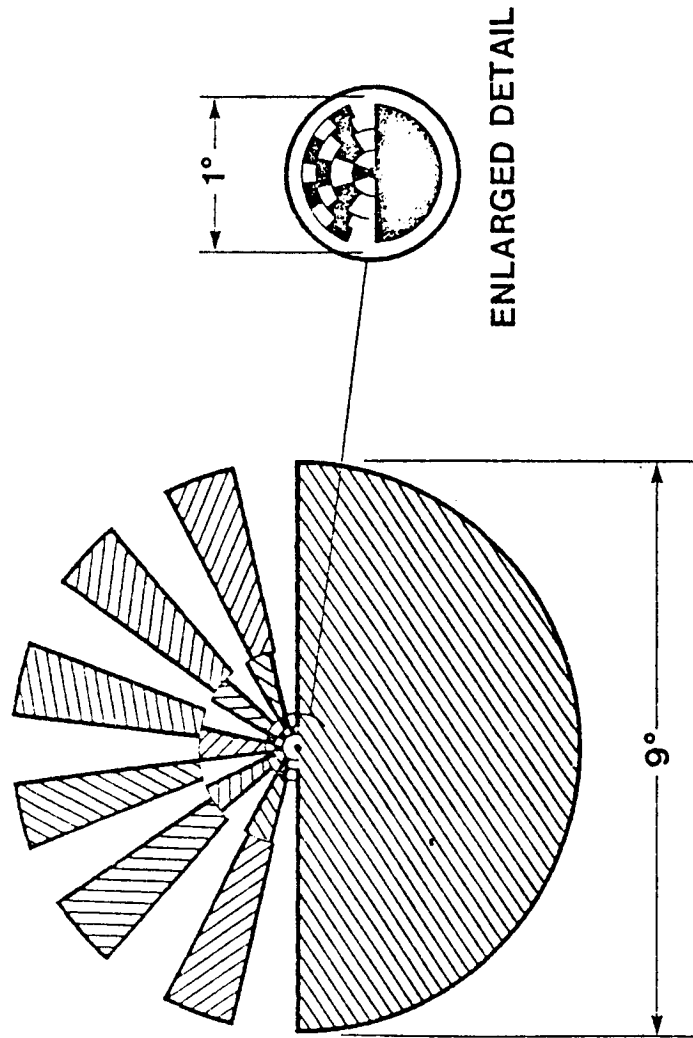
Reticle - The reticle shown in Figure 14 was designed specifically for the requirements of the Shuttle infrared imaging system. In the system, elevation and azimuth tracking requirements are quite different. Elevation accuracy is a driving function in determining the number of detectors required in the focal plane. Large azimuth errors are tolerable as long as the Shuttle remains in the tracking telescope's field-of-view. In the present design, we will actually bias in an error to keep the Shuttle off the reticle center (where there is no signal). Determination of the Shuttle vertical (elevation) position will be accomplished by the zero and 180° phase crossing of the opaque portion of the reticle by the Shuttle image.

The modulation by the reticle is by discrete frequencies. The radial position of the target image is determined by the frequency of modulation received by the detector. The center  $\pm 0.5^\circ$  is broken up into four discrete regions that vary from three to nine times the reticle rotation rate; the next  $1.0^\circ$  is designed to be 11 times the rotation rate. The last  $3.0^\circ$  are at 13 times the rotation rate. The center portion of the reticle is broken up into several increments to aid in servosystem design. The spoke width is set up to be greater than two Shuttle image lengths, including diffraction limit blur circle for the closest predicted crossing distance.

Detector and Filter - Indium Antimonide (InSb) is the detector chosen to be used in the acquisition tracking telescope. By reducing the long wavelength background irradiation to very low levels using a cooled bandpass filter, specific detectives,  $D^*$ , values of up to  $3 \times 10^{12}$  will be arrived at for a 4.5-mm diameter detector. The detector will be cooled with a Joule-Thompson cooler to 90 K. The combination of high  $D^*$  and good frequency response (necessary for accurately determining elevation errors) narrowed the choice to the reliable InSb detector.

# TRACKING SCOPE ROTATING RETICLE

FIG. 14



The cooled bandpass filter (Fig. 15) (1 to 2.6 micrometer) serves to reduce background irradiation and therefore detector noise. It was also determined that any target signal lost in the region beyond 2.6 micrometers is not a serious loss due to excellent signal-to-noise (S/N) values for the present system. In addition, this limit significantly eases the optical design complexity. The 1 micrometer lower wavelength limit serves to adequately reduce the solar background but aids in acquiring stars during boresighting operations (see calibration section, page 55).

Signal-to-Noise (S/N) - Figure 16 shows the system parameters for reference and the acquisition signal-to-noise (S/N) values for the listed conditions. These predicted S/N values are exceptionally good; they assure target acquisition within the telescope field-of-view. Such high S/N values ease the burden on the electronics and software system in the processing of error signals.

The servo system required to enable the acquisition system to perform its function is described in the following paragraphs. Portions of this servosystem are part of the AIRO telescope stabilization system and only require slight modification. Figure 17 shows an overall block diagram of the acquisition and stabilization system as designed for this task, using as much existing capability as possible.

There are six major loops to consider for the C141 system.

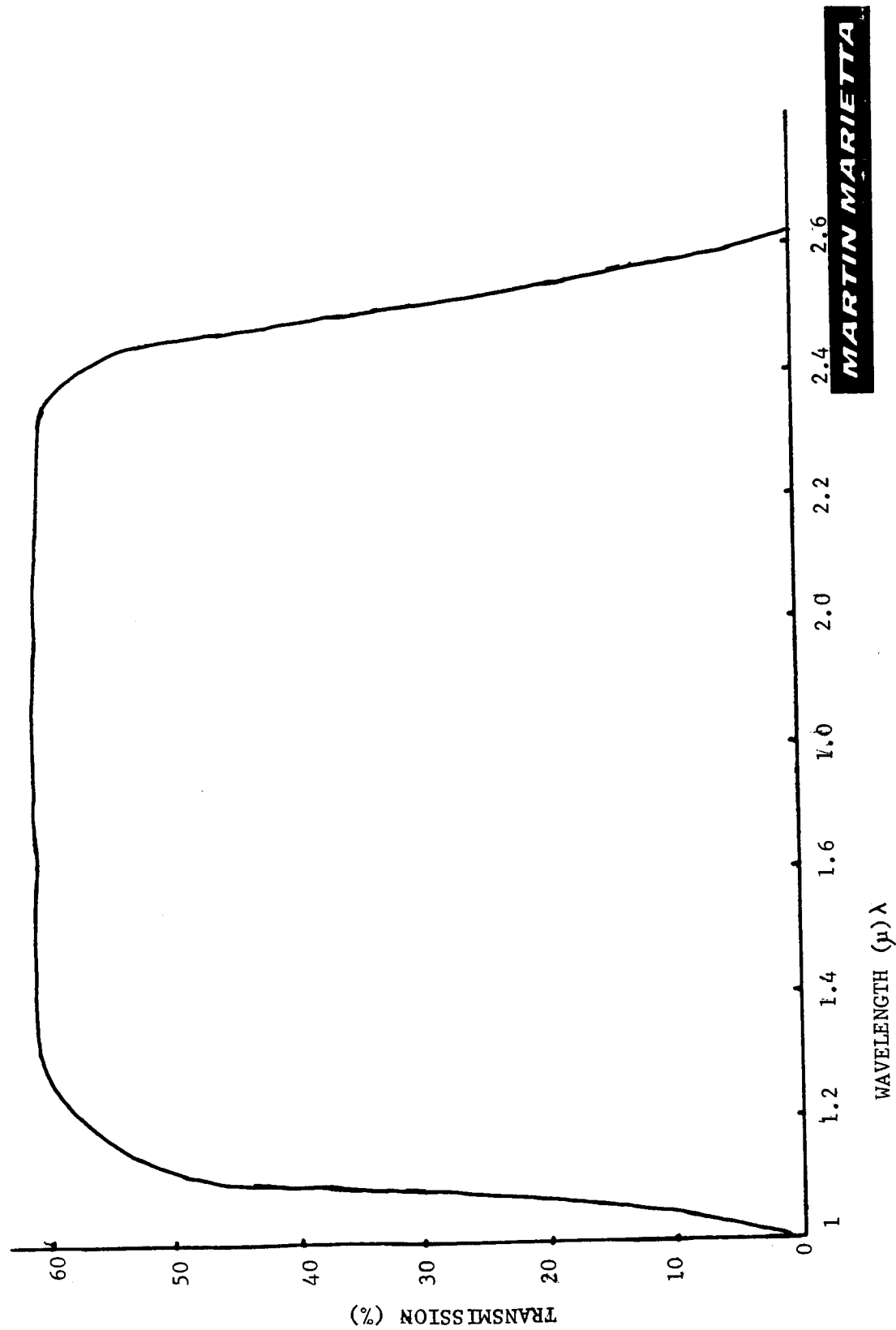
Azimuth Telescope Stabilizing Loop - This existing loop will stabilize the telescope in azimuth and will provide an inertial hold (see Fig. 18). It will provide the initial pointing system with an incremental bias on pointing angle. It may be required to provide a low bandwidth centering function in its  $\pm 2^\circ$  travel at initialization.

LOS Telescope Stabilizing Loop - Presently an operator observes a TV CRT to center the LOS axis manually via a joy stick. This function will be refined with a closed-loop servo using an angular pick-off similar to the AZ and EL system (see Fig. 19). This axis should remain centered to within 1/2 to 1/4 degree at initialization. The actual value of this error must be fed to the Elevation Initialization as a bias.

Azimuth and Elevation Tracking Loops (4 Loops) - Figures 20 and 21 show these loops. The existing system capability was evaluated as to maximum torquing accelerations and rates (see Fig. 22). The elevation axis has a maximum acceleration of  $3.77^\circ/\text{sec}^2$  which is adequate. The elevation gyro package is capable of torquing the gyro at  $3^\circ/\text{s}$  and is presently electronically limited to slew at 225 arcsec/sec. For our application, this should be increased to  $0.5^\circ/\text{sec}$  by electronic mods.

FIG. 15

ACQUISITION SYSTEM - FILTER

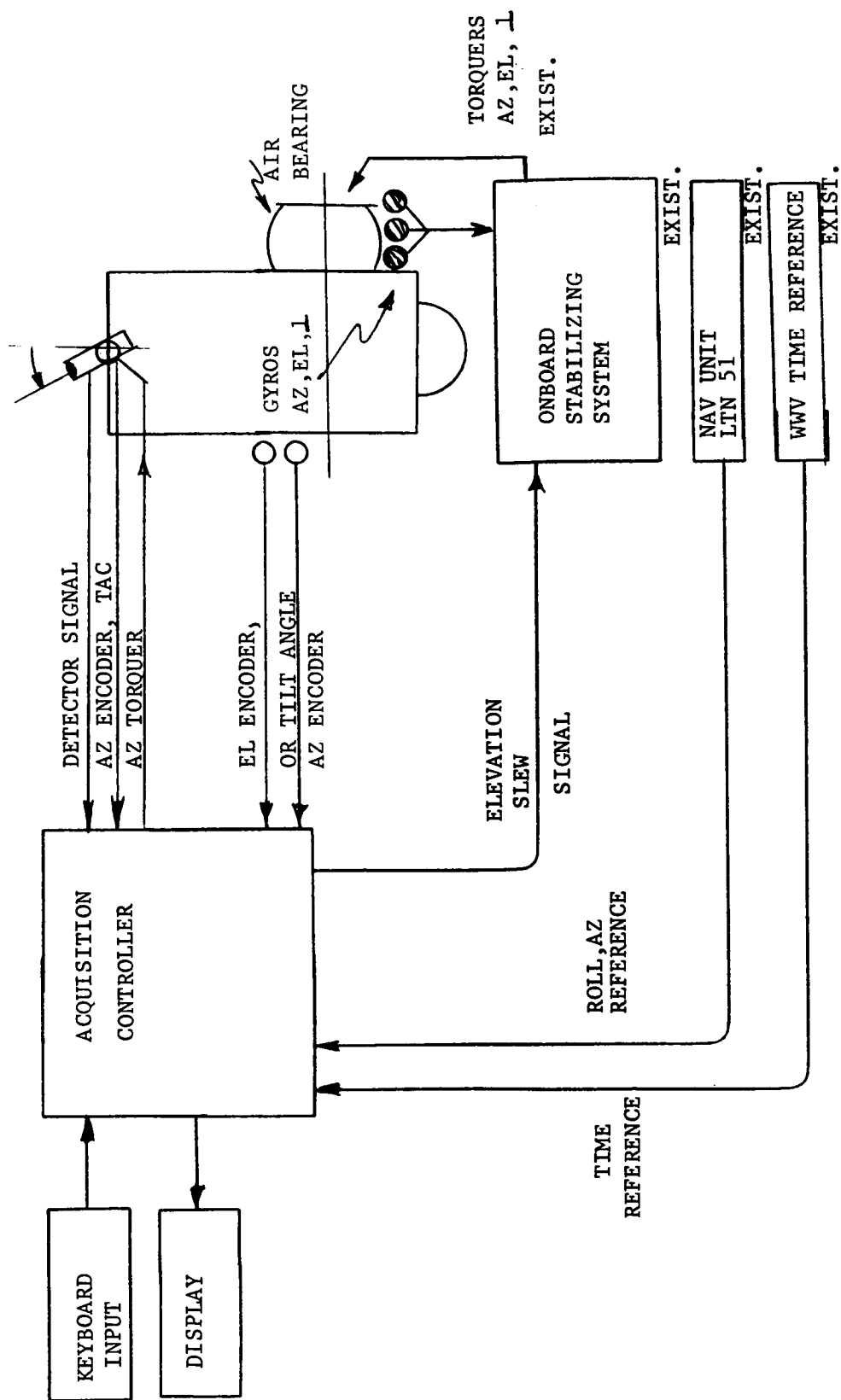


MARTIN MARIETTA

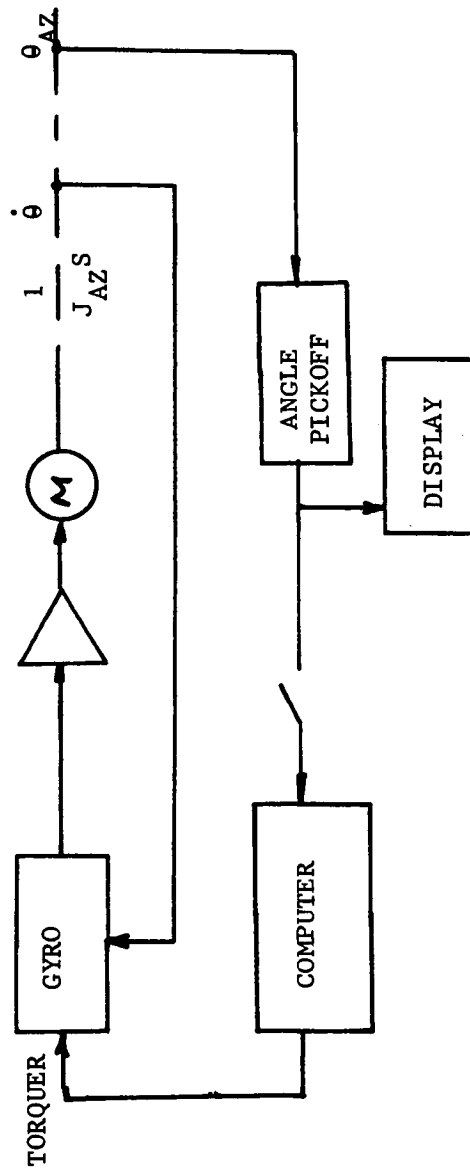


# ACQUISITION AND TRACKING SYSTEM PARAMETERS

SYSTEM PARAMETERS		ACQUISITION PARAMETERS			
COLLECTOR DIAMETER	62.5 mm	TIME FROM REENTRY	282	544	791
FOCAL LENGTH	125 mm	OFT-1 (SEC)	922	YF12	
DETECTOR DIAMETER	4.5 mm	MEAN TEMPERATURE	1250°K	1100°K	1000°K 1050°K 700°K
ELECTRICAL BANDWIDTH	25Hz	RANGE	162KM	131KM	92KM 72KM 30KM
DETECTOR $\lambda_1 = 1.0\mu$ $\lambda_2 = 2.5\mu$	InSb	SIGNAL TO NOISE	2680	1900	2065 4580 200
DETECTOR TEMP	$\approx 77^\circ K$				
FOV	$9^\circ$				
SHUTTLE AREA	362 METER <sup>2</sup>				
YF-12 AREA	70 METER <sup>2</sup>				
C = 0.3*					

**MARTIN MARIETTA**

- o POSITION NULL ADDITION TO MAINTAIN AZ CENTERED
- o PRESENTLY BEING DONE BY TRACKER SCOPE SIGNAL



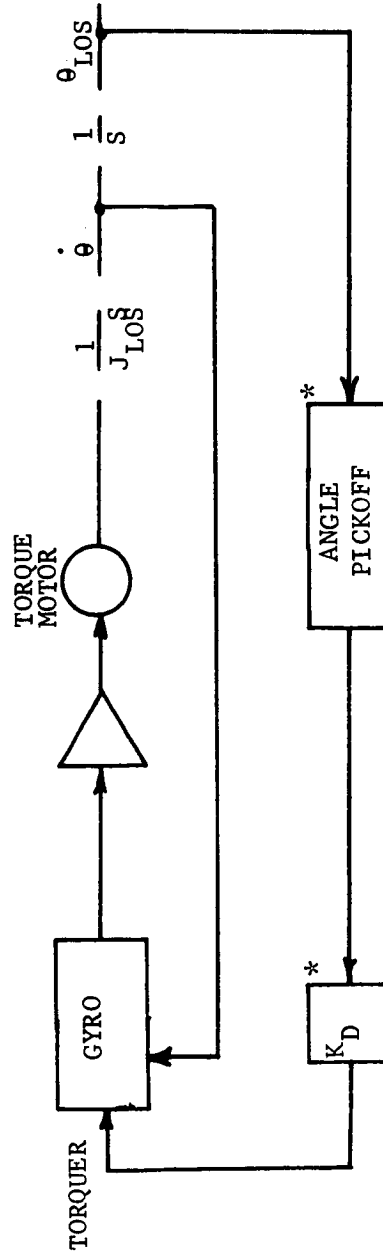
REQUIRED

\*ADD SOFTWARE TO CLOSE POSITION LOOP  
ALL HARDWARE EXISTING

LOS SERVO LOOP (91.5 cm TELESCOPE)

30

POSITION NULL TO MAINTAIN LOS CENTER  
PRESENTLY DONE BY OPERATOR OBSERVING TV DISPLAY

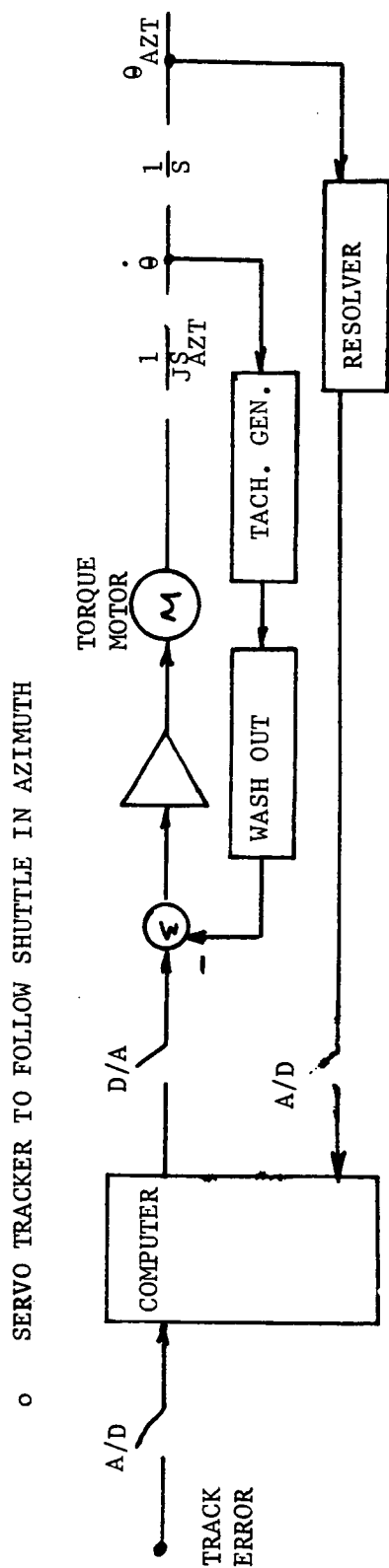


REQUIRED

- \*ANGLE PICKOFF (SIMILAR TO EXISTING AZ, EL)
  - \*COMPUTER INPUT
  - \*COMPUTER OUTPUT
  - \*SOFTWARE
- OR ANALOG HARDWARE

# AZ TRACKER SERVO LOOP (NEW ACQUISITION TRACKER)

FIG. 20



## REQUIRED

\*ALL ANALOG HARDWARE

\*SOFTWARE TO CLOSE LOOP AND SET INITIAL POSITION

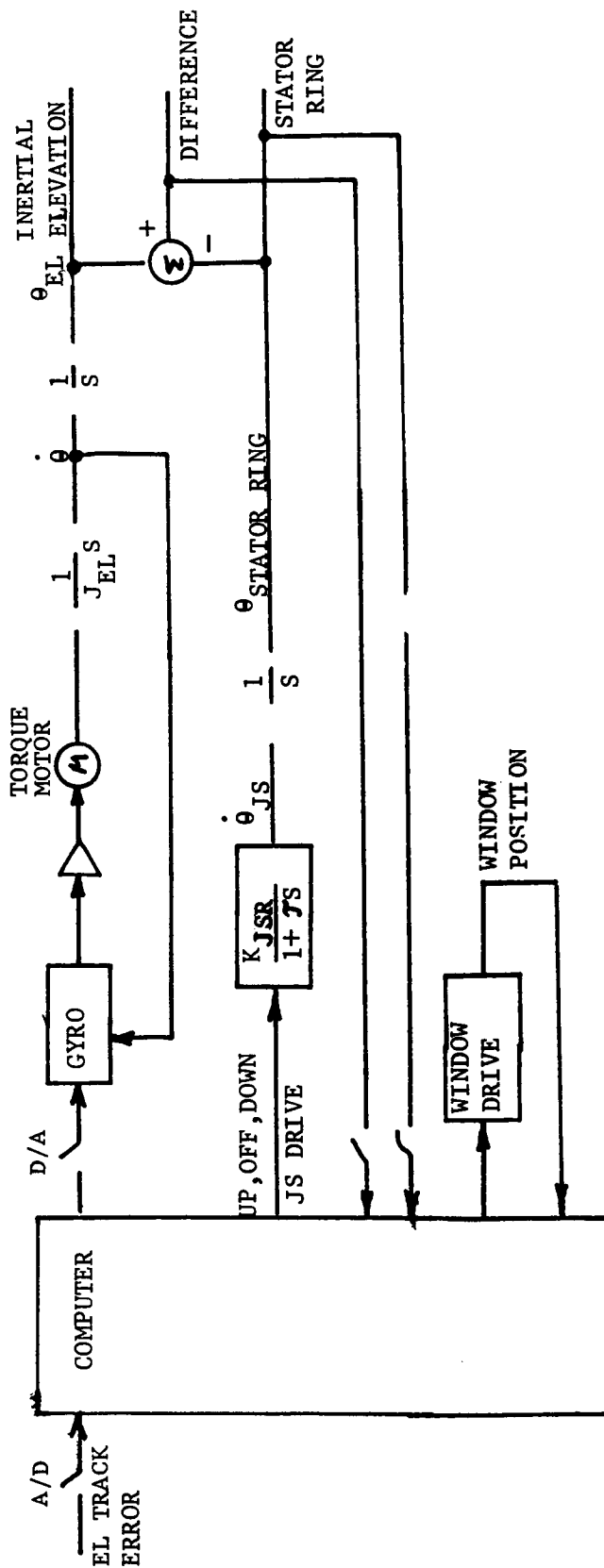
MARTIN MARIETTA

# ELEVATION SERVO (91.5 cm TELESCOPE)

FIG. 21

32

- o ELEVATE TELESCOPE TO NULL TRACK SCOPE EL ERROR
- o MAINTAIN STATOR RING IN CENTER OF TRAVEL VIA EXISTING JACK SCREW
- o MAINTAIN WINDOW IN CENTER OF TRAVEL VIA EXISTING DRIVE



## REQUIRED

- \*EL TRACK ERROR INPUT
- \*STATOR RING POSITION INPUT
- \*WINDOW POSITION INPUT
- \*JACK SCREW COMMAND OUTPUT
- \*WINDOW COMMAND OUTPUT
- \*SOFTWARE TO HANDLE ABOVE AND SET INITIAL POSITION

MARTIN MARIETTA

## ACCELERATION AND RATE CAPABILITIES

## ○ MAX TELESCOPE ACCELERATION

$$\text{EL T/J} = \frac{25' \text{ LB}}{380 \text{ SF}^2} \rightarrow 3.769^\circ/\text{S}^2$$

$$\text{AZ T/J} = \frac{25}{945} \rightarrow 1.515^\circ/\text{S}^2$$

$$\text{LOS T/J} = \frac{25}{835} \rightarrow 1.715^\circ/\text{S}^2$$

## ○ MAX GYRO TORQUE RATE

30/S @ .7° STOP

ELECTRONICS PRESENTLY LIMIT TO 255 S/S

## ○ MAX JACK SCREW RATE

≈ 390/S

## ○ MAX WINDOW RATE\*

≈ 270/S

\*THERE IS APPROXIMATELY +1° DEGREE EXTRA OPENING

The jack screw or stator ring and port movement were clocked at  $0.39^\circ/\text{sec}$  and  $0.27^\circ/\text{sec}$  respectively. These two servos will be driven from the computer so as to maintain center of the stabilizing system and window port. A deadband of  $1/2^\circ$  appears feasible to maintain center and not pick up aircraft motion. The slew rates appear to be compatible with the mission requirements. The angular sensor for a stator ring servo will be the existing elevation sensor. The sensors for the window port will be the existing window port elevation sensor, plus the stator ring elevation sensor, plus the stator ring elevation pot. The azimuth tracker loop will be accomplished by an analog rate loop and a digital position loop. The conflicting requirements of large tracking rates and low-limit cycle activity about the sensor deadband require a wash out filter on the rate feedback. An angular encoder is required to achieve accurate initial pointing.

The elevation servo will operate much as it does now with the tracker scope elevation signal being used instead of the present tracker signal. With the present system, a settling time of 5 sec is required after the initial slew rate (see Fig. 23).

Simulation of Azimuth and Elevation Control - A computer simulation code of azimuth and elevation dynamics was written to determine overall system response. Figure 24 shows elevation motion of the telescope which operates at maximum rate until elevation error reaches roughly  $1/2^\circ$ . The system then tends to settle for 5 sec to the final value of elevation. Figure 25 is the elevation rate. Humps indicate crossing of the center bands of the acquisition reticle.

As the main telescope is moving, the stator ring must follow to maintain the torque motors in their  $\pm 2^\circ$  operating range. Figures 26 and 27 show this motion. Upon reaching  $1/2$  degree error between the main telescope and stator ring, Figure 26 shows the stator ring slewing at maximum rate until this error is once again within the  $1/2$  degree band. Figure 28 shows the difference between stator ring and main elevation. At first the main telescope out travels the stator ring, then the stator ring catches up. This condition is worst-case in that the error peaks at  $2^\circ$ .

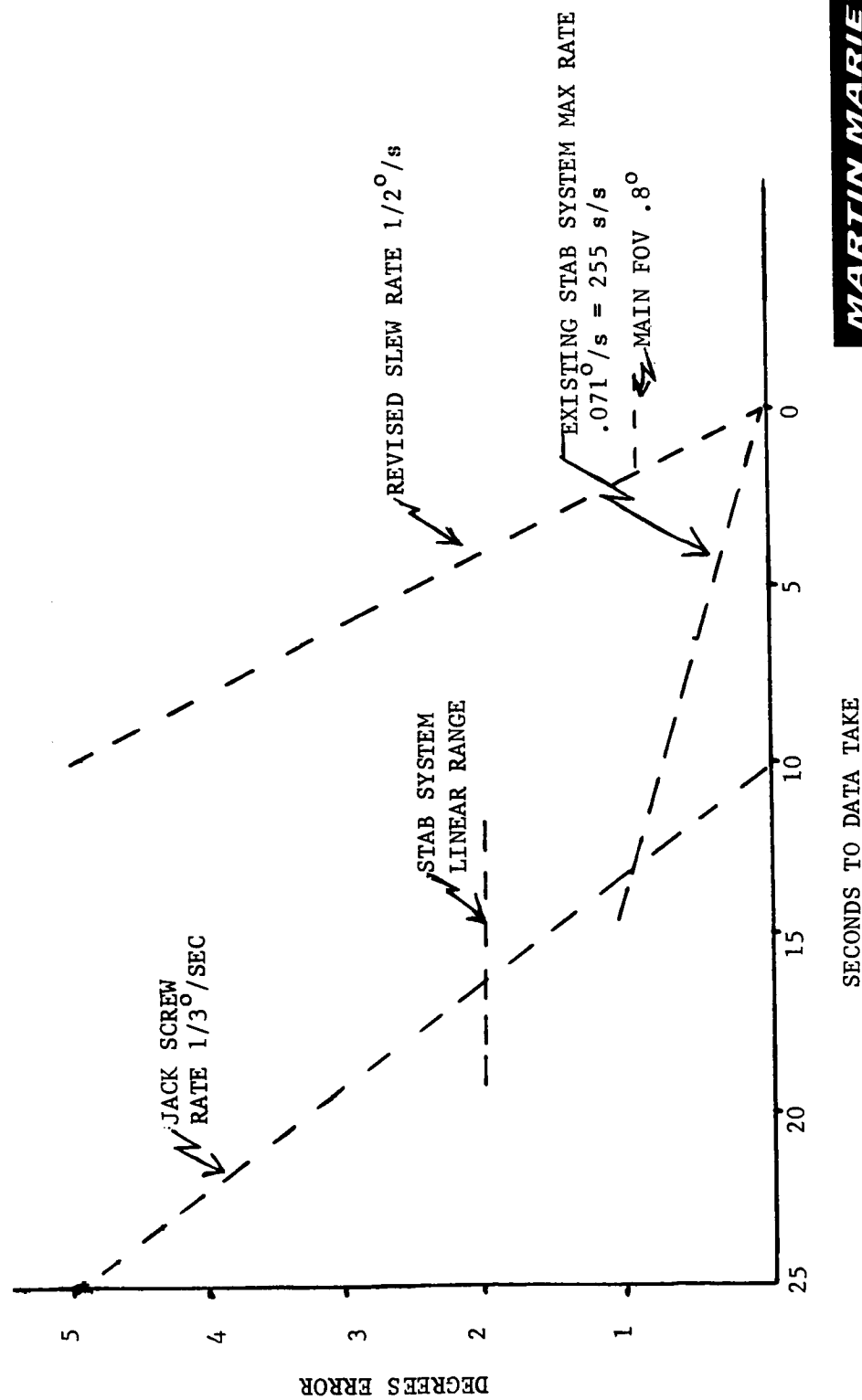
The azimuth gimbal on the tracking scope picks up the Shuttle at roughly  $70^\circ$  aft of perpendicular to the aircraft. Figures 29 and 30 show azimuth angle and rate. Jumps in Figure 30 show the system moving between reticle bands.

Figure 31 shows the image motion in the reticle plane in azimuth and elevation. This case is for an initial error of  $5^\circ$  in elevation and 1 degree in azimuth. (System initially pointing below and aft of the Shuttle). Figure 32 shows the same plot but with the system initially pointing below by  $2^\circ$  and forward by  $4^\circ$  of the Shuttle.

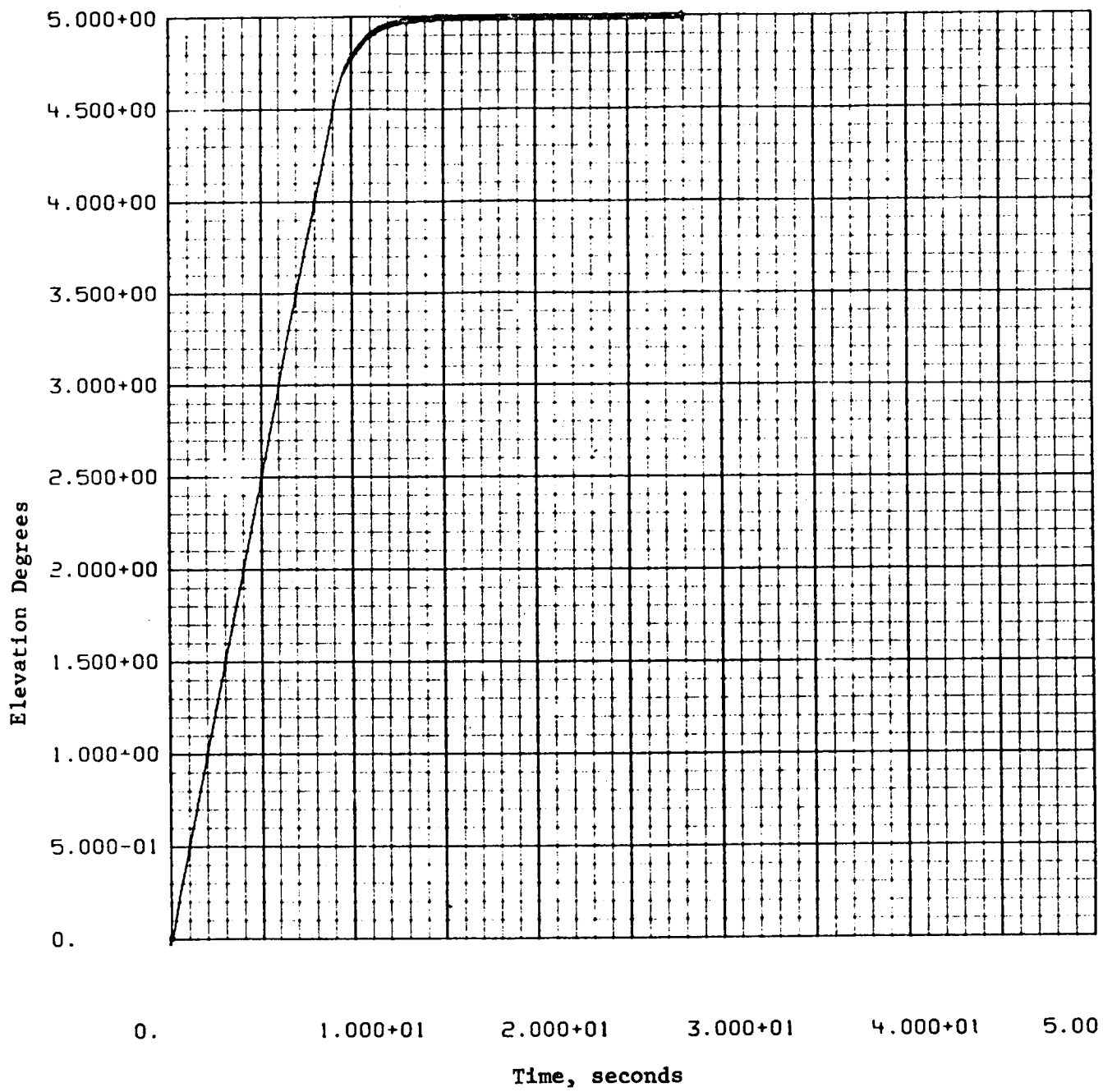


FIG. 23

ACQUISITION, TRACK & SETTLE TIMING VS. MAX SLEW RATES

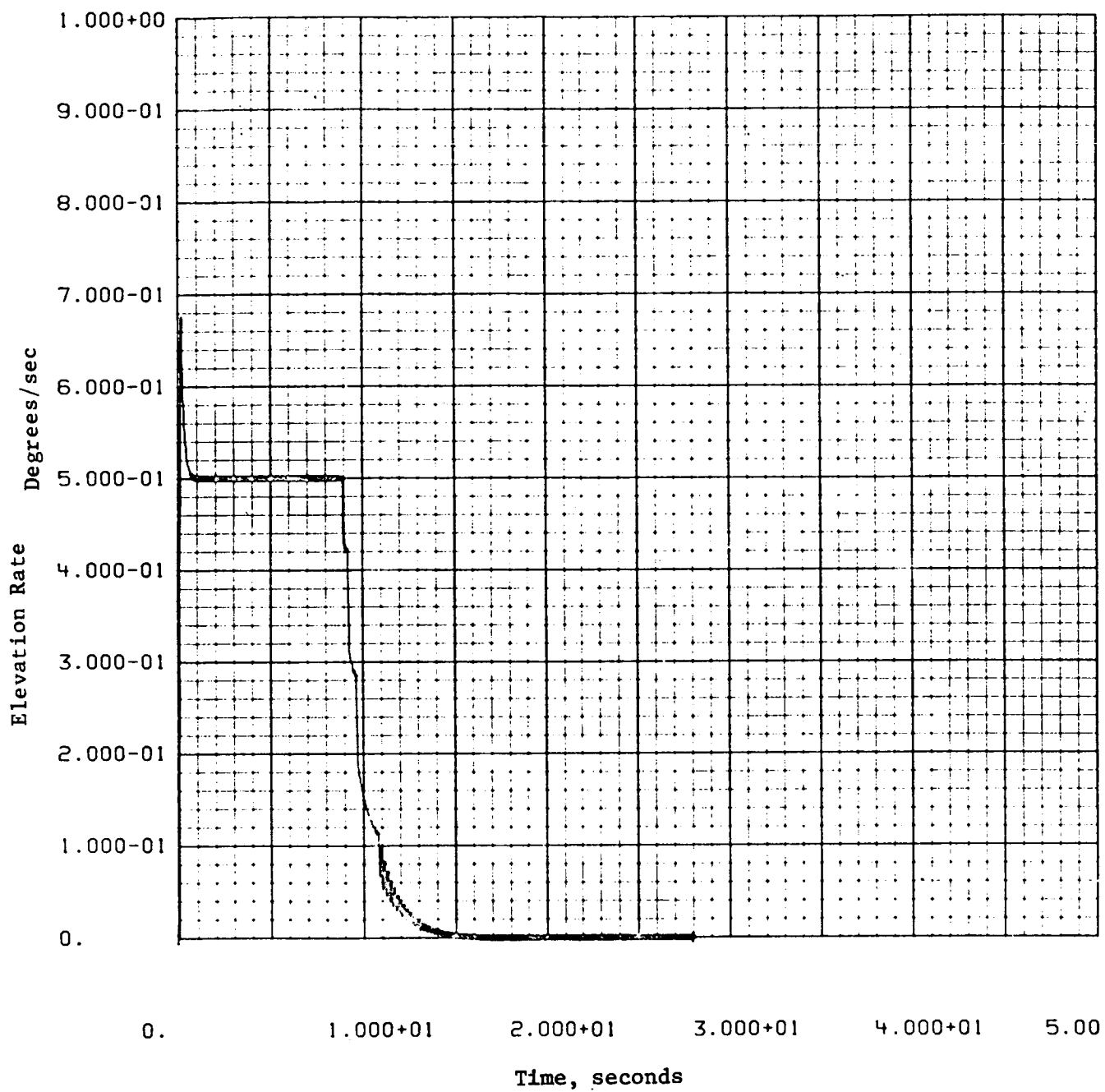


MARTIN MARIETTA



1 SIMULATION OF EL AND AZ CONTROL

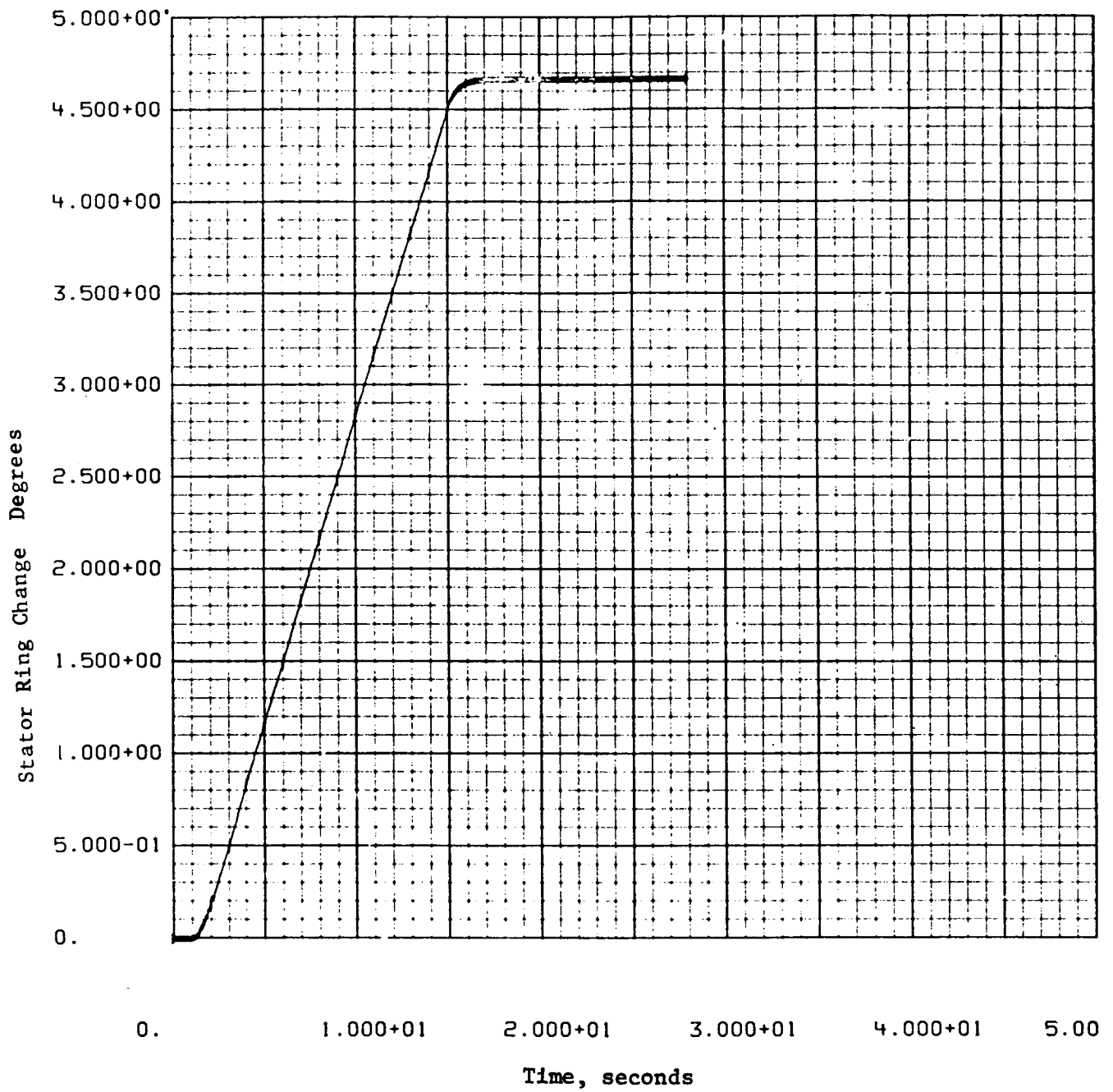
Figure 24



1

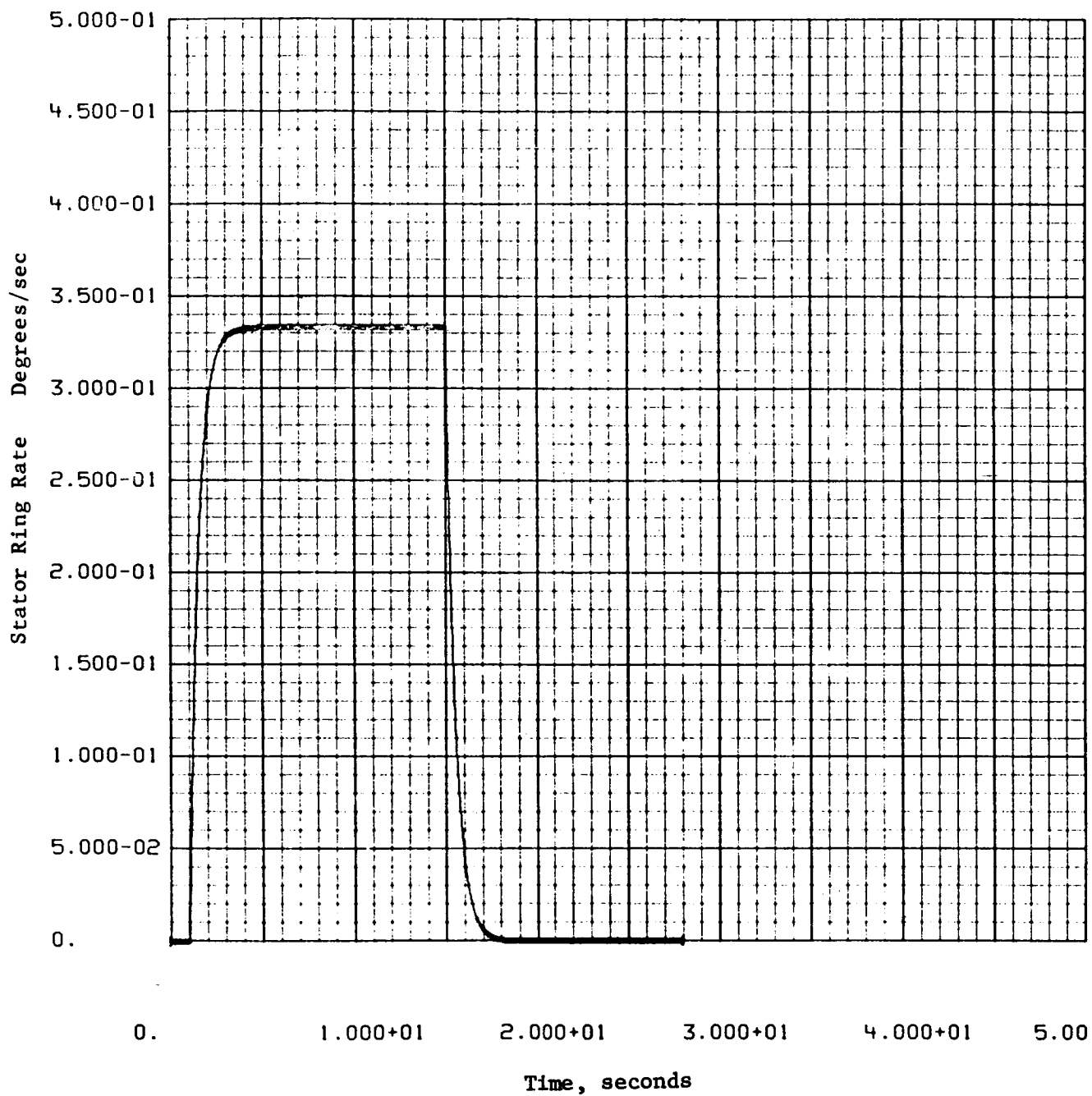
SIMULATION OF EL AND AZ CONTROL

Figure 25



1 SIMULATION OF EL AND AZ CONTROL

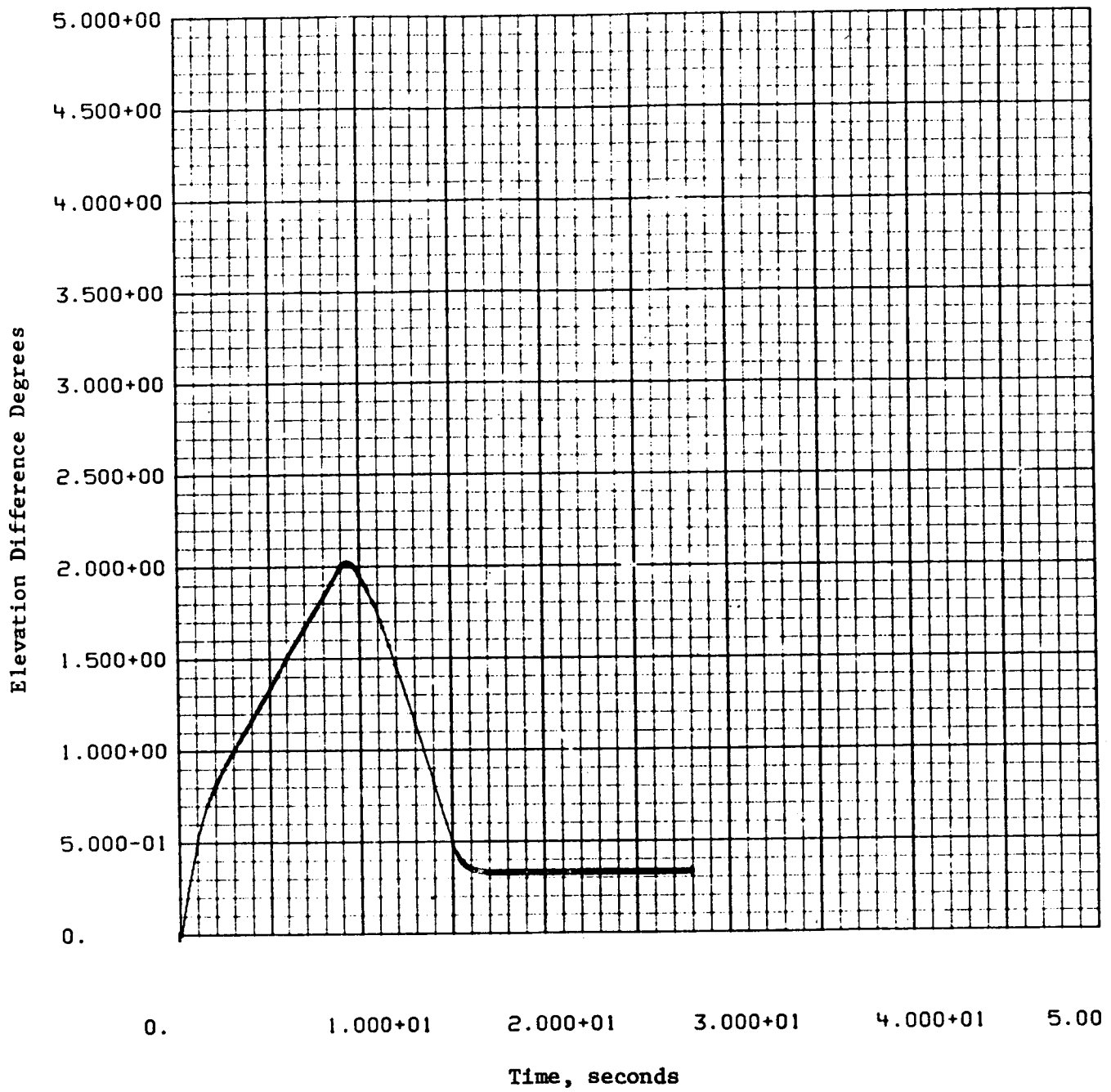
Figure 26



1

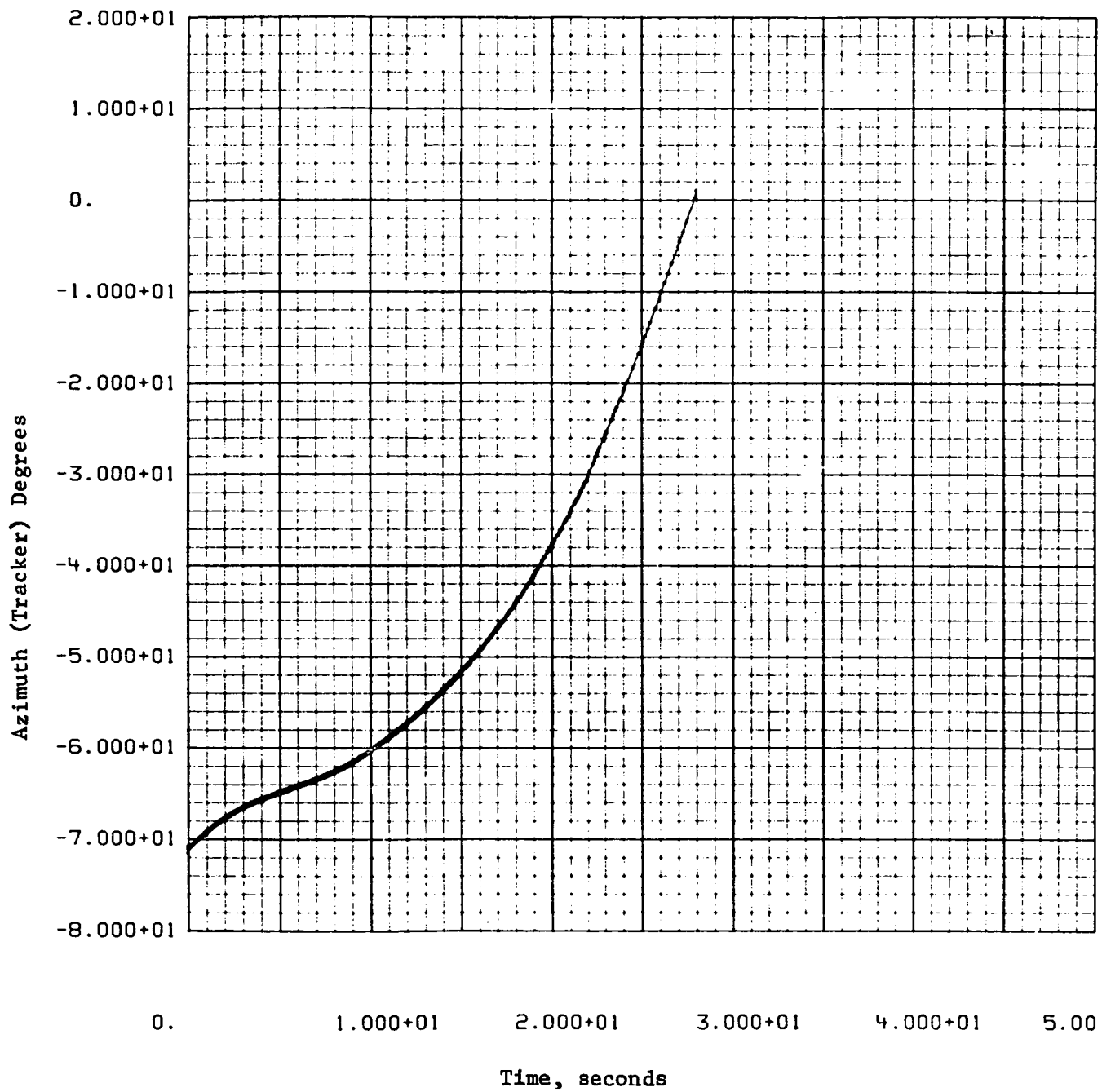
SIMULATION OF EL AND AZ CONTROL

Figure 27



1 SIMULATION OF EL AND AZ CONTROL

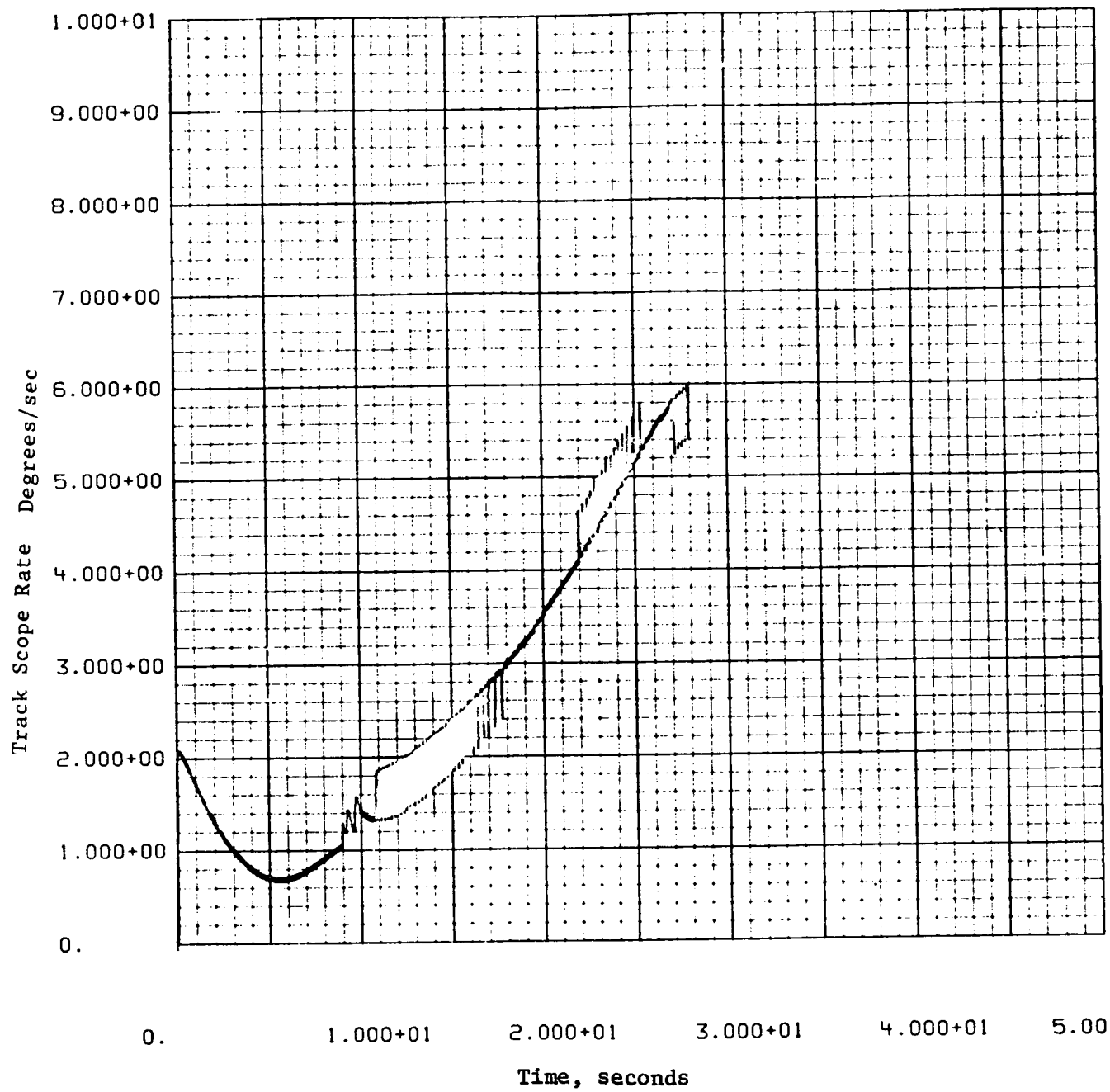
Figure 28



1

SIMULATION OF EL AND AZ CONTROL

Figure 29



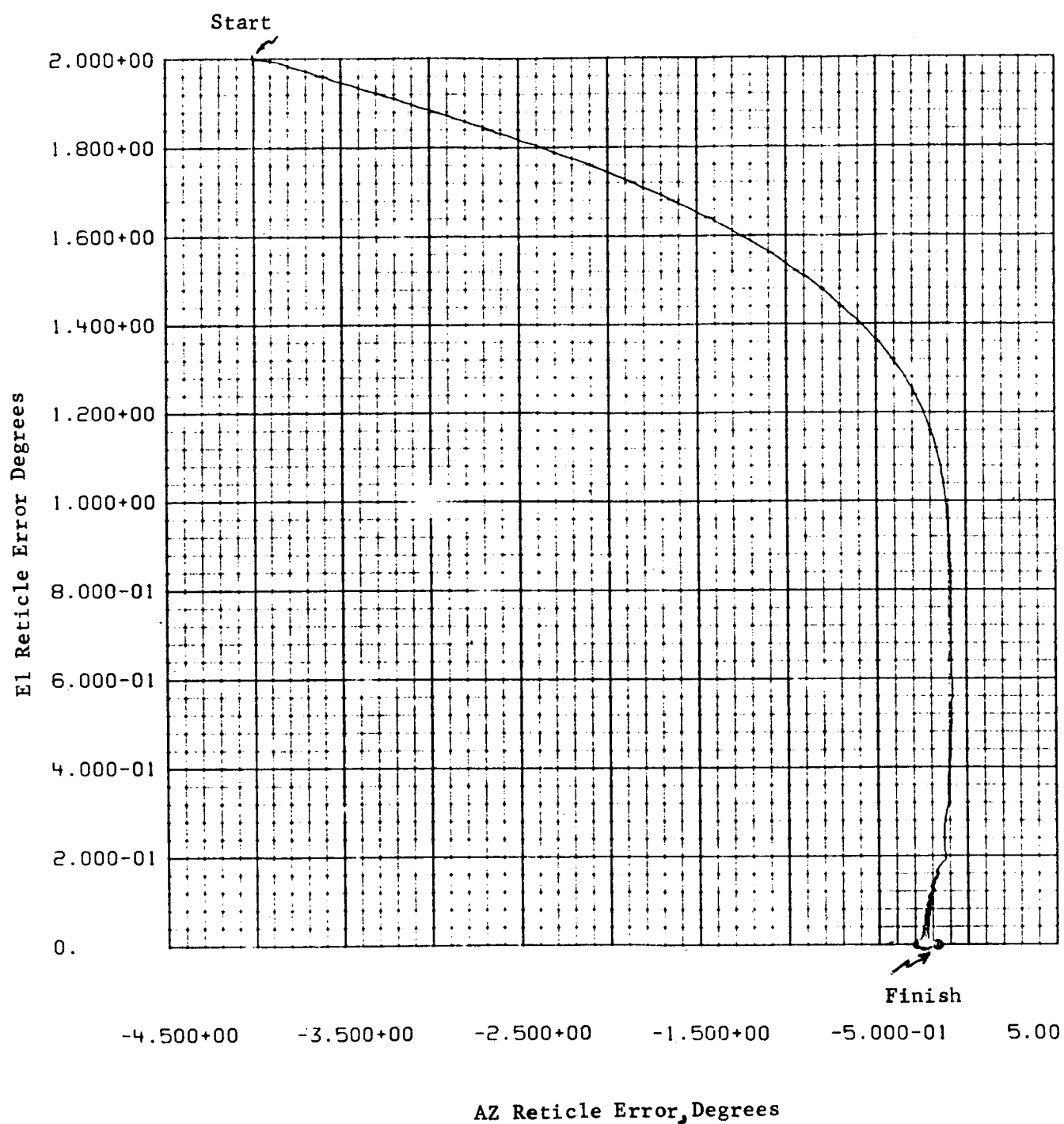
1

SIMULATION OF EL AND AZ CONTROL

Figure 30







1

SIMULATION OF EL AND AZ CONTROL

Initial Condition  
 EL error = +2°  
 AZ error = -4°

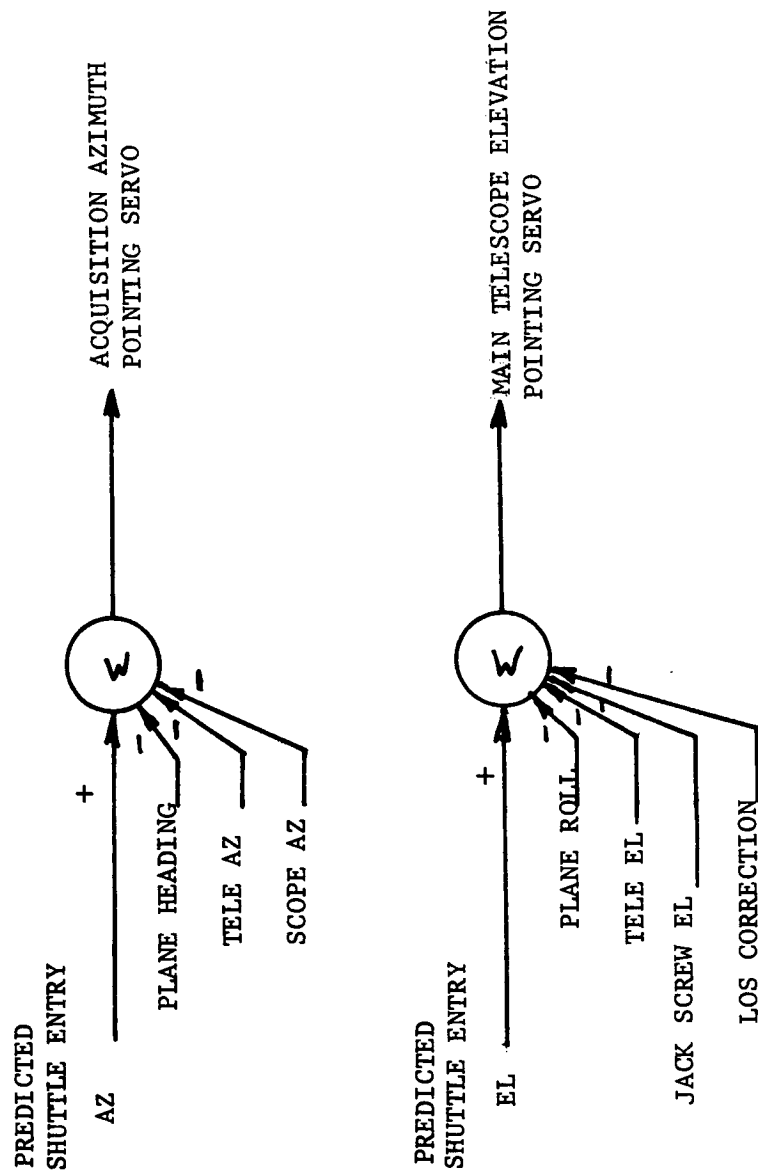
Figure 32

Initial pointing of the acquisition and tracking scope will be accomplished as follows. Predicted Shuttle entry azimuth will be compared to the sum of plane heading, telescope AZ and acquisition scope AZ. The difference will be used to torque the scope servo. Predicted Shuttle entry elevation will be compared to the sum of plane roll angle, telescope El, stator ring elevation and LOS angle correction. The difference will be used to elevate the telescope servo and stator ring. At the time of go-ahead, determined by predicted Shuttle entry time versus WWV time standard, the acquisition scope will be positioned and begin tracking (see Fig. 33).

Acquisition Scope Errors - Sensor errors in azimuth are mainly due to reticle radial quantization of 7 arcmin per band. The elevation axis must be much more precise. Errors are broken down into point source errors and finite image size errors (Fig. 34). Point source errors are as follows. An off-the-shelf lens will give a resolution of 82.2 arcsec, while a special-built lens will reduce this resolution to approximately 15 arcsec. Boresite alignment will probably be around 30 arcsec and may be reduced by calibration procedures that may be corrected partially by an electronics bias. A reasonable reticle resolution will be 7 arcsec. Detector response may be tailored, but a reasonable value is 16 arcsec from a 25 kc bandwidth. Demodulation errors appear to be bounded by the outer clock band resolution. A refined fiber optics light source for this should yield 7 arcsec accuracy. Errors from the finite image size are difficult to evaluate at present. At worst, this should be 75 arcsec, but with an extra signal processing this should reduce to 14 arcsec. The HP 2100 will be required to handle this task and would act as the demodulator (see Fig. 35). A breadboard of the system will be needed to establish firm error numbers; however, at present, RSS errors of 41 arcsec in elevation appear feasible.

ADAMS - Servo Interface - It appears feasible to use the ADAMS system for much of the servoprocessing. This will be accomplished by coding one HP2100 for servofunctions. The unit will be overseen by the ADAMS executive processor. It is expected that the executive will handle CRT terminal input and output and act as a monitor and parameter input. The interface to the servoprocessor will be via an electronics box furnishing the signals not already existing in the ADAMS. Figure 36 lists the existing and additional signals required. The repetition rate will be based on the basic acquisition sample rate of 50 sps. One HP2100 appears adequate to handle the coding and computation requirements. This approach should be extremely flexible and allow modifications and revisions, as required, without last minute hardware changes.

INITIAL POINTING ANGLE CALCULATIONS TO BE DONE IN HP2100 FIG. 33

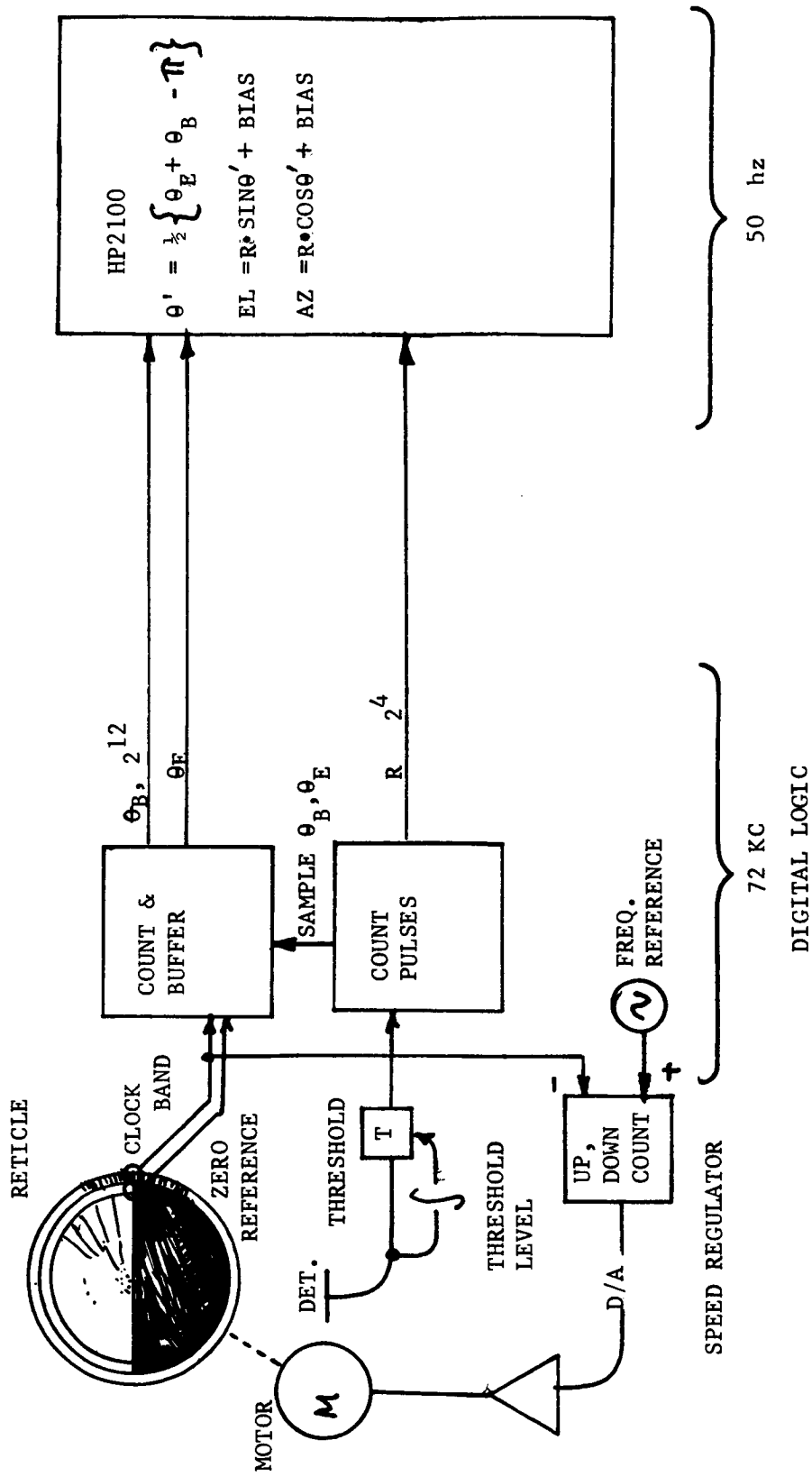


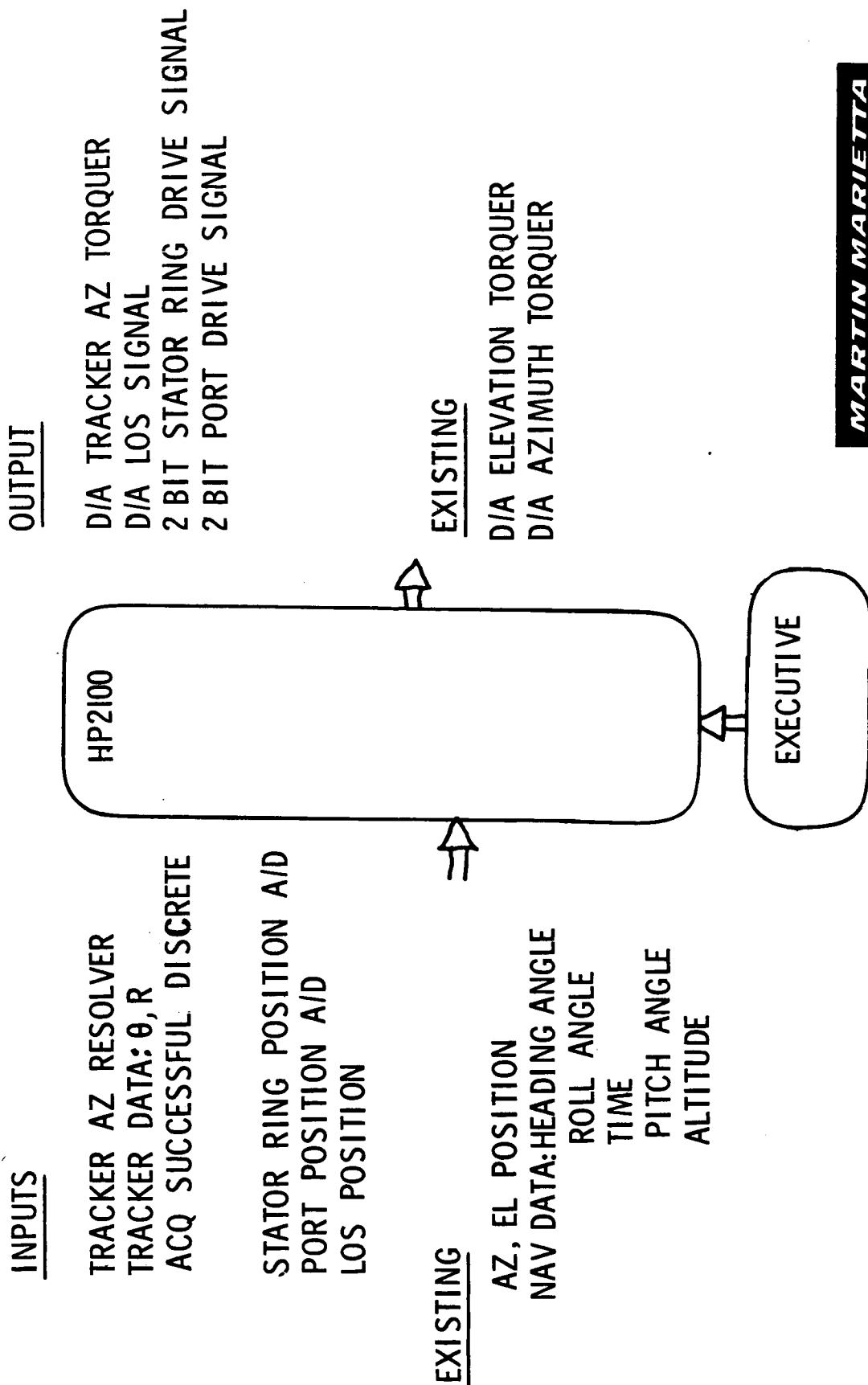
POINT	OPTICS	PRELIM.	→	REFINED
SOURCE	BORE SITE	82.2 S	REV LENSE	15 S
ERRORS	RETICLE	30 S		30 S
	DETECTOR RISE	7 S		7 S
	DE MOD	8 S	LOWER BW	16 S (25KC)
		29 S	REFINE	7 S
				LIGHT SOURCE

FINITE IMAGE  
SIZE  
ERROR

75     $\S$      $\xrightarrow{\quad}$     COMPUTER 14  $\S$   
PROCESS

$\Sigma 89 \S, \text{RSS } 41 \S$





MARTIN MARIETTA





## IMAGE PLANE SYSTEM

---

The design requirements for the Image Plane System are:

- 1) maintain a state-of-readiness until the Shuttle image enters any detector field-of-view,
- 2) be compatible with the 91.5 cm f/13.5 telescope image plane but autonomous in performance,
- 3) provide redundancy, and finally
- 4) provide adequate signal output to the data handling system under the worst-case encounter parameters with either the Shuttle or YF-12 calibration aircraft.

The streak camera approach to infrared imaging of the Space Shuttle imposes the following general requirements on the image plane detector array system:

- 1) The resolution elements (each detector) must be consistent with the target resolution requirements (e.g., 0.050 mm);
- 2) The image must be contiguous (no space) in the streak direction;
- 3) The detector must respond to grey body radiation in the temperature range from 600 to 1900 K;
- 4) The detector-filter combination must be in a wavelength region so that the first derivative  $\left(\frac{dW}{dT}\right)$  is large enough to yield the required Shuttle temperature resolution, i.e., 5% (2½% design goal).

The time constant of the detectors must be short enough not to be a major contributor to limiting the spatial resolution of a 40-microsec detector element crossing (i.e., the 40-microsec element crossing time will be at least five time constants of the detector).

The first task undertaken was to determine the best available IR sensor compatible with the experiment objectives.

The requirement of measuring the radiance from a rapidly moving target with portions ranging from 600 to 1900 K presents constraints limiting the choice of detectors. The short wavelength region was chosen for maximum temperature resolution; however, it could not be too short or it would be insensitive to the lower temperatures. An array of detectors was necessary because of the measurement's short duration.

The selection of detectors considered and some of their characteristics are as follows:

Detector	Sensitivity	Detector Temperature, K	Response	Wavelength Range, $\mu\text{m}$
Lead Sulphide	$D^* 5 \times 10^{11}$	193	2 msec	0.6 to 3
Silicon	$D^* 10^{12}$	300	1 $\mu\text{sec}$	0.3 to 1.1
Pyroelectric Vidicons	$D^* 10^9$	300	10 msec	Thermal only
Lead Selenide	$D^* 3 \times 10^{10}$	77	20 $\mu\text{sec}$	1 to 4.5
Indium Arsenide	$D^* 5 \times 10^{11}$	77	5 $\mu\text{sec}$	1 to 3
Mercury/Cadmium/Telluride	$D^* 2 \times 10^{10}$	77	0.5 $\mu\text{sec}$	8 to 15
Indium Antimonide	$D^* 3 \times 10^{11}$	77	0.5 $\mu\text{sec}$	1 to 5.5

The requirements include a spectral response from 1 to 3 micrometer, a  $D^*$  above  $1 \times 10^{11}$  and a response time of 1 microsec or faster.

Only indium antimonide meets all the requirements necessary for the detector and can be manufactured in an array format.

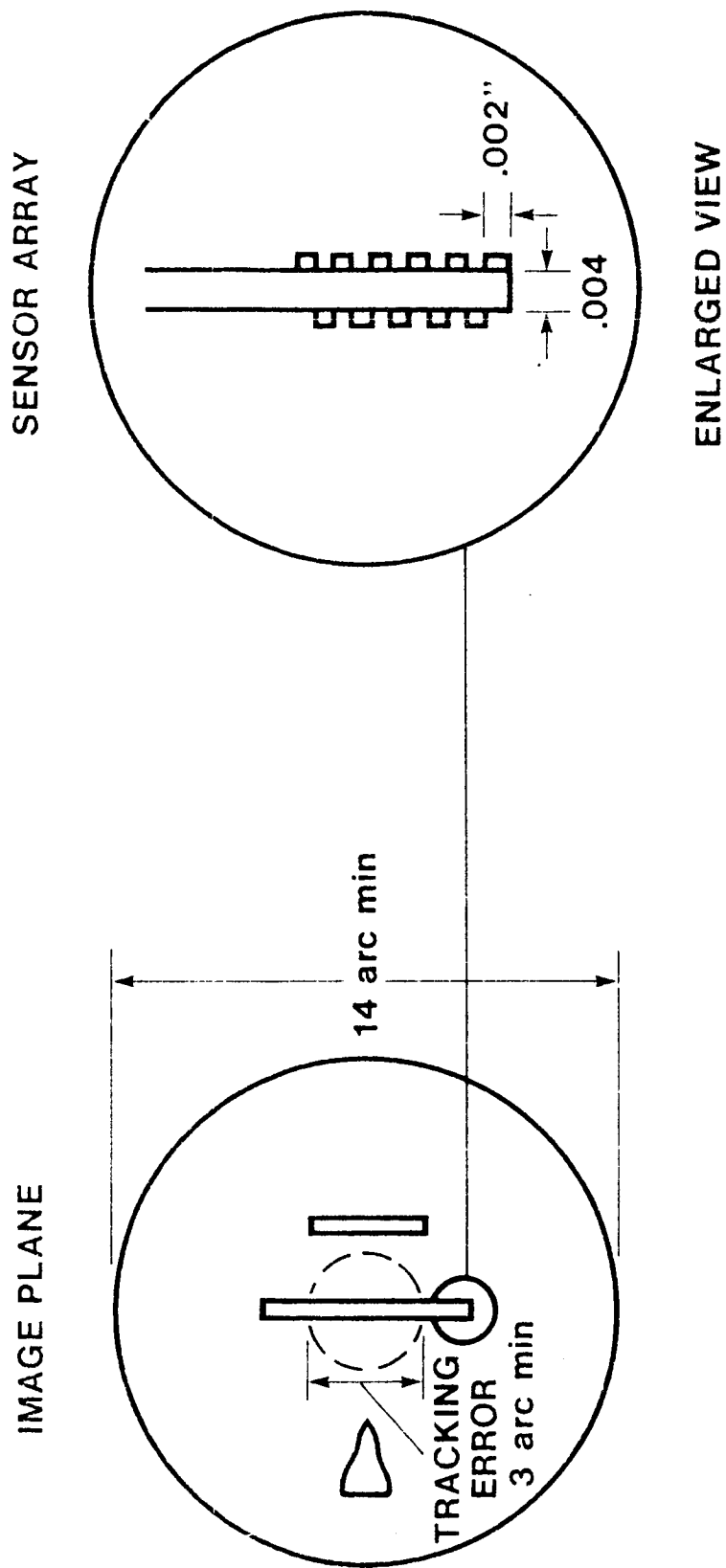
Detector Array - To reduce cost and complexity of the detector system, a major goal was to reduce the number of detectors. By adding up the tracking uncertainties and using the worst- (largest image) case trajectory, it was found necessary to have approximately 320 detector in a linear array. Taking a conservative approach, 40 detectors were added to each end bringing the total to 400. For the 2nd row, it was determined that 200 detectors would meet the requirement if the RSS of the error sources is used.

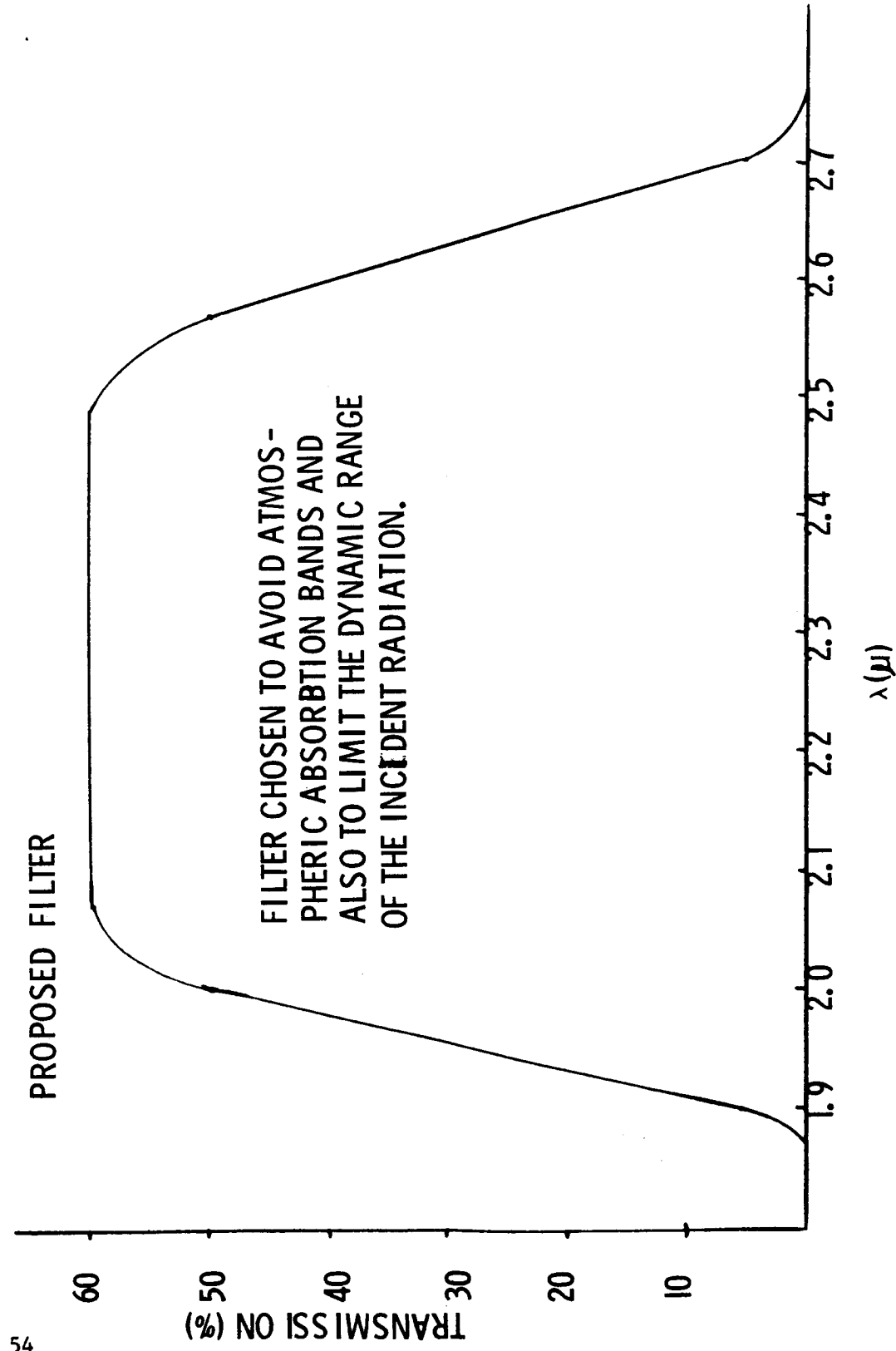
Detector Array and Filter - The detector arrays shown in Figure 37 consist of two linear InSb (PV) arrays in the image plane. One array contains 400 detectors, the other 200 detectors. The 200-element array is added for redundancy. As shown in the enlarged view, each detector element is 0.002 in. (0.050 mm) square with a crosstrack spacing of zero. Because of measurement conditions, namely that the Shuttle image will cover only a portion of either array, it is possible to reduce the number of leads leaving the focal plane by connecting two or more detectors together. A scheme for connecting three detectors together, thereby reducing the total number of leads to 200, is shown in Figure 41, Data Handling Schematic.

The filter shown in Figure 38 is designed to accomplish three tasks. It significantly reduces background irradiation and therefore the noise. It cuts off a major absorption band thus easing the data reduction problems. And finally, it reduces the irradiation (on the short wavelength side) from the higher target temperatures to reduce the dynamic range. This allows (as discussed later) a better quantization of the lower target temperatures using a 12-bit system.

FIG. 37

# PRIMARY TELESCOPE IMAGE PLANE





Dewar Assembly - The Dewar assembly shown in Figure 39 is an approach to housing the detector array and amplifier assemblies to the main telescope while keeping the seal integrity of the airplane-to-telescope interface.

The detector array is located at the focal plane of the main telescope. The Dewar is designed to cool the detector arrays and the bandpass optical filter. The detector leads will pass through the Dewar walls and then through hermetic seals to the amplifier boards located in the area around the Dewar. The amplifier board mounting system will allow easy access for troubleshooting and board changing.

Calibration of Detector Array - For an extended source, if the F-number is kept the same, then the following relationship exists (subscript A = telescope and subscript B = auxillary calibration system).

$$K_{A,A} D_{A,A}^2 \theta_A = K_{B,B} D_{B,B}^2 \theta_B$$

where

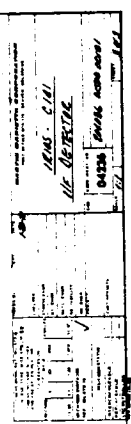
$K_{A,B}$  is the optical transmission of each system.

Using the system shown in Figure 40, we will illuminate approximately 137 detectors at each position setting. The procedure would be to mount the Dewar/detector array to the calibration system as shown and move the collector lens in a stop-and-take-data scheme. This procedure would be repeated for a number of source temperatures. It would use the entire amplification and data taking system. After the Dewar is mounted to the main telescope, there will be an electronic check capability of all amplifier gains.

Preliminary Prep/Flight Procedure - Following installation of the acquisition and imaging system in the C141 AIRO, a preflight alignment is necessary. This can be accomplished in the AIRO hanger using the calibration test equipment as follows:

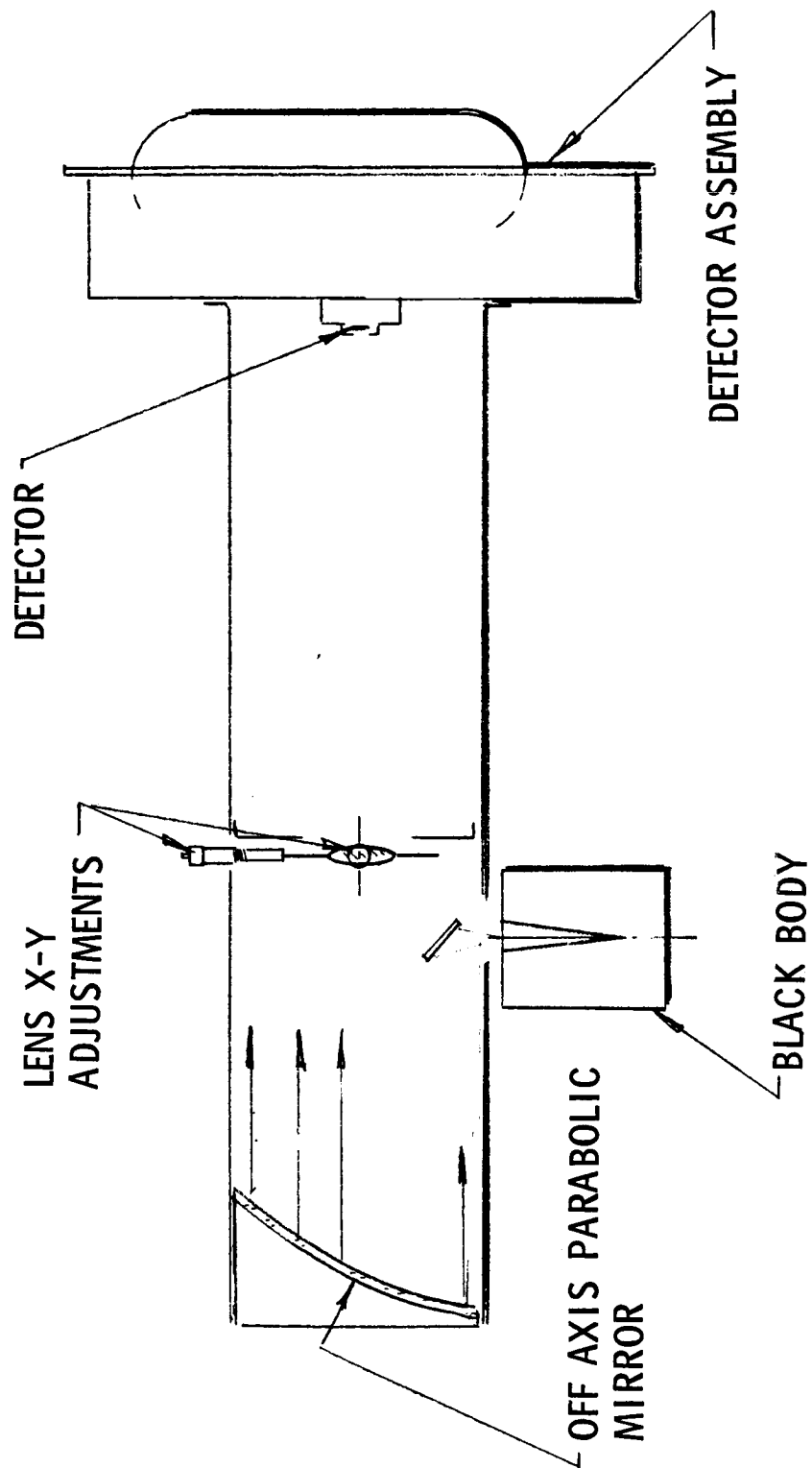
- 1) Mount the blackbody source/collimator in the hanger so it can be viewed by the telescope/acquisition system. (Maximum image size is 1 arcmin.)
- 2) Acquire and lock-on with the acquisition system.
- 3) Electrically bias the acquisition system error signals in evaluation and aximuth until the 1 arcmin image is centered on the 400 element array of the image plane system.

**FIG. 39**



# DETECTOR CALIBRATION

FIG. 40



Verification of alignment at altitude is desired and can be accomplished using a star. The procedure would be similar to that described above. During preflight preencounter alignment procedures, it is planned to obtain optical boresighting between the acquisition system and main telescope by viewing a star. The system sensitivity of the main telescope imaging system is approximately  $10^{-14}$  W/cm<sup>2</sup>. For the acquisition system, it is approximately  $2 \times 10^{-12}$  W/cm<sup>2</sup>. Several stars and planets have spectral irradiances in the range of 2 to  $5 \times 10^{-12}$  in the 1.0 to 2.5 micrometer region that will be usable as boresight targets. Another aspect of the system concerns focus and depth-of-focus. After boresighting on a star, the main telescope must be re-focused to properly view the Shuttle. A focus shift of at least 2 mm is required at the focal plane. This may be accomplished by movement of the secondary mirror. The depth-of-focus of the system is given by

$$\delta = F\beta(f/\#)$$

where

F = Focal Length

$\beta = 7 \times 10^{-6}$  rad

$f/\# = 13.5$

Depth-of-focus ( $\delta$ ) then is 1.12 mm or about half the required focus shift. This means the required accuracy for focusing the telescope is only  $2 \pm 1$  mm at the focal plane. Any adjustments required would compensate for thermal and aerodynamic distortion at altitude.

After alignment verification is made, the procedure for data taking is as follows:

- 1) Slew acquisition telescope to forward or aft acquisition angle depending on flight direction with respect to Shuttle.
- 2) Slew main telescope to nominal elevation angle for data pass.
- 3) Put acquisition system in stand-by/armed (reticle active but azimuth servo in hold).
- 4) Position C141 on ground track appropriate for particular data point.
- 5) Set time sequence with respect to anticipated Shuttle intercept.
- 6) At time of anticipated Shuttle acquisition (T = 25 sec), verify acquisition system switched from stand-by/armed to track.



- 7) By  $T = 10$  sec, verify acquisition system switched from track to lock.
- 8) Data system is automatically armed by acquisition lock.
- 9) Verify data system data acquired condition and dump to tape.



## DATA HANDLING SYSTEM

---

Design Requirements - In its simplest form, the Data Handling System is required to: (1) interface the 600 indium antimonide detectors that form the two linear detector arrays in the focal plane of the C-141 main telescope, and (2) provide to the C-141 ADAMS computer all the information produced during the passage of a single Shuttle image across the detector arrays. The design requirements come from two different sources. The first set of requirements derive from the selection of a detector type, the associated array geometry, and the image size dictated by the telescope optics and the Shuttle flight path relative to the C-141. These elements are covered in other parts of this report but they drive design requirements in the data system. The second source of design requirements is the final desired form of the information gathered by this system. Those requirements involve parameters like measurement range and resolution. Each of these two kinds of design requirements are treated as follows:

a. *Design Requirements Imposed by Interface Hardware Detectors*- Each diode detector is a current transducer that will convert IR flux to current. The baseline detector will produce approximately 0.8 nanoamp of current at a radiance representing 600 K and 1.17 microamp at 1700 K. At the maximum Shuttle temperature of 1900 K the output current is 2.75 microamp. For design purposes the first stage amplifiers must handle a current of 0 to 2.75 microamp  $\pm 10\%$ . The detector is a current generator in parallel with a  $10^8$  ohm resistance. Operation of the detector will be in the zero voltage mode so that neither detector source resistance or capacitance is a major concern in the design. Also, detector noise is not a major factor in the design. The feedback resistor in the first current amplifier is the major source of noise. A significant design requirement involves the constraining of the detector to amplifier wiring so that the cable capacitance is not modulated by aircraft vibration or sound. The detector-to-amplifier wiring is by far the most susceptible point in the signal processing path. Extreme case must be taken to eliminate stray electric or magnetic fields or currents in this wiring. An element of difficulty could be encountered here because all the detectors are single ended; providing their signals against a common ground reference. This means that none of the methods of common mode noise rejection can be used in this design. The noise sources must simply be kept from reaching this critical front-end circuitry.

The detector geometry and Shuttle image size (see Fig. 41) permits the 600 detectors to be segmented into 100 element arrays that are grouped into three sets of 200 each. The corresponding detectors in each set are then wired together to reduce the number of signal channels to 200. This is possible because the Shuttle image is small enough and the array is large enough because of tracking uncertainties, such that the Shuttle image can pass over only one detector of any parallel groups of three on any one pass. No problem is anticipated from paralleling detectors.

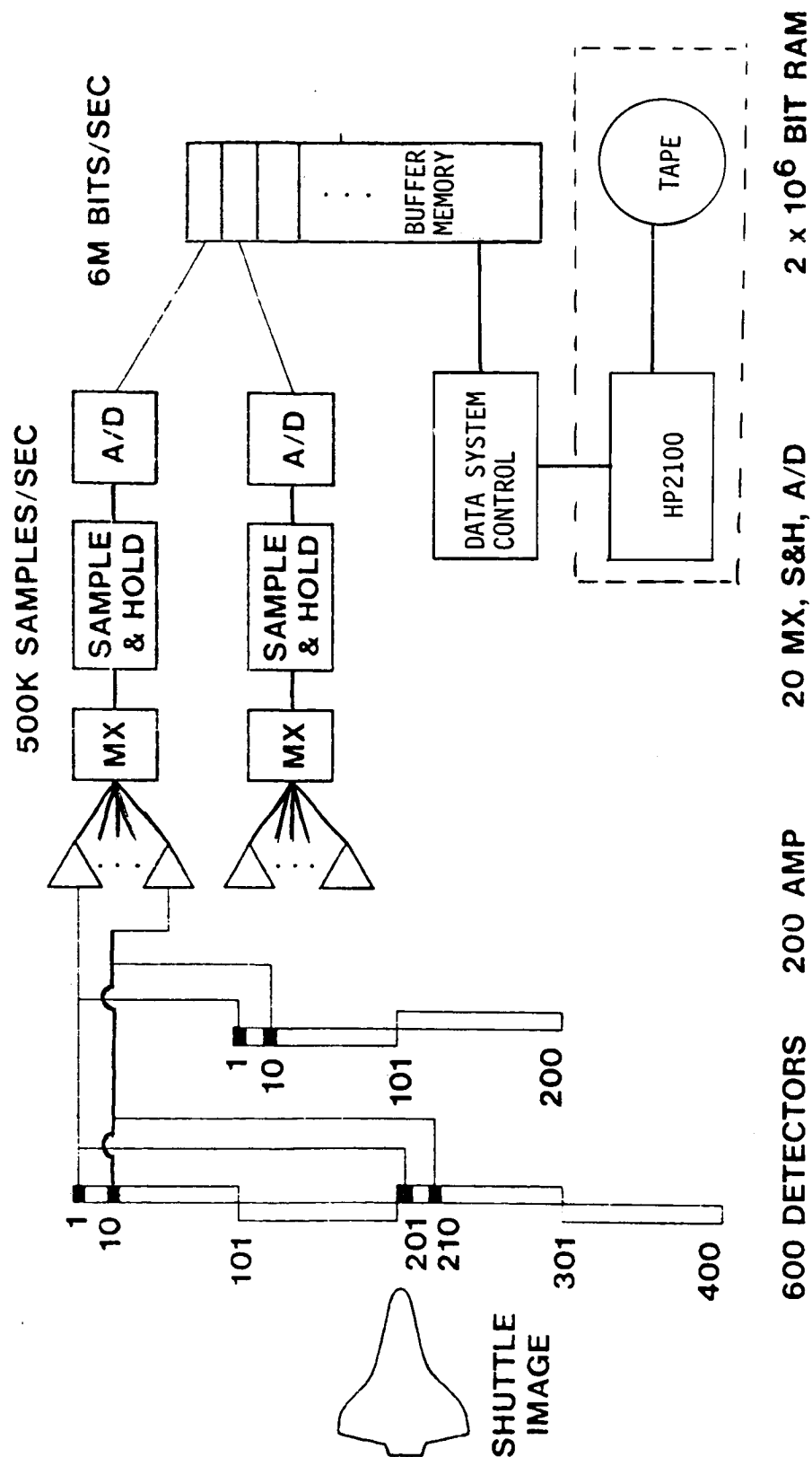
*ADAMS* - The ADAMS is a data processing system built around a pair of HP2100 computers. Their peripherals exist on the C-141 aircraft/ therefore, they will be used to checkout the detector data handling system and to write the detector output onto computer tape. The ADAMS will also issue operating mode commands to the data system, display calibration data, and perform the most important data present test. These design requirements will be expanded in the data system description section.

*b. Design Requirements Generated by the Project* - The temperature range is 600 to 1900 K. This range requirement is actually included in the current output specified from the detector but a measurement accuracy/resolution was not treated. A measurement accuracy of 2½% of full scale is desired; however, it is not a meaningful concept due to the extreme nonlinear nature of the measurement. Instead of setting a requirement, analysis of the measurement and the possible methods of implementing the measurement led to the conclusion to digitize the measurement and to digitize down into the noise level. The overall system signal-to-noise ratio will not be known until the system is built and installed on the aircraft. The lower noise limit is set by the thermal noise in the feedback resistor around the 1st stage amplifier. Analysis shows this to be in the order of at least one significant bit for 12-bit encoding. Therefore 12-bit encoding is specified as a design requirement.

The frequency response amplifier also has a somewhat arbitrary design requirement. The 3 dB down-point is to be at 50 kHz or greater. The sample rate for A/D conversion is not set by the frequency response number but by a requirement to keep the pixels square. An analysis of all Shuttle passes indicates pixel rate between 10,000 and 20,000 per sec with some margin. That is the design requirement for the measurement sample rate. Further study may indicate that a slew rate criteria will be more appropriate than a frequency response criteria but that is not clear at this time.

FIG. 4I

# DATA HANDLING SCHEMATIC

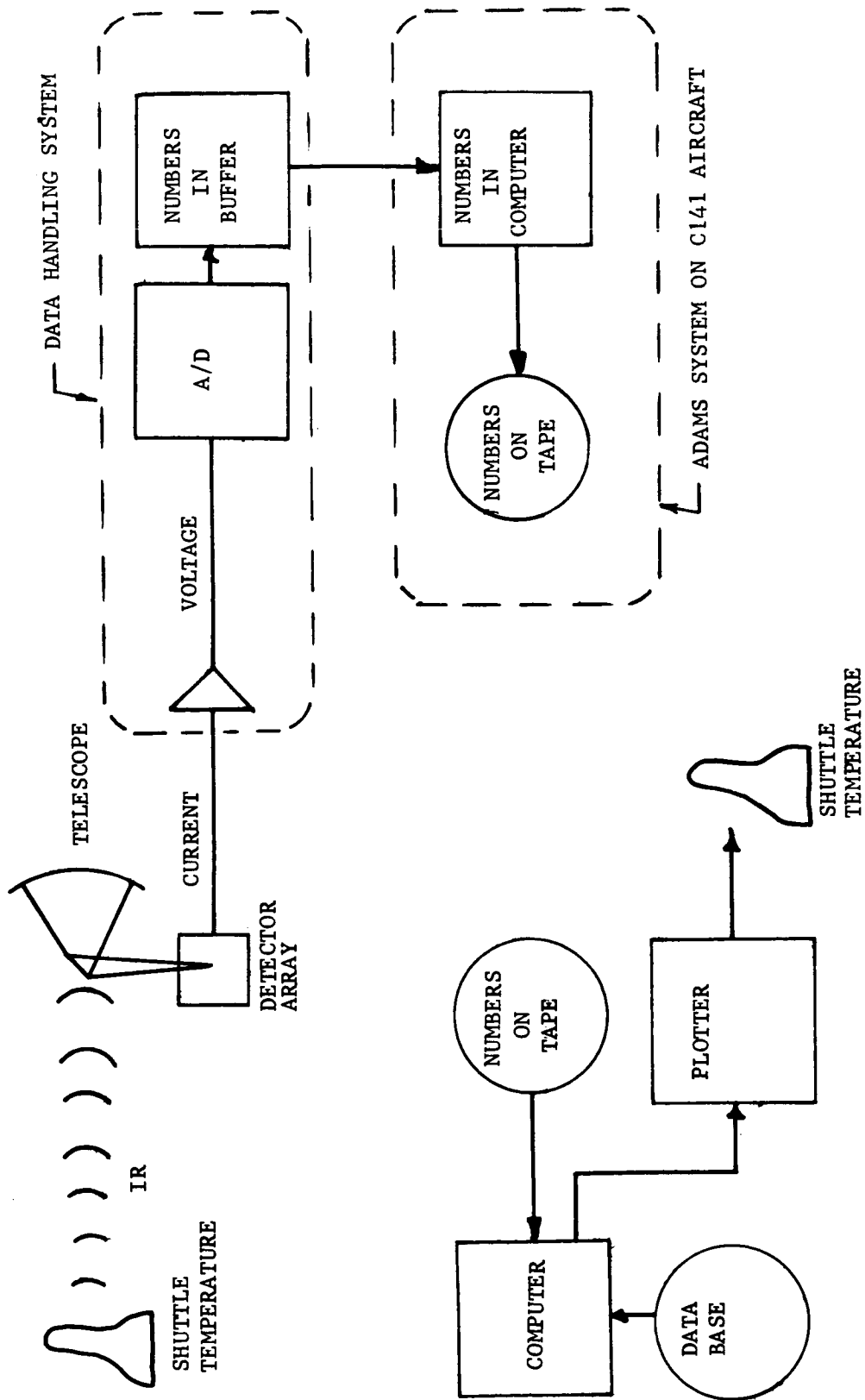


The total throughput data rate is simply the maximum sample rate (20,000) times the number of channels (200) times the word length (12) or 48 mbs. Note that this rate never really occurs in the system because the data are handled in many parallel channels, with each channel running at a much lower rate. The ability to change the system clock is another somewhat arbitrary design requirement that must be established. The design requirement is that the system clock must allow operation of the system within 5% of any A/D sampling rate desired between 10,000 and 20,000 samples/sec (sps) on a given channel. A data storage requirement can be arrived at based upon the highest pixel rate and the longest Shuttle pass. That is, 15901 sps for 13.82 msec or 527,404 bits. As a design requirement, a memory of at least twice this size is specified to allow for the storage of a block of data and its subsequent test by the ADAMS for Shuttle image content, during the period that the second block of data is being written.

Data Handling System Design - This section describes the baseline system design arrived at during the study but does not attempt to justify the system.

Overall Design Description - Figure 42 shows the overall flow of information from the Space Shuttle to the C-141 telescope through the detectors and into the data system. The data are accumulated in the data system buffer and then read into the ADAMS computer and written onto computer tape. The figure clearly shows the system interfaces; however, it must be remembered that the ADAMS is an intrinsic part of the functional system and what is referred to in this report as a data handling system is only a part of a system and will not function in a flight mode without the ADAMS.

Figure 41 is a more detailed data flow schematic and shows the paralleling of the 600 detectors into 200 analog measurement channels. Each measurement has a 1st stage amplifier and a 2nd stage amplifier. The outputs of the 200 2nd stage amplifiers are assigned by groups of 10 to 20 different but identical multiplexer, sample and hold, and A/D modules. These data modules will be purchased as complete operating systems. The Datel DAS250 system has been baselined for this module. The outputs of the 20 data system modules are read into the 1 megabit Static Ram Memory. The memory is accessed by the ADAMS system through the data system control unit. That access is either in the test-for-data mode where only selected channels are tested to see if data are present during the actual Shuttle pass or access is in a mode where the entire contents of memory are read into the ADAMS and placed on tape, or displayed.



Detailed Design - A detailed design was not performed in this phase but some material exists that will be useful in the detailed design phase.

*a. Measurement Amplification* - Specific amplifiers were not selected but a firm decision to use operational amplifiers was made. Some discussions of the amplifier channel follow.

The detector size and type has been established in other portions of this study. Based upon the detector characteristics and some typical FET input amplifier characteristics, the amplifier input signal is 0.8 nanoamp at 600 K and 3.0 microamp at 1900 K. With a  $10^6$  ohm feedback resistor in the first amplifier, its output voltage will be 0.8 mV to 3.0 V. The second stage of amplification will produce 2.6 mV to 10 V. By calculation, and with a safety factor of 3, the noise at the output of the second amplifier is 1 mV peak.

This sets the minimum size for the resolution element. If that element were twice the peak-to-peak noise, then it would be 4 mV or one part out of 2500. Ten-bit encoding is 1/1024, 11 is 1/2048, and 12 is 1/4096. It is apparent that encoding beyond 12 bits will not increase the information provided by the measurement. For instance, if a 0- to 10-V signal is digitized to 13 bits, the least significant bit will represent slightly more than 1 mV but it will change continuously due to the 2-mV peak-to-peak system noise, and therefore will provide no useful information. The following table shows the delta temperature represented by the noise voltage as a function of temperature. It is not a single number because of the extreme nonlinear nature of this measurement. See Figure 43.

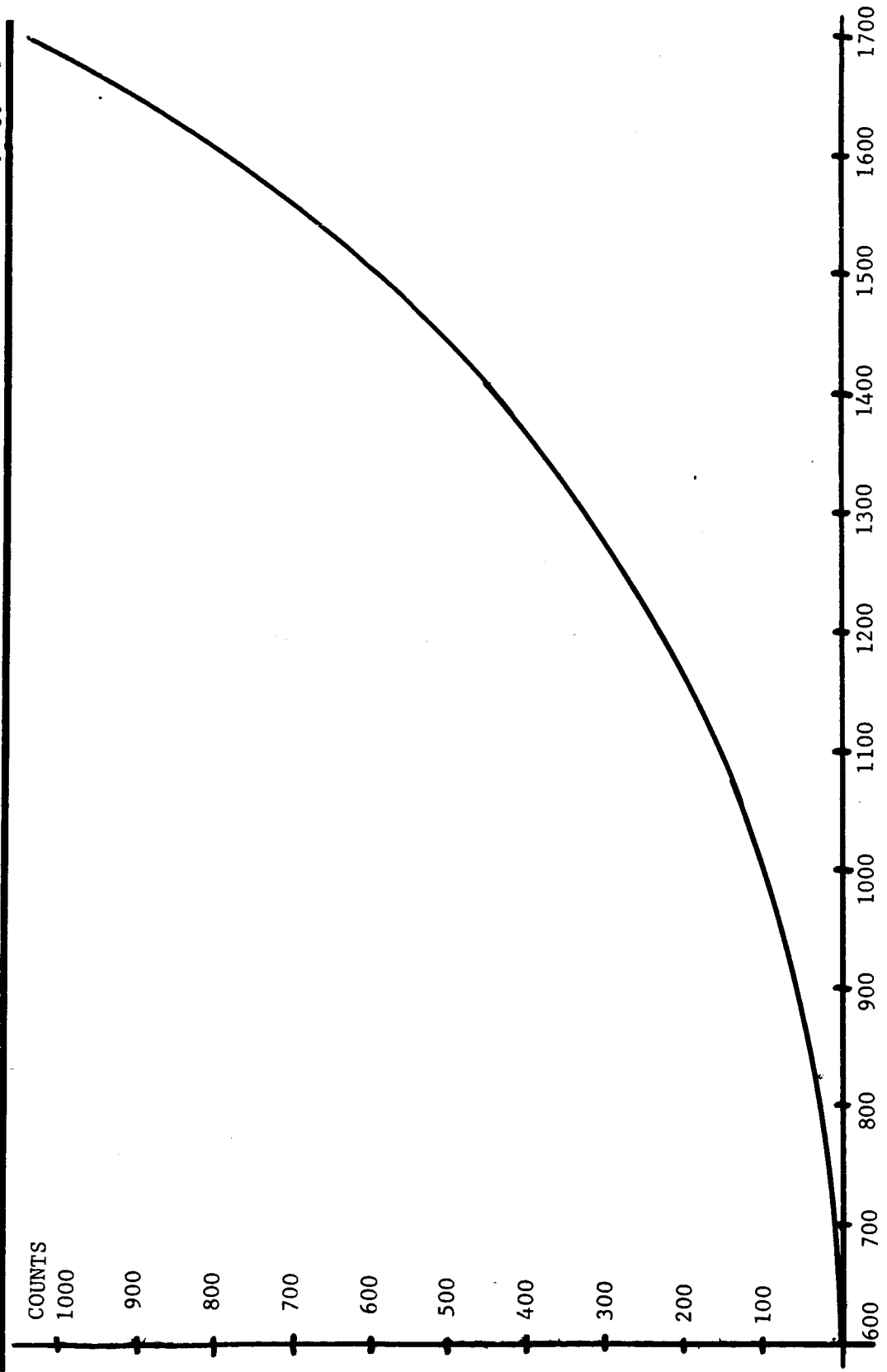
Temperature, K	NEAT, K
600	13
700	4
800	2
900	1

A second major consideration is the temperature resolution *desired*. Two numbers have been used, 5% of reading as a requirement and  $2\frac{1}{2}\%$  of reading as a goal. Because of the nonlinear measurement response, the measurement is most difficult to make at 600 K. At that temperature,  $30^\circ$  must be resolved to meet the requirement and  $15^\circ$  is desirable. A 10-bit conversion of the 600 to 1700 K measurement range yields only about 48 K resolution at 600 K. Either an increase in the digitizing level or a decrease in measurement range is necessary to meet the 5%, 30 K criterion. Encoding to 11 bits meets the 5% criterion and encoding to 12 bits meets the  $2\frac{1}{2}\%$ , 15-K criterion. It should be



FIG. 43

TEMPERATURE VERSUS COUNTS



TEMPERATURE K

MARTIN MARIETTA

remembered that 15 K resolution is approximately the same amplitude as the calculated system noise of 13 K. Again, the conclusion is that 12-bit encoding is desirable.

Some effort was expended trying to make the measurement more linear. This type of problem has been solved previously by using a transistor for the feedback resistor around the first measurement amplifier. Its effective resistance is an inverse function of the feedback current. This produced a logarithmic measurement response relative to radiation flux and a more nearly linear response relative to temperature. Unfortunately, discussions with the design people involved indicated that it would not be possible to increase the frequency response of that type of circuit to that required in this application. Another approach is to make two or more measurements out of each measurement and expand the scale of each; however, neither of the above approaches looks feasible for this task.

The basic conclusion reached is that two linear operational amplifiers are required for each measurement. The 1st stage amplifier should be a high quality, low noise, FET input amplifier operating as a transimpedance or current amplifier. The most serious concern when using this amplifier is the gain bandwidth product required and the desirability of a very flat gain curve over the information bandwidth. The second stage of amplification appears to be very straightforward and any number of amplifiers can do this job.

*b. Datel DA5250 Data Module* - This module will accept 16 single-ended measurements at a throughput rate of 250,000 sps with each sample converted to a 12-bit number. The following table summarizes its major characteristics.

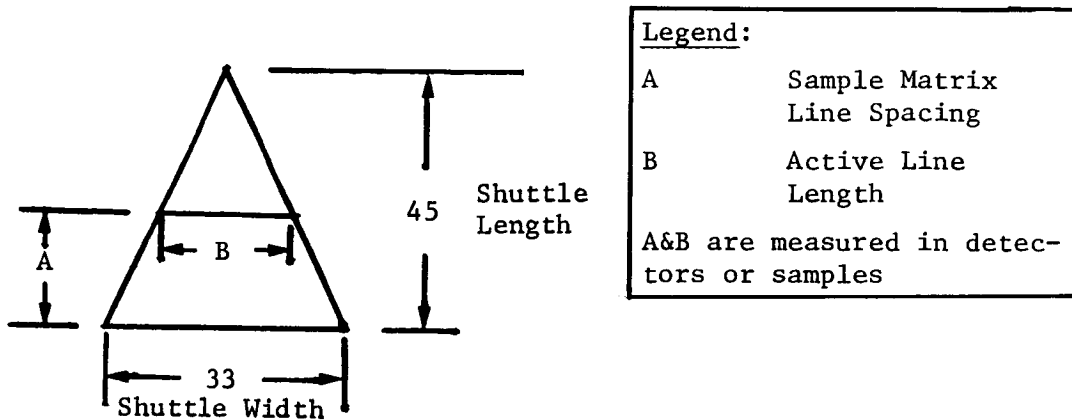
Number of Channels	16
Input Type	Single-Ended
Input Voltage Range	0 to +10 V
Input Impedance	100 M $\Omega$
Channel Addressing	4-bit code
Address Logic Compatibility	DTL/TTL
Resolution	12 bits
Nonlinearity Maximum	1/2 LSB
Maximum Error at Maximum Throughput	0.025%
Temperature Coefficient Maximum	40 ppm/°C
No Missing Codes	0 to 70°C
Throughput Rate Maximum	250,000 kHz
Acquisition Time	2 $\mu$ sec
Conversion Time	2 $\mu$ sec
Aperture Time	20 nsec
Output Coding	Binary and 2 Complement
Voltages Required	$\pm$ 15V, +5V
Package Size	12.7x11.4x3.8 cm
Operating Temperature Range	0 to 70°C

The use of this existing data system module greatly simplifies the design of the overall system and is very cost effective. The specifications listed for this module are remarkable and if maintained in the system design will be transparent in the end-to-end measurement transfer function.

c. *Static Memory* - A specific memory was not selected but the EM&M SEMS12 memory which is off-the-shelf could do this job. It is a 16K by 18-bit unit. At least four memories are required to support the total bit rate and storage requirement. More design must be done to thoroughly understand the best approach to implementing the memory. Each memory module is approximately 16.2x22.8x3.5cm and weighs 1.68 kg.

d. *Memory Save Criteria* - In addition to the two other interesting characteristics of this system, the high data rate and the relatively small amount of information generated, a third characteristic exists. That is, it is not exactly known when the information will be generated. If a very large storage medium such as magnetic tape was available, then the system would simply be turned on well ahead of time and run until it was verified that the Shuttle pass had occurred. With the selection of electronic memory for storage, because it reduces cost, it is necessary to develop a method of testing these data for the presence of Shuttle information so that the system can be stopped when it is verified that two complete Shuttle images are stored. Because of the computing power available in the ADAMS system, such a test is possible.

With digitized data, a redundancy removal or threshold detection is easy except that the system runs fast. A substantial amount of hardware would be required to process all these data in any manner. A possible way around this problem is to use two buffer memories and write them alternately. Then test a few selected channels and times and determine if Shuttle information is present. If it is, then that memory is saved and the next memory is saved and then the system is stopped. The minimum sampling array that is guaranteed to obtain at least one sample containing Shuttle data is derived below.



$$B = 33 - \frac{33}{45} A$$

Let  $N$  = number of detectors in the sampling rectangle

$$N = AB = A \left( 33 - \frac{33}{45} A \right)$$

$$\frac{dN}{dA} = 33 - \frac{33 \times 2}{45} A = 0$$

$$A = 22.5 = 22 \text{ samples}$$

$$B = 16.87 = 16 \text{ detectors}$$

The result is then for the smallest Shuttle image, every 22nd sample of every 16th detector must be tested. This is the minimum test that will guarantee the detection of Shuttle data if there are no bad detectors or noise affects anywhere in the system. Using the new baseline of 200 detectors in the first array, the test rate for the data from one array is:

$$\text{Test Rate} = \left( \frac{200}{16} + 1 \right) \frac{15558}{22} = 13.5 (707.18) = 9547 \text{ tests/sec}$$

A test must occur every 108.8 microsec on an average. The ADAMS HP2100A can do a memory cycle in 980 nanosec and execute most of its instructions in 1.96 microsec. A potential program might involve reading the ambient outputs of the detectors selected for data test, adding the threshold criteria to the ambients and storing the table. When the data-take starts, data to be tested must be read into the arithmetic unit, the criteria number must be read from the criteria table, a subtraction must be performed, and a test of equal to or greater than zero performed. If the result is less than zero, the computer will continue to test, if greater than zero it will generate a memory save signal. The time involved for a single test appears to be equal to two memory cycles and two instruction times or 5.88 microsec. In 108.8 microsec, eighteen tests should be performed where one is the minimum that will detect data. The conclusion reached is that it is feasible to use the HP2100A in the ADAMS to perform the data test.

*e. Electronic Calibration* - A good set of ambient measurement outputs are obtained in this system by its nature. It would appear worthwhile to check the ambients against a criteria stored in the computer and provide violations to the system engineer. In addition, it appears desirable to perform a gain check through each channel by injecting a calibration current into the first amplifier. Again the results of that check should be available. These calibration data would be stored on tape and used during data reduction. One calibration step would probably be adequate, but several would be desirable.

*f. Checkout* - Because of the relatively few times this system will be used, it would seem proper to do a fair amount of manual checkout using conventional test equipment. This is particularly true of steady-state functions like power supply voltage. As detailed design proceeds, careful attention should be paid to bringing out test points on each box that will allow the detection of a malfunctioning box.

A second level of checkout involves the use of a computer. The computer tests would verify that all storage locations are properly addressed and that all bits in each location are working. Every bit of each A/D could be tested if an additional calibration source is used at the A/D inputs.

The calibration sequence itself provides a good overall system checkout.

*g. Controls and Displays* - Power system controls and displays are probably all that are required as part of the data system. All other controls and displays should be adequately provided by the ADAMS and test equipment.



## IMAGING SYSTEM PERFORMANCE

---

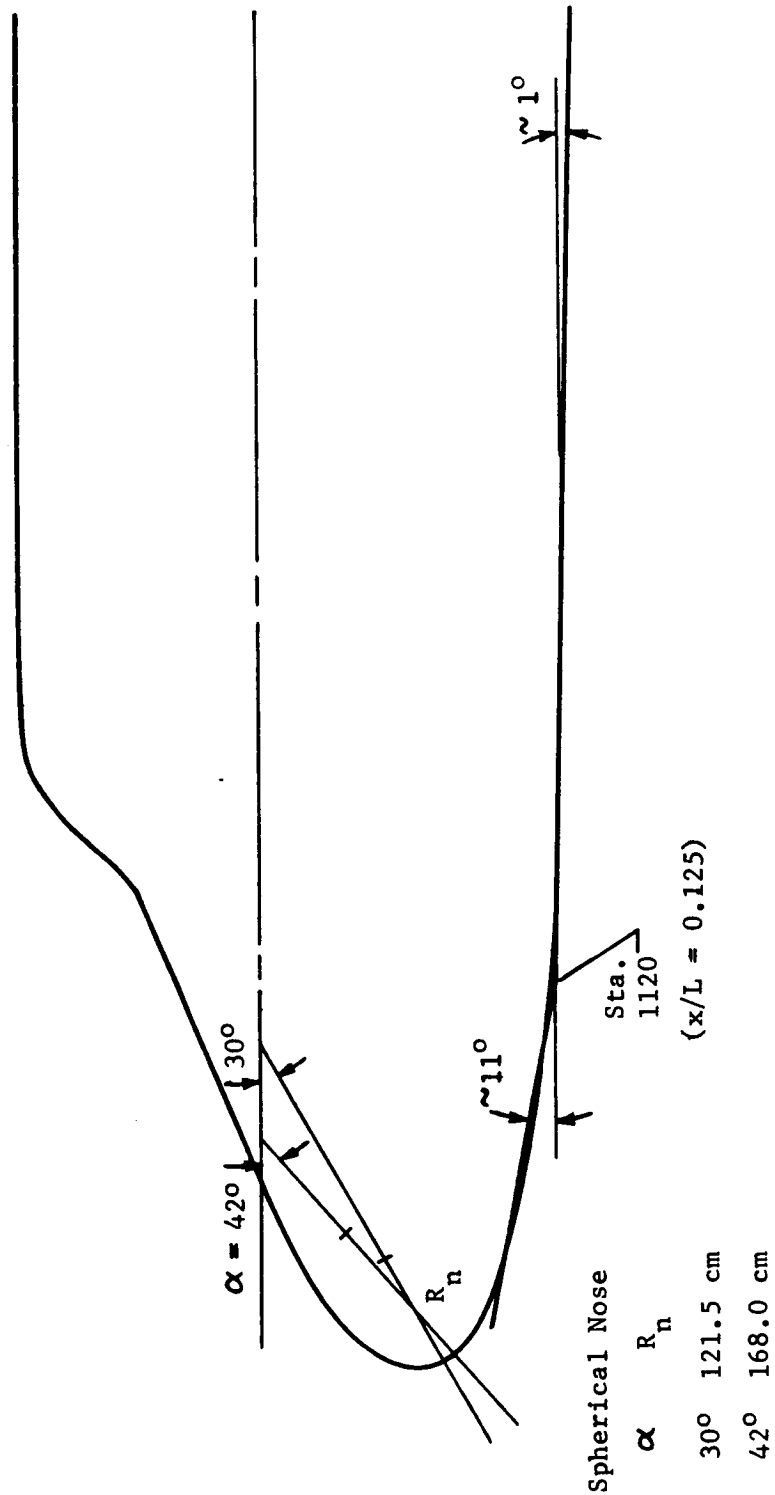
The imaging system performance has been analyzed from the radiation source to the data storage point and includes the following effects; Shuttle flow field, atmospheric, aircraft flow field, telescope optics, image stabilization, detector, and background.

The Shuttle flow field was synthesized by computer modeling (see Fig. 44). The Orbiter shock layer model for two points in the reentry trajectory is shown in Figure 45. Results from this analysis are given in Figures 46 and 47. Figure 46 shows pressure, temperature, and standoff distance of the shock layer as a function of station along the Shuttle undersurface. Figure 47 illustrates the radiative equilibrium temperature also as a function of station.

Figures 48 and 49 depict the variation in heat flux at the Shuttle wall with heat flux at the shock layer and the contribution of energy (line structure) due to self-radiation of the shock layer ( $Q_{IS}$ ). In all cases the energy density emerging from the shock layer is almost identical with that on the Shuttle wall ( $Q_{CW} = Q_{CS}$ ) indicating no effects due to the shock layer in the region of 0.5 to 6.2 micrometers. Variations of pressure by a factor of 1.5, temperature by a factor of 1.25, and density by a factor of 3 also indicated no difference between the Shuttle-radiated energy and that at the shock layer. Spatial resolution effects were also assessed by evaluating the modulation transfer function of the interviewing bow shock. Figure 50 indicates no modulation loss down to a spatial frequency corresponding to one arcsec.

The atmospheric effects include transmission as a function of wavelength (Ref. 10) and spatial resolution losses from upper atmospheric turbulence. Figure 51 depicts the atmospheric transmittance as a function of wavelength from an aircraft altitude of 12.5 km looking upward  $35^\circ$  from the zenith. No appreciable losses occur in the wavelength band from 1.5 to 2.5 micrometers that has been chosen as optimum for Shuttle radiative energy transfer.

The modulation transfer function of the upper atmosphere is shown in Figure 52. It has been described by Hufnagel and Stanley (Ref. 9) and by Farhat and Decon (Ref. 11). The atmospheric structure constant (Ref. 12) has been evaluated numerically between 12.5 and 70 km for one case and 12.5 and 40 km for case two. The associated zenith angles for Case 1 corresponds to conditions found early in the Shuttle reentry profile and Case 2 to the later, lower altitude conditions. The atmospheric effects have a significant effect on the system performance. Increasing the aircraft



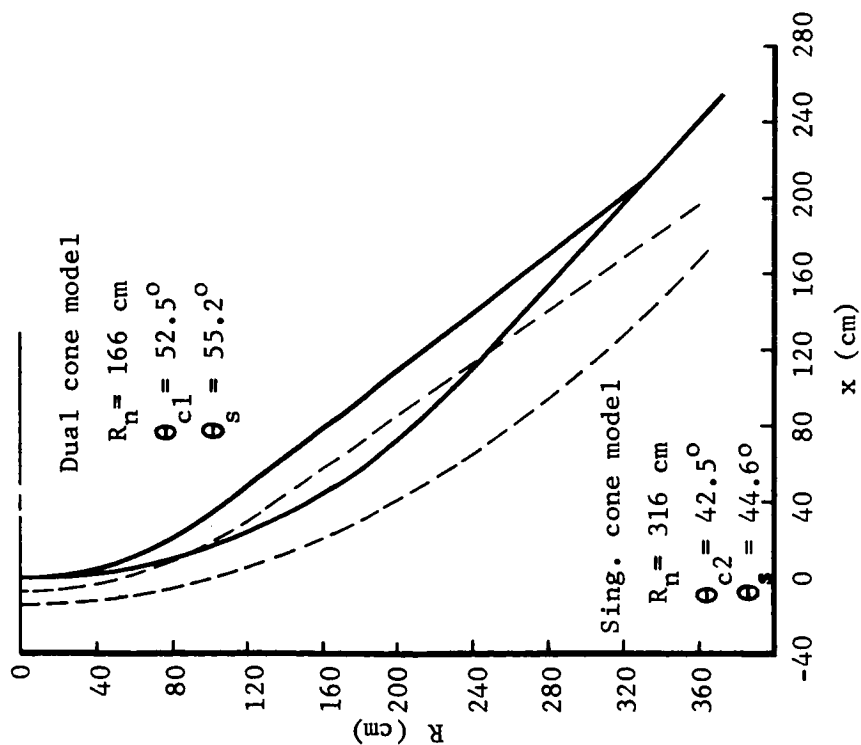


# ORBITER SHOCK LAYER MODELS

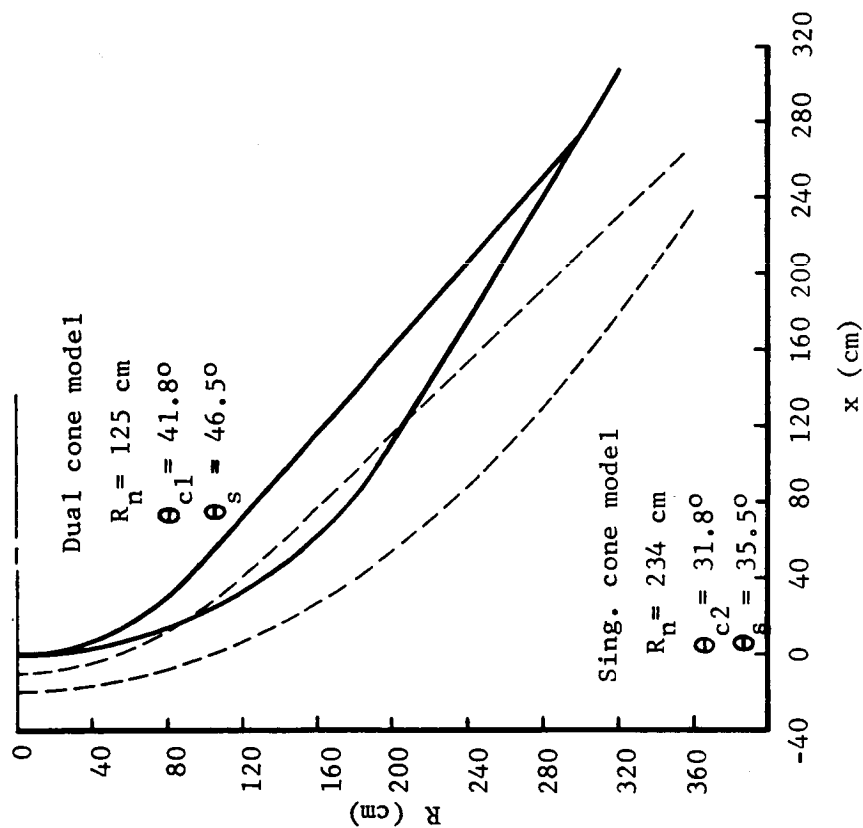
FIG. 45

Orbiter trajectory 14414.1

Traj. time 450 s



Traj. time 1200 s



MARTIN MARIETTA

# TRAJECTORY CONDITIONS & SHOCK LAYER PROPERTIES

FIG. 46

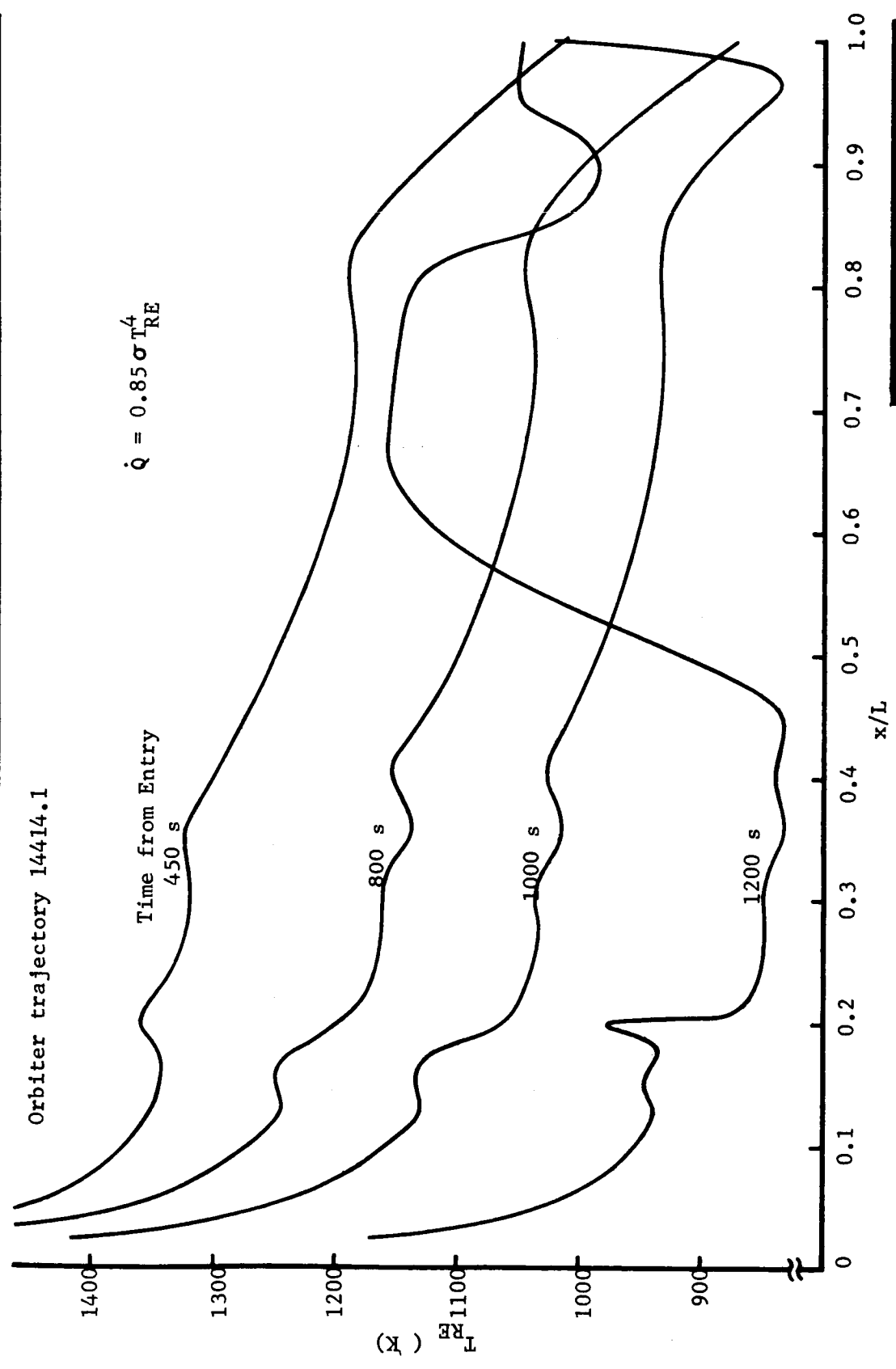
Orbiter trajectory 14414.1

76

Trajectory Parameters	Nose Cap	Sta. 1120 $x/L = 0.125$	Sta. 1200 $x/L = 0.200$	Sta. 1400 $x/L = 0.400$	Sta. 1600 $x/L = 0.600$	Sta. 1800 $x/L = 0.800$	Sta. 1996 $x/L = 1.000$
$t = 450$ s	0.0247	0.0165	0.0120	0.0120	0.0120	0.0120	0.0120
$Z = 74.5$ km							
$V = 7.5$ km/s	5969	5377	4951	4951	4951	4951	4951
$\alpha = 41.5^\circ$	7.25	28	37	61	85	109	133
$t = 800$ s	0.0547	0.0283	0.0183	0.0183	0.0183	0.0183	0.0183
$Z = 63.8$ km							
$V = 5.7$ km/s	5465	4064	3004	3004	3004	3004	3004
$\alpha = 32.8^\circ$	7.50	34	43	65	88	111	134
$t = 1200$ s	0.0960	0.0485	0.0306	0.0306	0.0306	0.0306	0.0306
$Z = 49.4$ km							
$V = 3.1$ km/s	3057	2313	1682	1682	1682	1682	1682
$\alpha = 30.8^\circ$	10.97	46	62	104	145	187	229

MARTIN MARIETTA

ORBITER WINDWARD & RADIATIVE EQUIL. TEMPERATURES FIG. 47



MARTIN MARIETTA

# ORBITER WINDWARD $\odot$ RADIATIVE HEAT FLUX

FIG. 48

Orbiter trajectory 14414.1

78

Traj. Time(s)	Nose Cap	Sta. 1120 $x/L = 0.125$	Sta. 1200 $x/L = 0.200$	Sta. 1400 $x/L = 0.400$	Sta. 1600 $x/L = 0.600$	Sta. 1800 $x/L = 0.800$	Sta. 1996 $x/L = 1.000$
450	$\dot{Q}_{Cw} (w/cm^2)$	41.0	16.2	13.4	10.0	9.32	4.83
	$\dot{Q}_{Cs} (w/cm^2)$	41.0	16.2	13.4	10.0	9.33	4.84
	$\dot{Q}_{Ls} (w/cm^2)$	$3.2 \times 10^{-5}$	$1.0 \times 10^{-7}$	$1.7 \times 10^{-7}$	$2.4 \times 10^{-7}$	$3.1 \times 10^{-7}$	$3.7 \times 10^{-7}$
800	$\dot{Q}_{Cw} (w/cm^2)$	36.3	9.32	8.23	5.91	5.52	2.70
	$\dot{Q}_{Cs} (w/cm^2)$	36.3	9.32	8.23	5.91	5.52	2.70
	$\dot{Q}_{Ls} (w/cm^2)$	$7.3 \times 10^{-6}$	$9.2 \times 10^{-15}$	$1.4 \times 10^{-14}$	$1.9 \times 10^{-14}$	$2.4 \times 10^{-14}$	$2.9 \times 10^{-14}$
1200	$\dot{Q}_{Cw} (w/cm^2)$	11.9	4.27	2.33	7.11	7.73	5.58
	$\dot{Q}_{Cs} (w/cm^2)$	11.9	4.27	2.33	7.11	7.73	5.58
	$\dot{Q}_{Ls} (w/cm^2)$	$1.0 \times 10^{-13}$	$\sim 10^{-26}$	$\sim 10^{-26}$	$\sim 10^{-25}$	$\sim 10^{-25}$	$\sim 10^{-25}$

Constant property shock layer using post shock conditions.

Frequency range 2.5 ev to 0.2 ev ( $0.5 \mu m$  to  $6.2 \mu m$ ).

$\dot{Q}_{Cw}$  = Heat flux at the shuttle wall. (Continuum)

$\dot{Q}_{Cs}$  = Heat flux at the shock layer. (Continuum)

$\dot{Q}_{Ls}$  = Heat flux at the shock layer. (Line Structure)

MARTIN MARIETTA

# EFFECT OF SHOCK LAYER PROPERTIES ON $\delta$ RADIATIVE HEAT FLUX FIG. 49

Orbiter trajectory 14414.1  
Trajectory time 450 s after entry.

Variation		Nose Cap	Sta. 1200 $x/L = 0.200$	Sta. 1600 $x/L = 0.600$	Sta. 1996 $x/L = 1.000$
$P = 1.5P_s$	$\dot{Q}_{Cw} (w/cm^2)$	41.0	16.2	10.0	4.83
	$\dot{Q}_{Cs} (w/cm^2)$	41.0	16.2	10.0	4.84
	$\dot{Q}_{Ls} (w/cm^2)$	$6.1 \times 10^{-5}$	$2.0 \times 10^{-7}$	$4.7 \times 10^{-7}$	$7.4 \times 10^{-7}$
$T = 1.25T_s$	$\dot{Q}_{Cw} (w/cm^2)$	41.0	16.2	10.0	4.84
	$\dot{Q}_{Cs} (w/cm^2)$	41.0	16.2	10.0	4.86
	$\dot{Q}_{Ls} (w/cm^2)$	$2.5 \times 10^{-2}$	$1.7 \times 10^{-4}$	$3.9 \times 10^{-4}$	$6.2 \times 10^{-4}$
$\delta = 3.0\delta_s$	$\dot{Q}_{Cw} (w/cm^2)$	41.0	16.2	10.0	4.84
	$\dot{Q}_{Cs} (w/cm^2)$	41.0	16.2	10.0	4.85
	$\dot{Q}_{Ls} (w/cm^2)$	$9.7 \times 10^{-5}$	$3.1 \times 10^{-7}$	$7.1 \times 10^{-7}$	$1.1 \times 10^{-6}$

MARTIN MARIETTA

$$T = e^{-\frac{4\pi S^2}{\lambda^2}} + \frac{f^2}{K^2 + f^2}$$

where

$$S = \frac{3 \times 10^{-6} \delta \rho M^2}{1 + .1 M^2}$$

- T = Modulation
- K =  $\delta/10\lambda R$
- f = Spatial Frequency
- M = Mach no.
- $\delta$  = Shock Wave Standoff or Boundary Layer Thickness
- $\rho$  = Pressure Ratio ( $6.8 \times 10^{-5}$  from Sea Level to 70 KM)
- R = Focal Length

See Reference (8)

Mach No. = 4  
Pressure Ratio @  $\frac{70KM}{12KM} = 1.8 \times 10^{-5}$   
Boundary Layer  $\delta = 100$  cm  
Wavelength  $\lambda = 2 \times 10^{-4}$  cm  
Focal Length R = 1236.2 cm

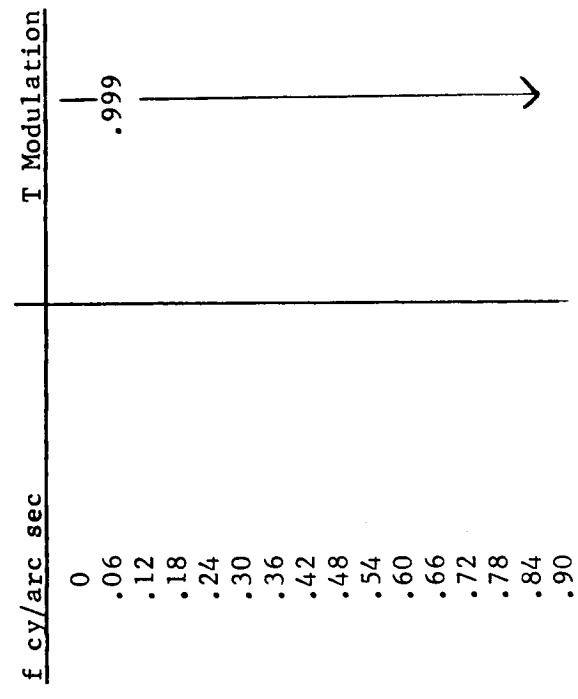
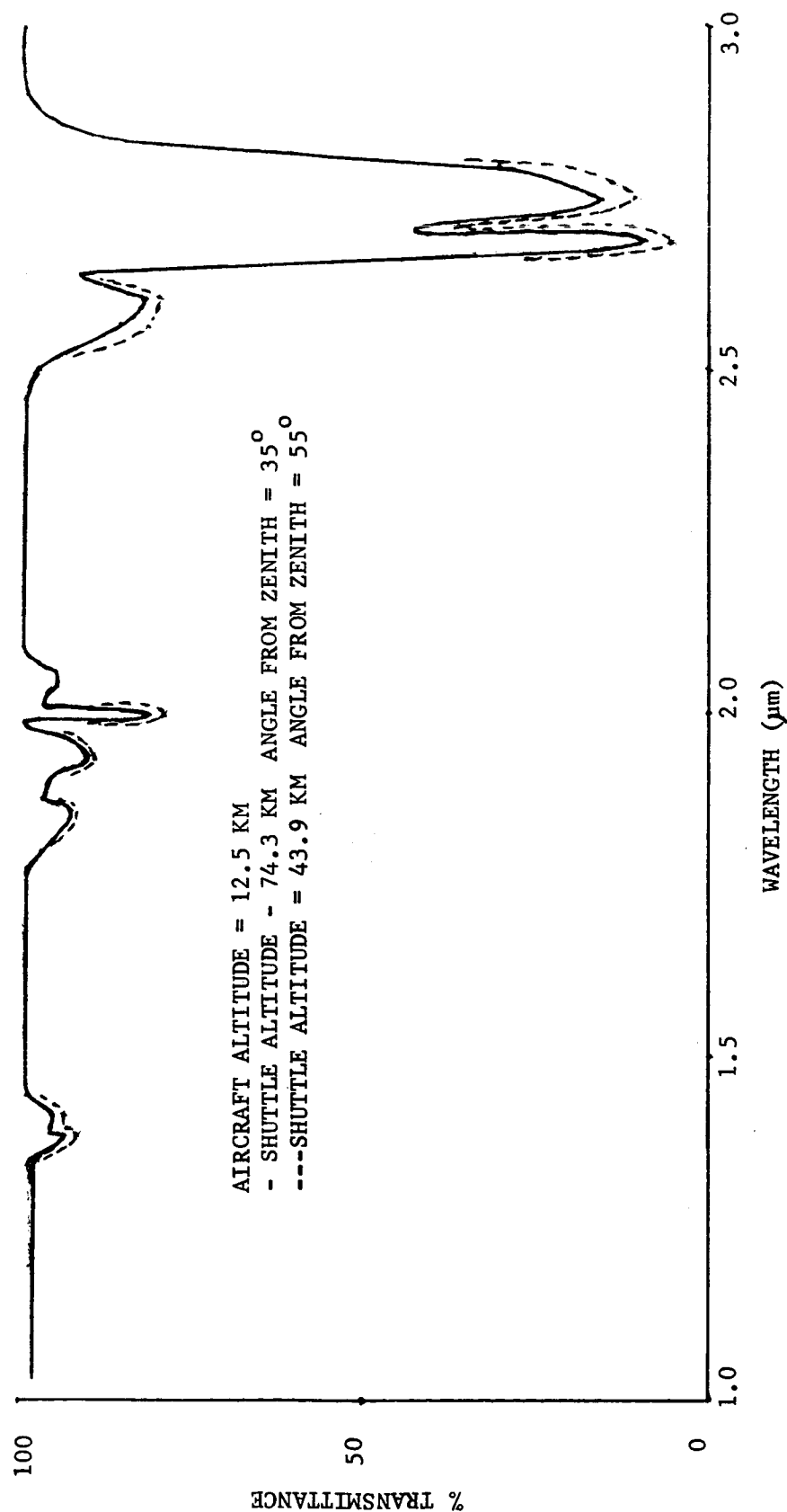


FIG. 51

ATMOSPHERIC TRANSMITTANCE (C141)



$$T = e^{-\frac{1}{2}D^2} \quad D = 2.91 \frac{4\pi}{\lambda^2} (f\lambda R)^{5/3} \text{ SEC } \alpha \int_{\text{cn}}^2$$

$$\Sigma C_n^2 = 3.96 \times 10^{-12} \quad \Sigma C_n = 3.98 \times 10^{-12} \quad R = 1236.2 \cdot 4^m$$

$$\alpha = 55^\circ \quad \alpha = 35^\circ \quad \lambda = 2 \times 10^{-4} \text{ cm}$$

$f/\text{CY/MM}$		$f/\text{CY/MM}$		$f/\text{CY/MM}$	
		$\text{arc/sec}$		$\text{arc/sec}$	
		$\alpha = 35^\circ$		$\alpha = 55^\circ$	
0	0	1.0	1.0	1.0	1.0
1	.06	.969	.956	.956	.956
2	.12	.904	.867	.867	.867
3	.18	.821	.756	.756	.756
4	.24	.728	.637	.637	.637
5	.30	.631	.520	.520	.520
6	.36	.536	.412	.412	.412
7	.42	.446	.318	.318	.318
8	.48	.365	.239	.239	.239
9	.54	.293	.175	.175	.175
10	.6	.232	.125	.125	.125
11	.66	.180	.087	.087	.087
12	.72	.138	.060	.060	.060
13	.78	.104	.040	.040	.040
14	.84	.077	.026	.026	.026
15	.90	.056	.017	.017	.017

$f$  = Spatial Frequency  
 $T$  = Modulation  
 $\lambda$  = Wavelength  
 $R$  = Focal Length  
 $\alpha$  = Angle from Zenith  
 $C_n$  = Atmospheric Structure Constant  
as a Function of Altitude



altitude from 12.5 to 14 km raises the MTF about 2%. Fortunately as the zenith angle increases, the range decreases such that the overall transfer function improves at lower altitudes.

The aircraft flow field or boundary layer is similar in analyses to that done for the Shuttle. Figure 53 again shows little effect.

The telescope on-board the NASA C141 is the 91.5-cm aperture f/13.5 Cassegrain system. The optical parameters for this telescope were obtained from the *C141 AIRO Users Handbook* and input to the Polypagos Optical Analysis Program (Ref. 13). The resulting MTF is shown in Figure 54. An energy-detected option in the computer program indicated 77.7% of the energy in the point spread function would be detected by a 50 x 50 micrometer detector. A graphical representation of the point spread function of the telescope is shown in Figure 55 and the MFT in Figure 56. The transmission efficiency of the optics at 2 micrometers is approximately 85% with three reflections.

Light falling on the detectors at the Cassegrain focal plane as a function of time is subject to the telescope stabilization jitter. The loss of contrast due to image motion has been discussed by Rosznau (Ref. 14). Figure 57 shows no effect due to the short exposure time per pixel (40  $\mu$ sec). For the C141 the telescope jitter is a maximum of 2 arcsec at an 8-Hz bandwidth. This corresponds to an image motion at the focal plane over that period of  $6 \times 10^{-7}$  mm.

The detector MTF, due to its physical size, is given by Seyrafi (Ref. 15) as a straight line function for square apertures and is shown in Figure 58.

The required electrical bandwidth for the front-end electronics is given by:

$$\text{FREQ (Hz)} = (A) (f)$$

where A is the maximum angular image rate and f is spatial frequency. To minimize the effect of the 3 dB rolloff, the frequency response was pushed out three time constants to provide 95% accuracy. The resulting bandwidth, as a function of spatial frequency, is shown in Figure 59 with 95% accuracy. The MTF of the electrical bandwidth has a negligible effect.

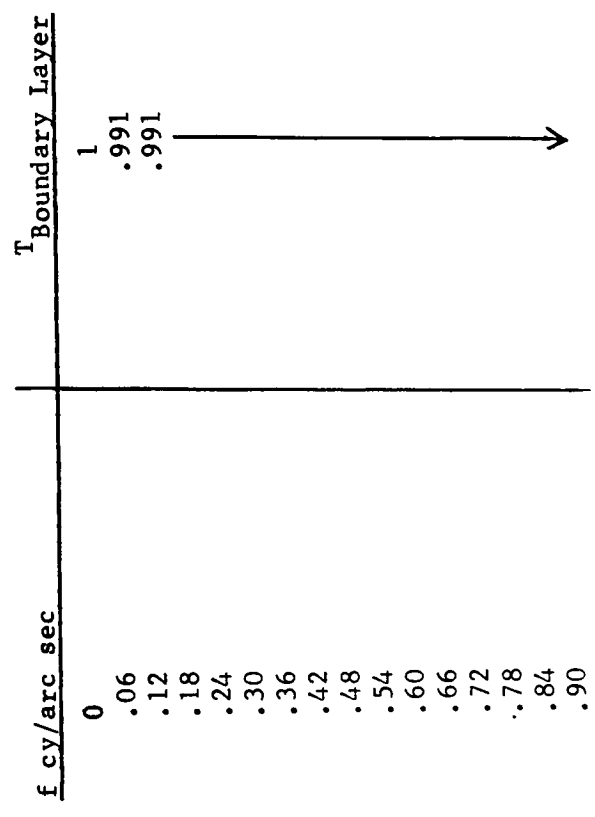
The calculated background irradiance at the 91.5-cm telescope entrance aperture and the acquisition telescope aperture at an altitude of 12 to 14 km is shown in Figure 60. The irradiance from the target for the worst-case (600 K) is still several orders of magnitude above any background source. The acquisition system does see scattered sunlight as a high signal; however, due to its uniformity compared to the Shuttle image, the background is

$$T = e^{-\frac{4\pi^2 S^2}{\lambda^2} + \frac{f^2}{K^2 + f^2}}$$
$$S = \frac{3 \times 10^{-6} \delta \rho M^2}{1 + .1 M^2}$$

$$K = \delta / 10 \lambda R$$

BOUNDARY LAYER

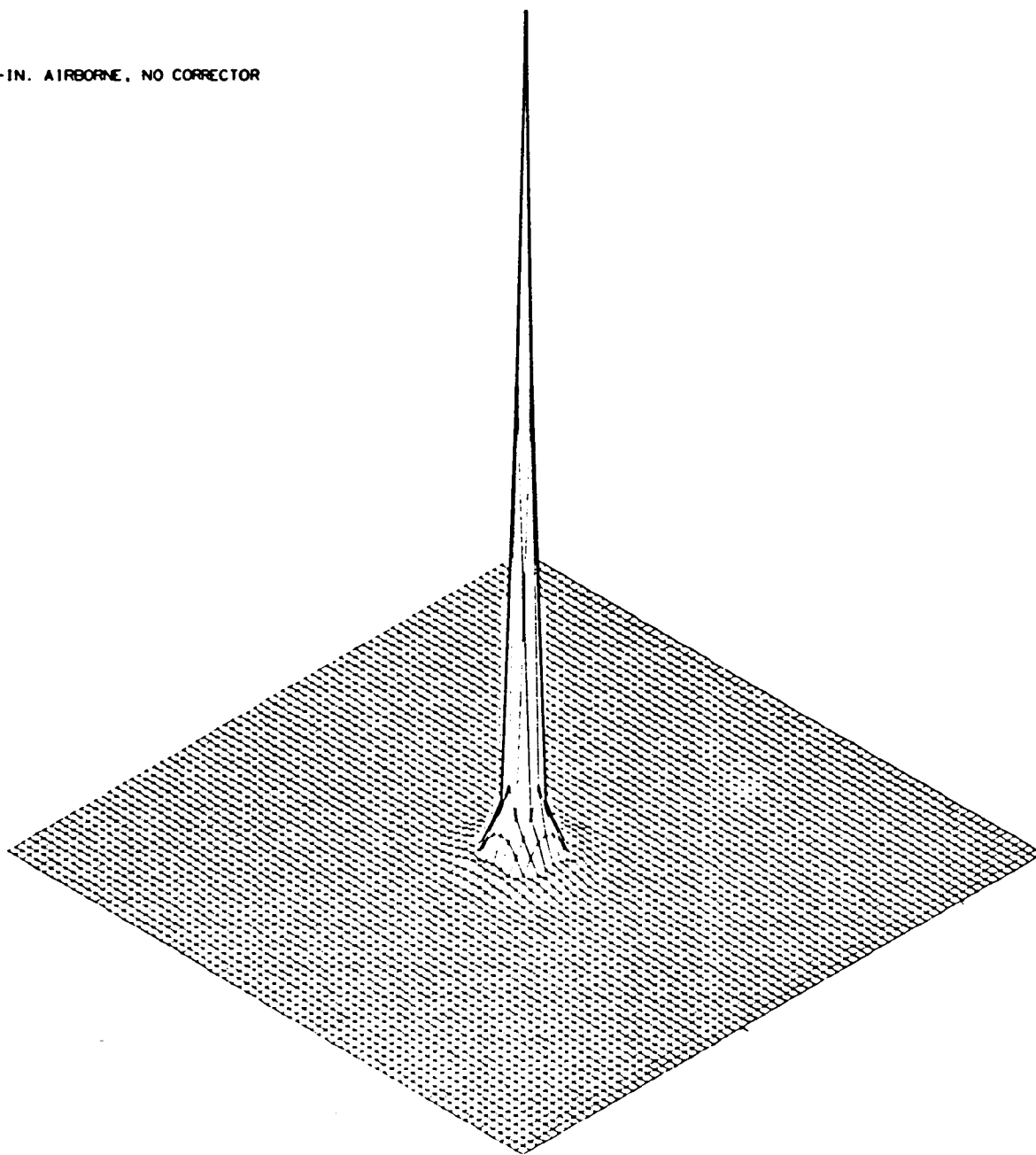
- M = Mach no.
  - $\delta$  = Shock Wave Standoff
  - $\rho$  = Pressure
  - $\lambda$  = Wavelength
  - R = Focal Length
  - f = Spatial Frequency
- m = .9
  - $\delta$  = 5 cm
  - $\rho$  = .27 @ 12 KM
  - $\lambda$  =  $2 \times 10^{-4}$  cm
  - R = 1236.2 cm



FROM POLYPAGOS COMPUTER PROGRAM

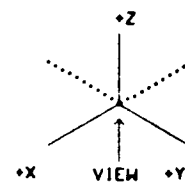
$f$ CY/MM	T
0	1.0
1	.95
2	.90
3	.85
4	.79
5	.77
6	.73
7	.70
8	.66
9	.61
10	.57
11	.54
12	.51
13	.49
14	.46
15	.45

35-IN. AIRBORNE, NO CORRECTOR

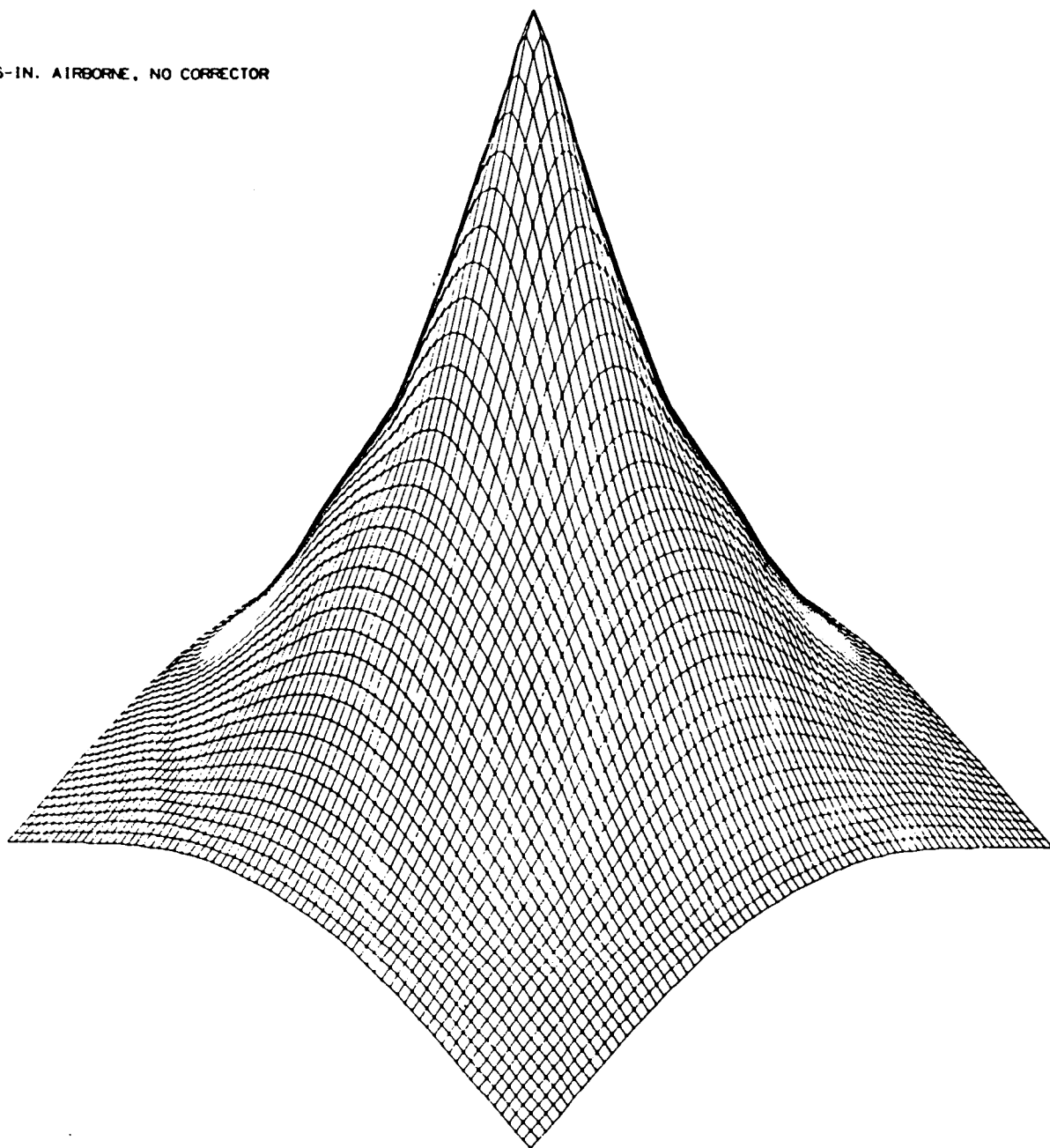


PSF K = 0.000

91.5 cm TELESCOPE  
POINT SPREAD FUNCTION



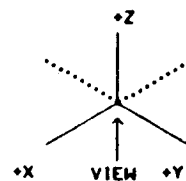
36-IN. AIRBORNE, NO CORRECTOR



MTF K = 0.000

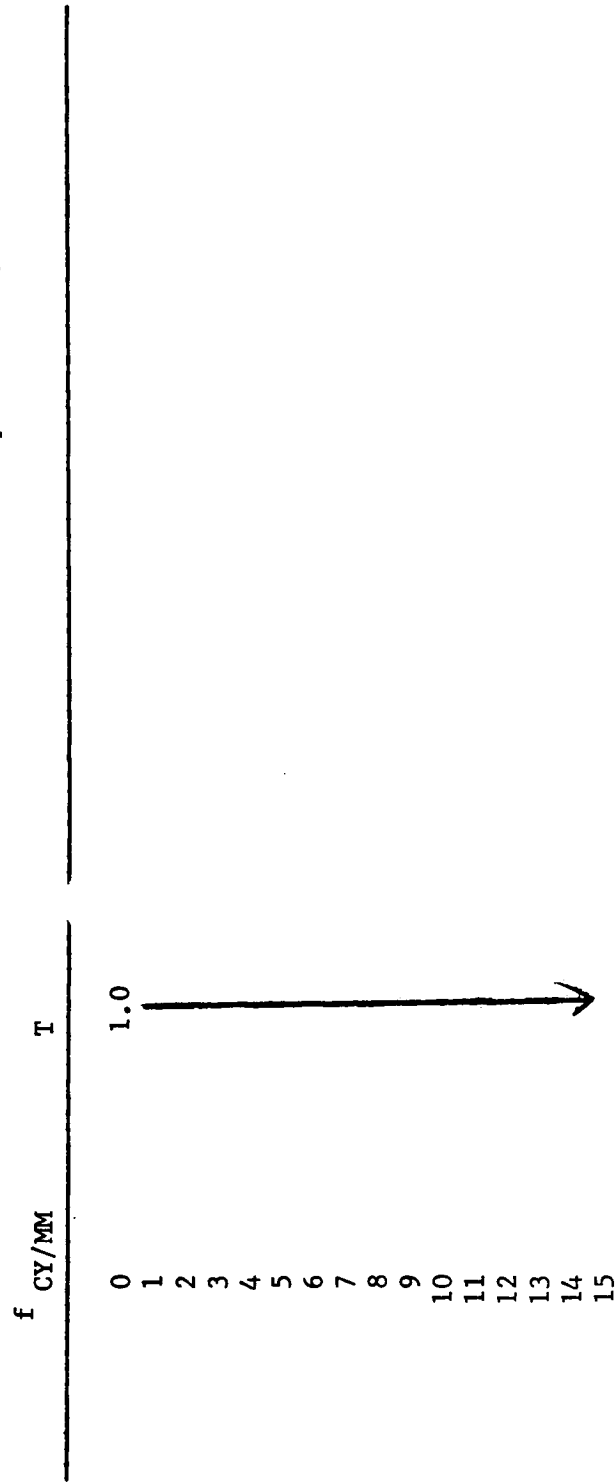
91.5 cm TELESCOPE  
MTF

FIG. 56



$T = \text{Modulation}$   
 $\alpha = 6 \times 10^{-7} \text{ mm}$  Maximum Image Motion  
 for Short Exposure  
 $K = \text{Spatial Frequency}$

$$T = e^{-2\pi^2 \alpha^2 K^2}$$



$$T = 1 - \frac{a}{l/K}$$

a = .05 mm Detector Size  
K = Spatial Frequency

$f_{CY/MM}$	T
0	1.0
1	.95
2	.90
3	.85
4	.80
5	.75
6	.70
7	.65
8	.60
9	.55
10	.50
11	.45
12	.40
13	.35
14	.30
15	.25

## ELECTRICAL BANDWIDTH

FIG. 59

90

$$\text{FREQ} = (A)(f) \quad A = \text{MAXIMUM ANGULAR IMAGE RATE} = 19983 \text{ ARC SEC/SEC}$$

f CY/ARC-SEC	FREQ(Hz) 3 db POINT	FREQ X 3 TIME CONSTANTS FOR 95% ACCURACY (Hz)
0	0	0
.06	1199	3597
.12	2398	7194
.18	3597	10791
.24	4796	14388
.30	5995	17985
.36	7194	21582
.42	8393	25129
.48	9592	28776
.54	10791	32373
.60	11990	35970
.66	13189	39567
.72	14388	43164
.78	15587	46761
.84	16786	50358
.90	17985	53955
.96		

**MARTIN MARIETTA**



# BACKGROUND IRRADIANCE AT ENTRANCE APERTURE

FIG. 60

	IRRADIANCE FROM		SCATTERED SUNLIGHT
	TARGET	ATMOS. EMISSION	
	$5.9 \times 10^{-9} \text{ Watts/cm}^2$	$1.2 \times 10^{-15} \text{ @ } -60^{\circ}\text{C}$	$5.4 \times 10^{-8} \text{ Watts/cm}^2$

ACQUISITION  
SYSTEM  
(T = 1100°K)  
RANGE = 131 KM  
 $\Delta\lambda$  (1.0 TO 2.5)  
FOV 9°

	$8.5 \times 10^{-14} \text{ watts/cm}^2$	$3.3 \times 10^{-24} \text{ watts/cm}^2$	$4.7 \times 10^{-17} \text{ watts/cm}^2$
--	--	--	--

IMAGING  
SYSTEM  
 $\Delta\lambda$  (1.9-2.6)  
(T = 600°K)

COMPARING TARGET TO BACKGROUND IRRADIANCE WE FIND THAT ONLY IN THE ACQUISITION SYSTEM DOES ANY COMPONENT OF BACKGROUND (SCATTERED SUNLIGHT) CAUSE CONCERN. BY AC COUPLING THE DETECTOR TO AMPLIFIER SYSTEM WE VERY EFFECTIVELY ELIMINATE ANY SIGNIFICANT CONTRIBUTION FROM UNIFORM BACKGROUND.

MARTIN MARIETTA

rejected. AC coupling then eliminates scattered sunlight as a signal source.

The summation of all effects governing MTF and ultimately spatial and temperature resolution is shown in Figure 61. Since only the atmospheric loss changes and the amount is not significant, all conditions of viewing are similar concerning MTF.

The NEAT for zero spatial frequency has been calculated for all temperatures and is shown in Figure 62 using 12-bit encoding. In an imaging system, however, modulation loss does occur. The system MTF shown previously is used to modify the NEAT as follows to obtain minimum resolvable temperature as a function of temperature and spatial frequency:

$$\text{MRT}(k, \Delta T) = \frac{\text{NEAT}(0 \text{ Spatial Freq})}{\text{MTF}(k)}$$

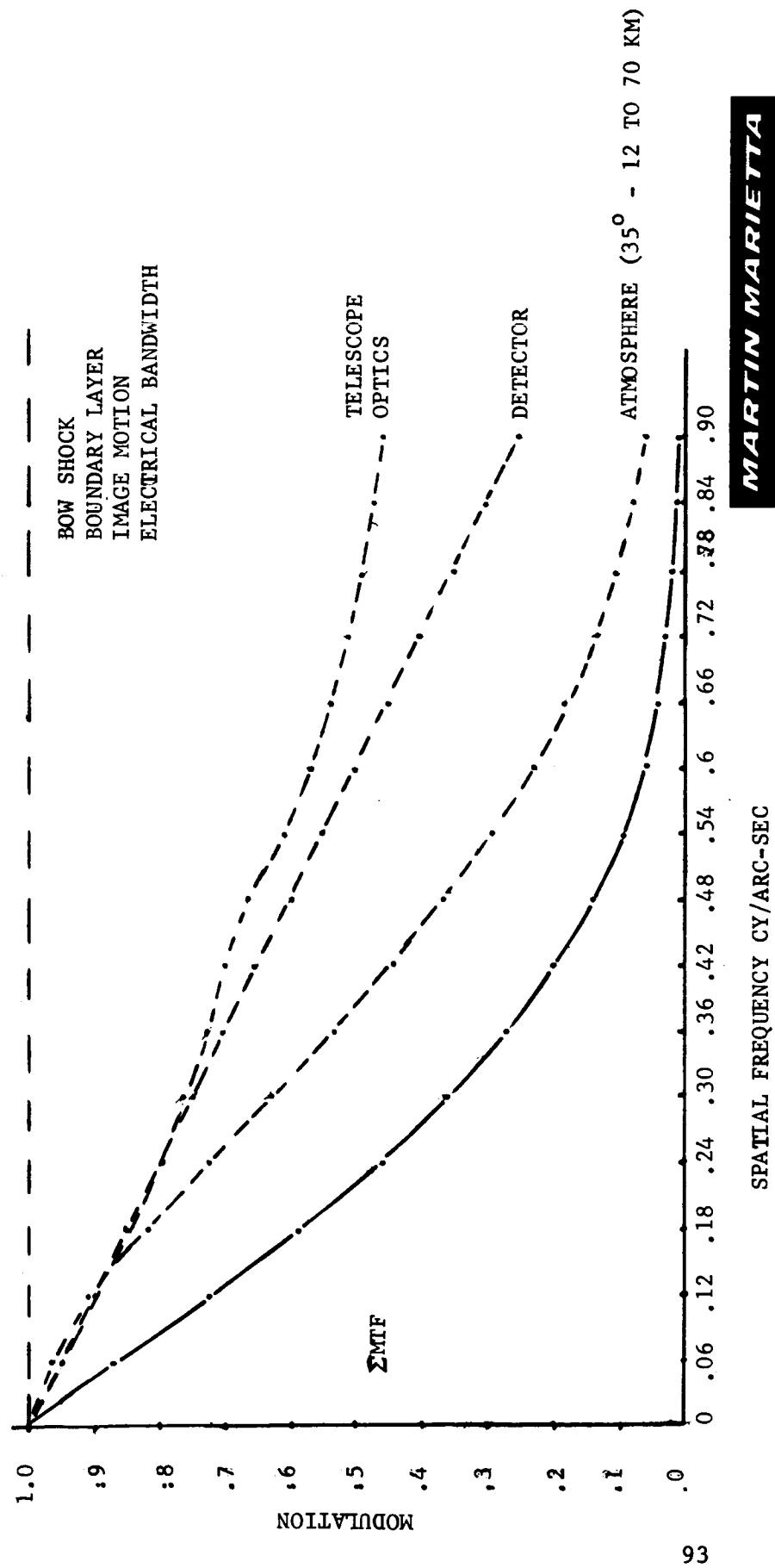
The MRT is shown in Figure 63 for several temperatures.

Spatial Resolution - Given the system MTF and the parameters for viewing the Shuttle in each case, the spatial resolution can be obtained. Spatial resolution is simply the reciprocal of spatial frequency times the range divided by the cosine of the angle between the line-of-sight and the Shuttle underside normal. (see Appendix.) This is shown in Figure 64. Also, using data presented in Figure 63, both the spatial and temperature resolution can be obtained for any case.

Figure 65 is a composite of the spatial resolution and minimum resolvable temperature for maximum range with the system performance bounded. The data can be processed to enhance either spatial resolution or minimum resolvable temperature at the expense of the other within the bounds defined by design goals. As an example, if the minimum temperature in a frame of data were 1000 K, the  $\Delta T$  could be allowed to slide to 2.5% improving spatial resolution or vice versa. Figure 66 is the same composite for the minimum range condition. Here much lower temperatures are resolvable within the system bounds.

$\Sigma$ MTF

FIG. 61



MARTIN MARIETTA

## IMAGING SYSTEM PARAMETERS

FIG. 62

$$D_0 = 91.5 \text{ cm}$$

$$F\# = 13.5$$

$$\text{FOCAL LENGTH} = 1236.2 \text{ cm}$$

DETECTOR (InSb)

$$\Delta f = 50 \times 10^3 \text{ Hz}$$

$$\lambda_1 = 1.9 \text{ u}$$

$$\lambda_2 = 2.7 \text{ u}$$

$$C = 0.3^*$$

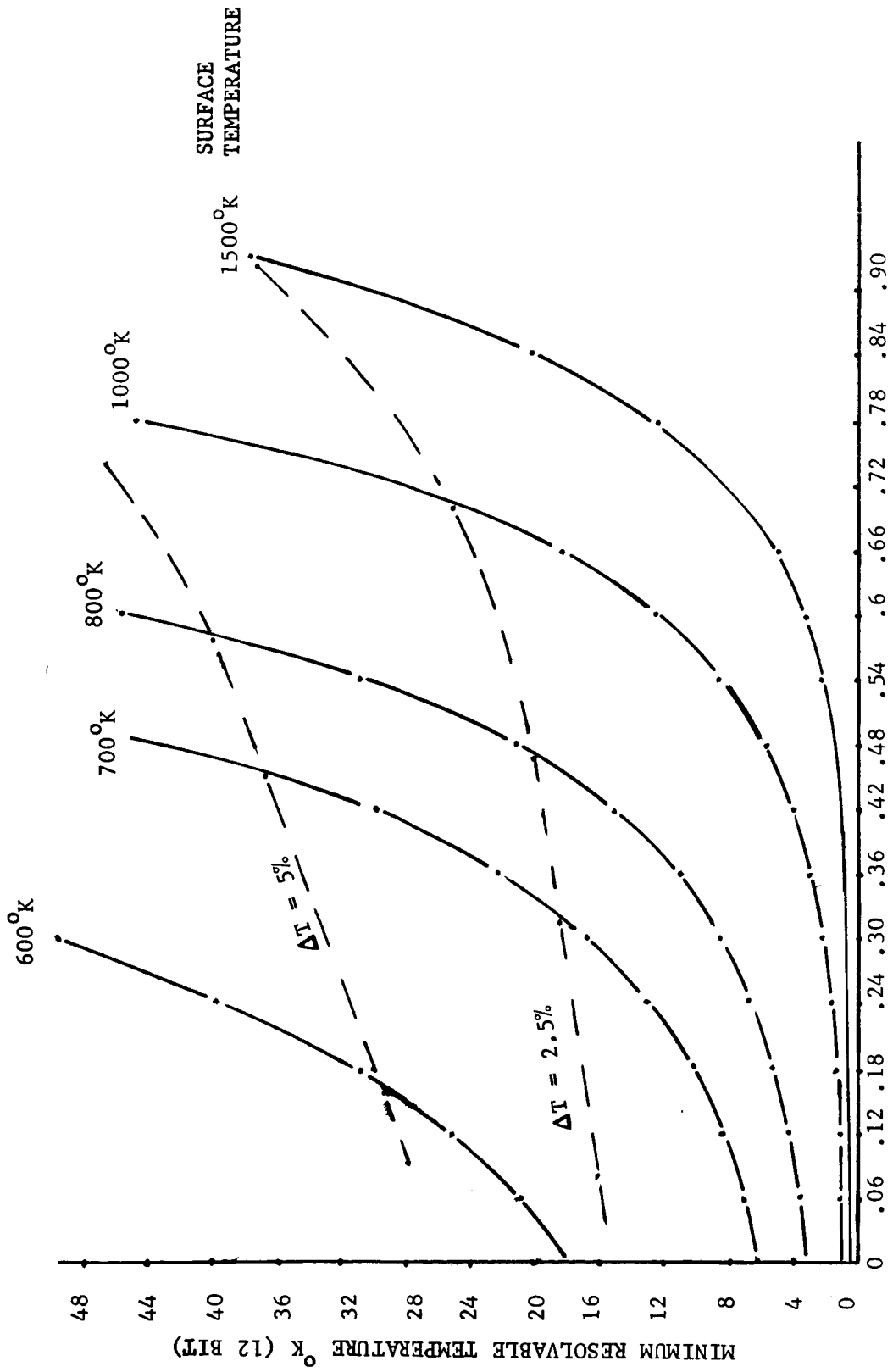
\*DERATING FACTOR

TEMP OF SOURCE(°K)	S/N	NEAT (°K)	NEAT (°K) DIGITAL 12 BIT
600	9	.7	18
700	36	2	6
800	108	1	3
900	250	.5	1.3
1000	500	.3	.8
1100	900	.2	.6
1200	1400	.16	.4
1300	2100	.13	.3
1400	3000	.1	.25
1500	4100	.09	.22
1600	5400	.08	.19
1700	6800	.07	.17
1800	8400	.06	.15
1900	10,000	.05	.14

MARTIN MARIETTA

FIG. 63

MINIMUM RESOLVABLE TEMPERATURE

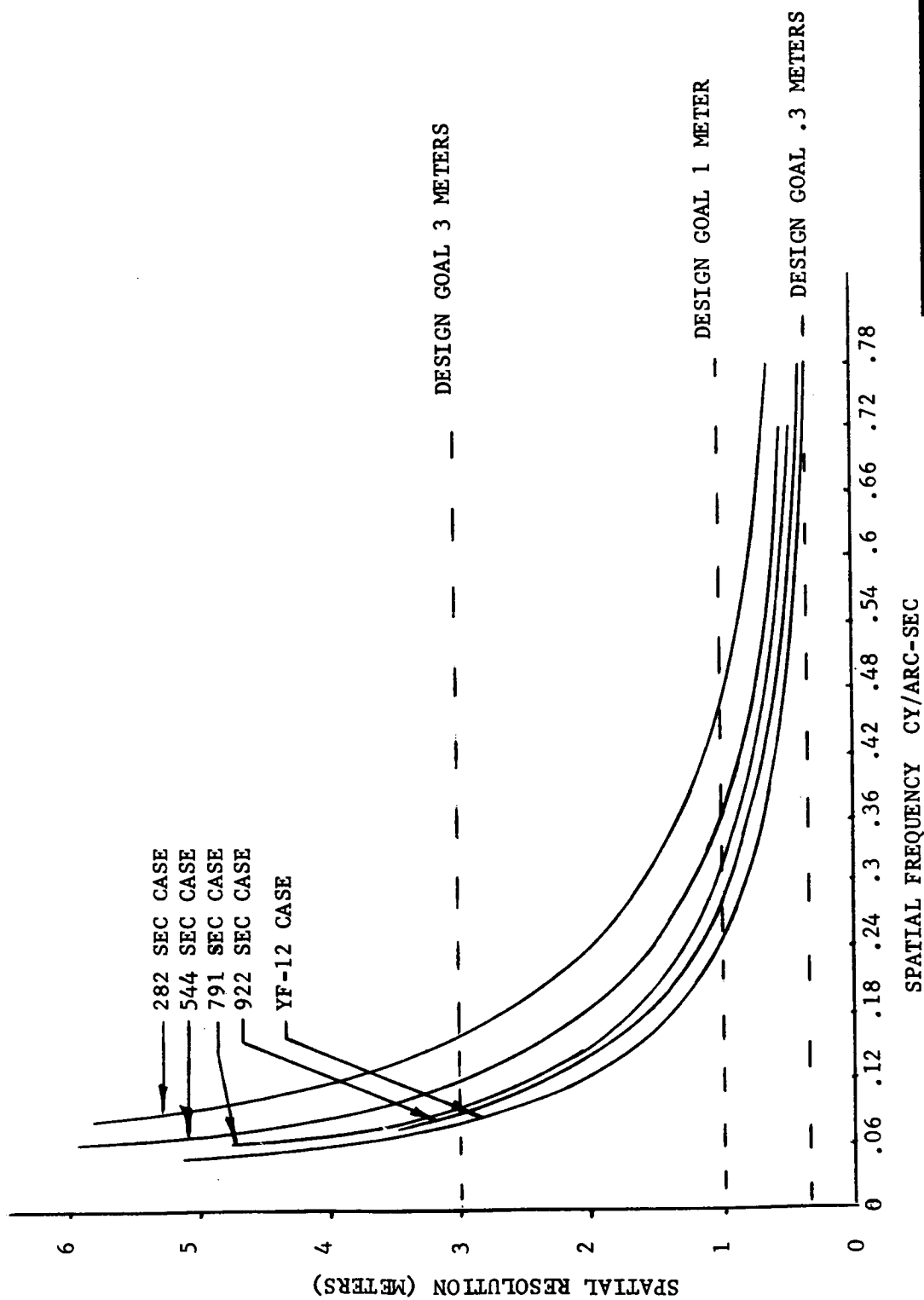


SPATIAL FREQUENCY CY/ARC-SEC

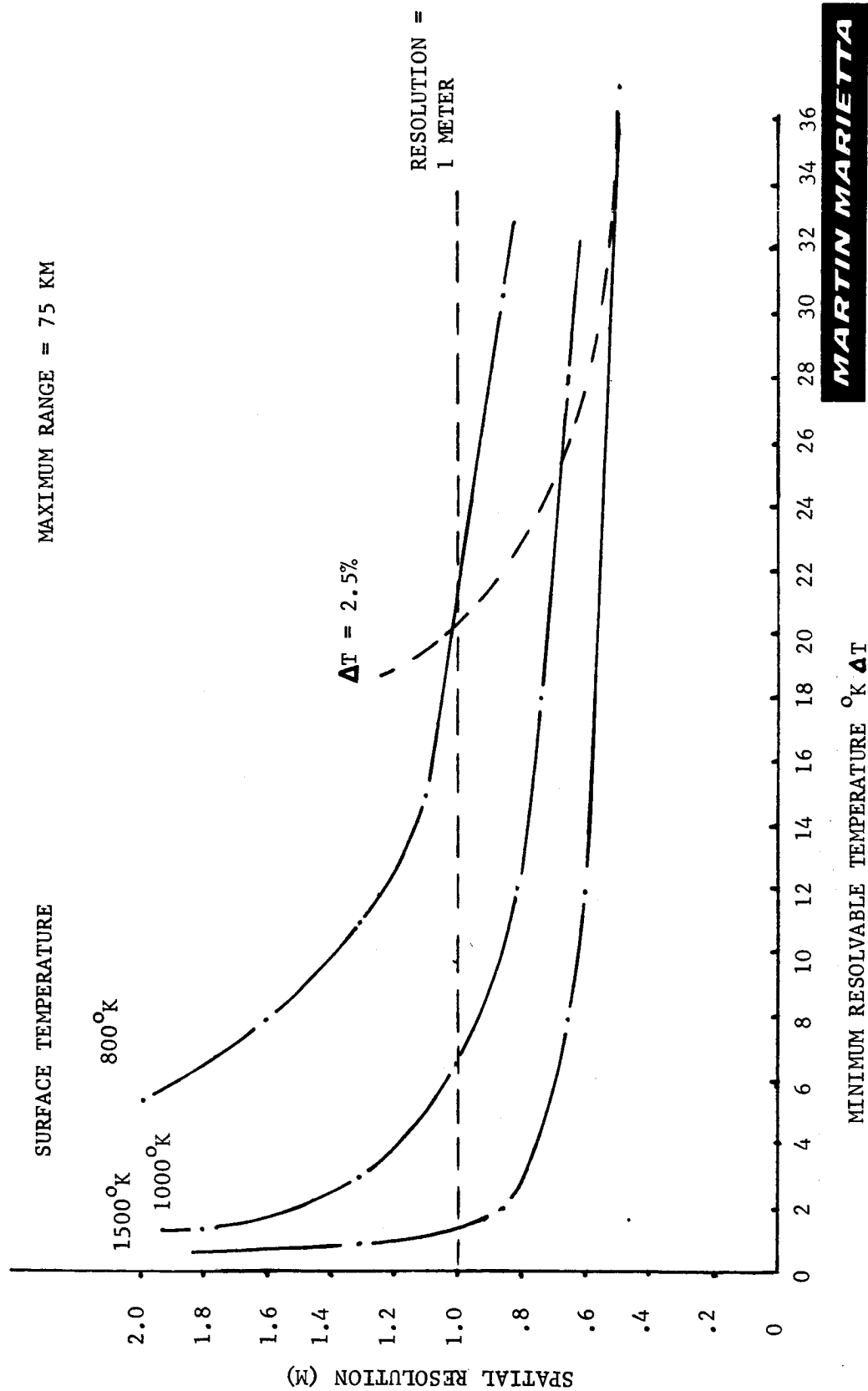
MARTIN MARIETTA

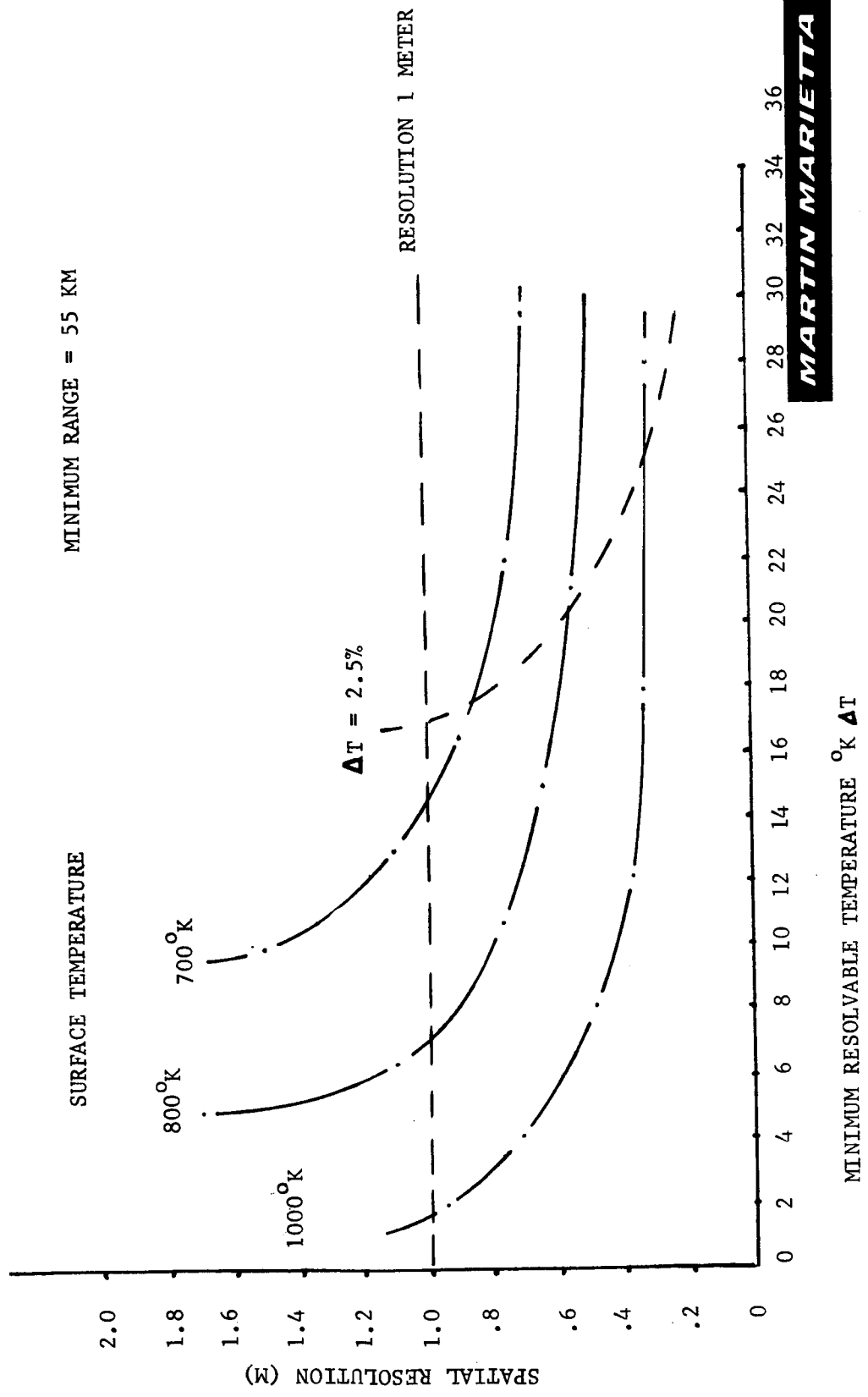
FIG. 64

SPATIAL RESOLUTION



MARTIN MARIETTA





MARTIN MARIETTA

1-2

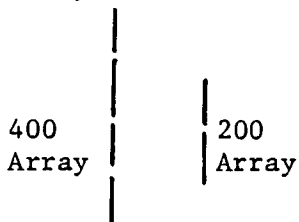


## DATA RECONSTRUCTION

---

After the data have been acquired and recorded, there will be several levels of processing required to go from the flight tape to an output tape containing calibrated and corrected data suitable for further analysis by NASA Ames Research Center. This processing will consist of five major steps; (1) unscrambling, (2) intensity correction, (3) reconstruction, (4) geometric correction, and (5) calibration. Each of these steps is discussed in detail in the following pages and processing flow diagrams are included.

Unscrambling - The unscrambling algorithms will depend on the final detector design and data acquisition logic and may change significantly if there is a design change. The following algorithms are based on the design as seen at this time. This involves 600 detectors, organized so there is an initial vertical array of 400 detectors followed by another centered vertical array of 200 detectors.



The system is designed to have a high probability for the Shuttle passage to be in the center 200 detectors in both banks. The extra 100 detectors on either side of this maximum probability area increase the chances of getting some useable data.

These data will be recorded so that the detector values are always in the order of 1 through 200 followed by 1 through 200. This will yield data groups of 400 values. Each physical tape record will be composed of an integral number of these data groups. The flight tape will also contain a number of pre-flight calibration data groups before the shuttle data-take and postflight calibration data after the data-take. The calibration data will be of the same basic format as the Shuttle image data and must be recognizable as being different. These could be flagged by a special code word in the data, by a different record size for the calibration data, or even by a hand written log of how many pre- and postflight calibration data groups were taken.

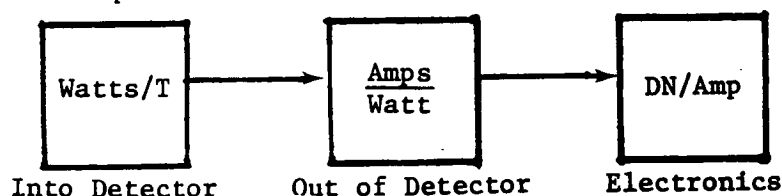
The calibration data must be pulled from the tape and operated on to yield a unique calibration value for each detector. These data will be stored on permanent disk file for later use in correcting the image data.

~~DO NOT REUSE PLANK NOT EJECT~~

At this point the image data can be straightforwardly read from the data tape and separated into two image arrays, one of size 400xNG, where NG is the number of data groups, and the other of size 200xNG.

Intensity Correction - Since the correction algorithms are in some cases dependent on detector calibrations, they should be applied while each image data value can be related to a unique detector and before any spatial cropping or recombination is performed.

Figure 67 shows how the flow diagram separates each identifiable correction or conversion required. However, several of these operations can be performed together. For example, the detector and filter response corrections, as well as the radiant emittance to temperature conversion can be combined.



The above sequence occurs during the data-take. The inverse operation can be used during the correction procedure.

$$DN/T = \left( C_{1SE} \frac{W}{T} \right) \left( C_{2SE} \frac{A}{W} \right) \left( C_{3SE} DN/A \right)$$

$$T = DN / \left( C_{1SE} \right) \left( C_{2SE} \right) \left( C_{3SE} \right),$$

where DN is the recorded digital number.

The radiant emittance to temperature conversion is included in the first correction function  $C_{1SE}$ . The radiant emittance,  $W = \epsilon \sigma T^4$ , where  $\sigma$  is the Shuttle surface emissivity.

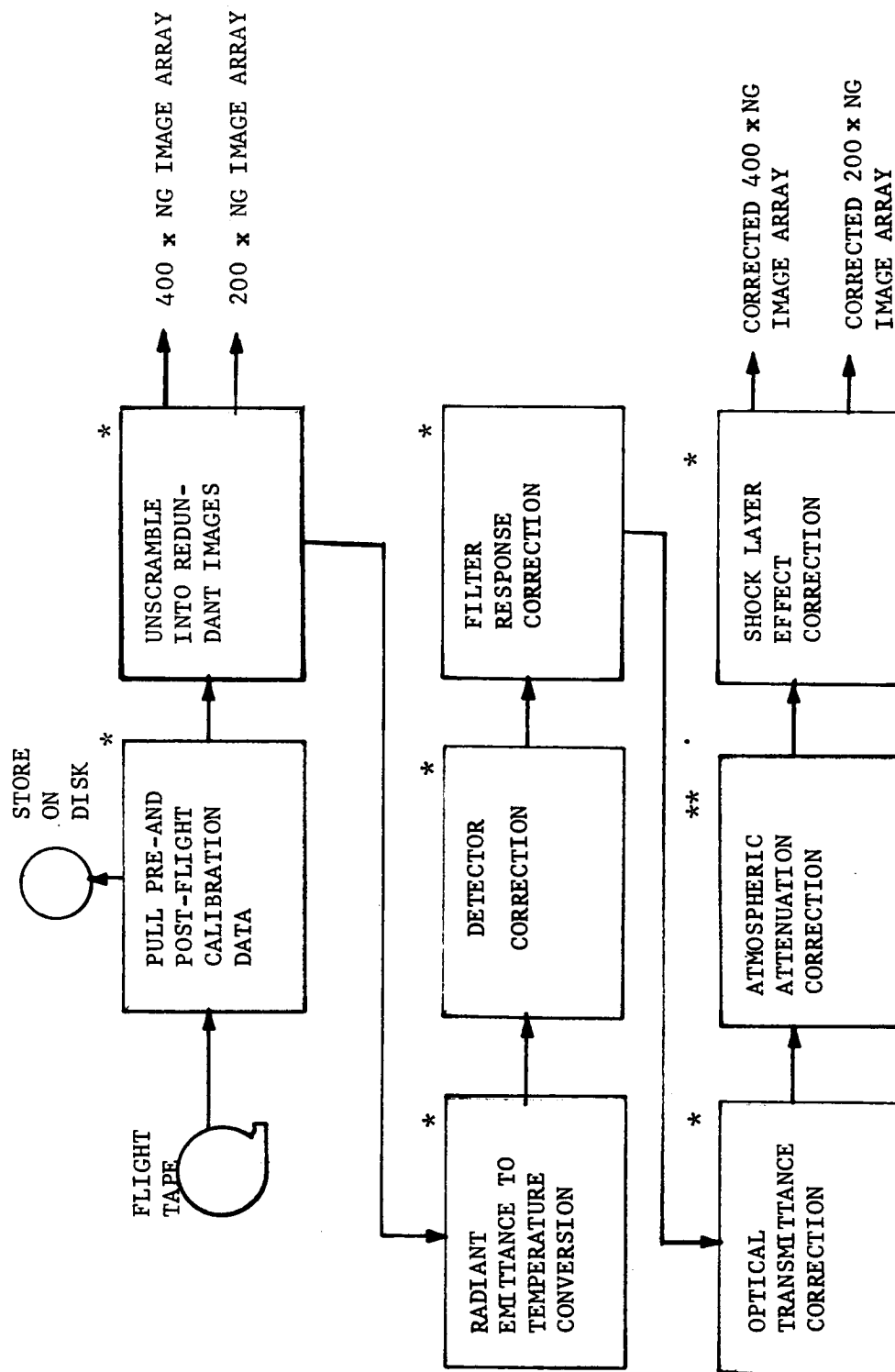
The optical transmittance is a function of wavelength, but will be fairly constant over the chosen wavelength band.

$$T_{Corrected} = T * C_{Optics}$$

The filter wavelength band was chosen to avoid atmospheric absorption bands. At a Shuttle altitude of 75 km, an aircraft altitude of 14 km, and a tropical atmospheric model, the attenuation is approximately constant at 1.5%. This may vary with different altitudes and ranges, and can be calculated using the LOWTRAN3 (Ref. 12) atmospheric transmittance computer program.

FIG. 67

IMAGE PROCESSING/UNSCRAMBLE AND INTENSITY CORRECTION



\* NEW DEVELOPMENT  
\*\*EXISTING SOFTWARE

MARTIN MARIETTA

$$T_{\text{Corrected}} = T * C_{\text{atmo}},$$

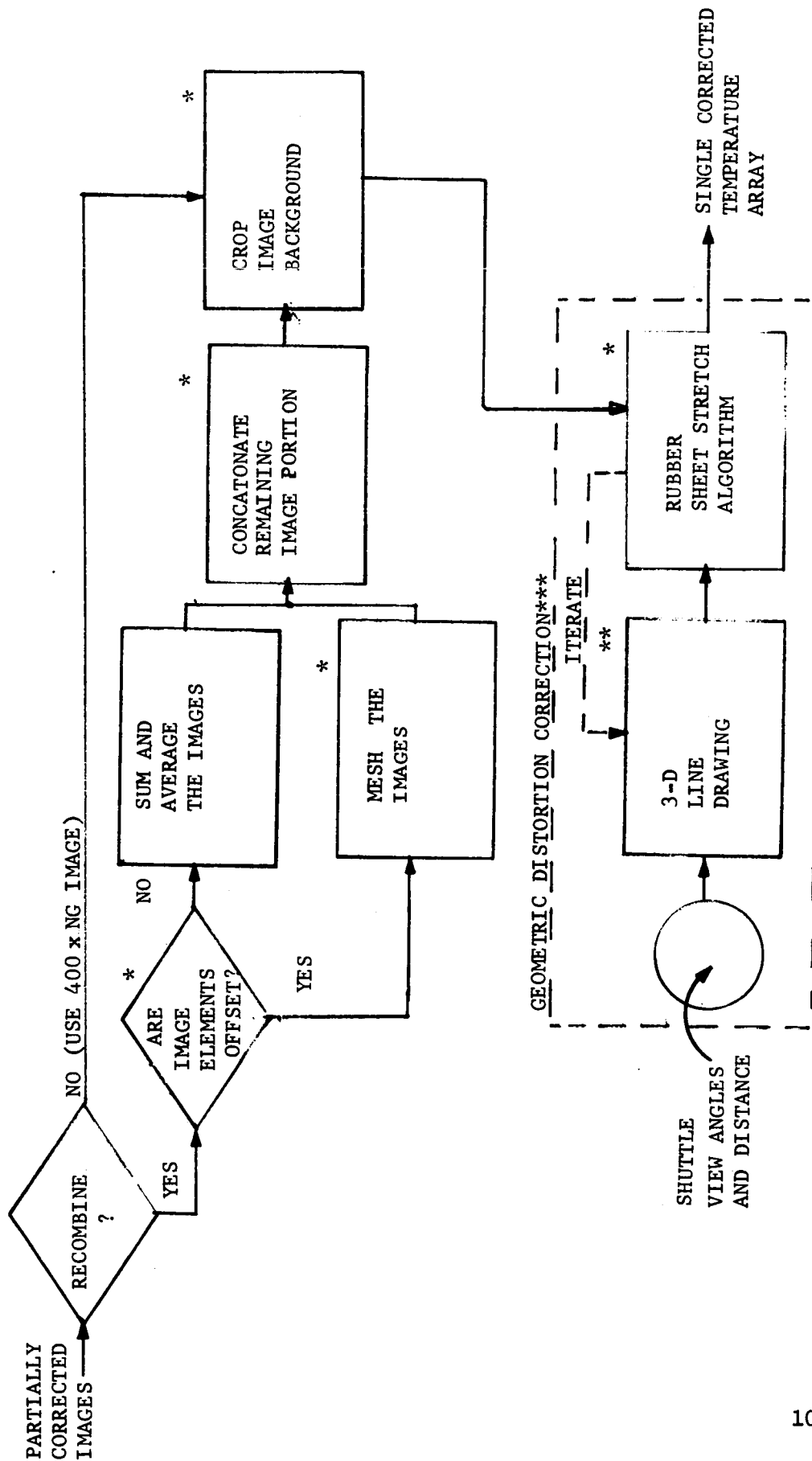
where  $C_{\text{atmo}} = f(\text{altitude, range})$ .

As seen in the flow diagram, a correction for shock layer effect was identified as required, but investigation has shown this effect to be negligible.

Reconstruction - The above processing produces two arrays of corrected temperature values. These arrays may be recombined to produce a single temperature image of improved resolution or less random noise (see Fig. 68). However, recombination may or may not be desirable. If the Shuttle passage was within the high probability central area of both detector banks, the middle 200 values of the 400 array can be beneficially combined with the 200 array. This may also be the case if the larger portion of the image falls within the mid-200 area. The remaining portion of the Shuttle image would then be appended to the single combined image. This would produce a result in which a small portion of the image would be of lower resolution or higher noise content than the rest. This could be acceptable if the delineation was considered during the analysis phase to prevent false interpretation. If, however, the Shuttle image is largely outside the mid-200 area, recombination is probably not warranted and only the 400 element array would be processed, proceeding directly to the edge cropping step.

Some form of display is necessary to enable the above decision. This can be a low resolution, quick-look method and only the 400 element array must be considered. If the recombination technique is chosen, only the mid-200 elements of the 400-element array are used producing two redundant 200xNG image arrays.

*a. Determine Optimum Recombination* - At this point, the optimum recombination of the two redundant images must be determined. Two choices are available: (1) the two images can be registered, summed and averaged, producing a single image with random noise removed; and (2) the images would be meshed or interlaced to produce one image with improved resolution. The optimum of the two methods is dependent upon the angle at which the Shuttle passes across the detector array. If the angle-of-passage differs little from the alignment angle of the redundant sensor elements, the redundant images will have little offset and the averaging procedure will be more desirable. Conversely, if the angle-of-passage is different from the sensor element alignment angle, the resultant offset will allow the images to be meshed.



\* NEW DEVELOPMENT  
 \*\* MODIFY EXISTING SOFTWARE  
 \*\*\*COULD BE PROCESSED AT JPL

MARTIN MARIETTA

Because the angle-of-Shuttle passage may not be accurately known at processing time, another way to determine the optimum method is desirable. This can be done by computing the best registration position of the two images, i.e., whether it is a full pixel offset, thus indicating averaging, or a half pixel offset indicating meshing.

To do this, each image element is replaced by a 2x2 array of identical values.

$X(2I - 1, 2J-1) = R(I,J)$   
 $X(2I-1, 2J) = A(I,J)$   
 $X(2I, 2J-1) = A(I,J)$   
 $X(2I, 2J) = A(I,J),$  where  $I=1, NR$  (no. of rows)  
 $J=1, NC$  (no. of columns)

If the above operation is done for both images, then X is the expanded version of image A and Y is the expanded version of image B.

By sliding image X over image Y one pixel at a time, the overall difference for each offset can be calculated. Start with a negative offset greater than the known possible maximum and do twice that number of overlays in both the horizontal and vertical directions offsetting one pixel at a time. Finally, the positioning that yields the lowest total difference is the best registration. If the final offset between X and Y is an even number of pixels, the averaging technique is indicated, and if odd, the mesh technique is better.

*b. Mesh Procedure* - The mesh procedure may be used on the expanded X and Y images immediately after registration. Using the expanded versions and summing and averaging them as registered produces a single image twice the number of rows and columns as the original image minus twice the offset and yields increased resolution.

$$P(I,J) = [X(I,J) + Y(I+VO, J+HO)]/2.$$

where  $I = 1, (2NR-2VO),$

$J = 1, (2NC-2HO),$

VO is the vertical offset of X from Y  
 and HO is the horizontal offset of X from Y

The edge overlap of the above image should be removed. This operation may be best performed at the time of registration before the summing and averaging.

c. *Average Procedure* - The averaging technique is best performed on the original images A and B, thus reducing the number of required operations. The proper registration of A and B is given by one-half the final vertical and horizontal offsets determined for the expanded images X and Y. The overlapping edges of A and B as determined by the offsets can be removed before the summing operation. If this is done, then the offsets need not be used in the indexing of the newly defined A' and B' during the summing.

$$A'(I,J) = A(I,J)$$

$$B'(I,J) = B(I + VO', J+HO'), \text{ where } \begin{aligned} I &= 1, NR-2VO' \\ J &= 1, NC-2HO', \\ VO &= VO/2, \\ \text{and } HO &= HO/2. \end{aligned}$$

d. *Concatenate Remaining Image Portion* - If the recombination procedure was used on the mid-200 element portion of the arrays and a portion of the Shuttle image fell outside of this area, it must now be concatenated to the recombined array. If the averaging technique was used, there will be a one-to-one element realignment relationship. However, if the meshing procedure was used, the outlying partial image array must be expanded with each element replaced by a 2x2 array so that the two arrays will match. The realignment in the horizontal direction will be dependent on the horizontal offset determined during recombination. The vertical alignment may require that the corresponding overlapping edge that was eliminated during recombination be restored to avoid a data discontinuity. A quick-look display at this point to check the concatenation is desirable.

e. *Crop Image Background* - The above recombination and realignment if required, will produce a rectangular array of picture elements containing the Shuttle image and a surrounding background area. To reduce the number of picture elements, and therefore, the number of operations needed for further processing, the background can be cropped leaving only a small border.

Average the first and last 5 elements in both horizontal and vertical directions to arrive at an average background level.

$$BKG = \frac{\sum A(I,J)}{N} \quad \begin{aligned} I &= 1,5 \text{ and } I = NR-5, NR, \\ J &= 1,5 \text{ and } J = NC-5, NC. \end{aligned}$$

and N = total number of elements summed.

Move across the image array in a horizontal direction looking for values greater than twice the average background. Note the positions of these occurrences and keep a running minimum and maximum horizontal location check.

Do for each row of the image.

If  $(P(I,J) > 2 \text{ BKG})$ ,

then  $JMIN = \text{Minimum of } JMIN \text{ and } J$ ,

and  $JMAX = \text{Maximum of } JMAX \text{ and } J$ .

Where  $J = 1, NC$  and  $I = 1, NR$  varying  $J$  first.

Repeat this operation in the vertical direction, finding the vertical minimum and maximum locations.

If  $[P(I,J) > 2 \text{ BKG}]$ ,

then  $IMIN = \text{Minimum of } IMIN \text{ and } I$ ,

and  $IMAX = \text{Maximum of } IMAX \text{ and } I$ ,

where  $I = 1, NR$  and  $J = 1, NC$

varying  $I$  first.

The resultant horizontal and vertical max and mins should indicate the outer most edges of the Shuttle image. These limits can be expanded to produce a small outer border and the outlying image elements eliminated.

Image display at this point is desirable because anomalous values in the background area could produce false limits. If this occurs the processing can be repeated on the new image and more accurate results produced.

The result of the above processing is a single array containing corrected temperature values with extraneous background removed. These data have not been adjusted to reflect the on-board Shuttle centerline calibration measurements, nor have any corrections been made to remove geometrical distortions or to rotate the image to a plan view. A tape containing the temperature array data at this level of processing can be provided.

Geometric Distortion Correction - The temperature image data will contain geometric distortions due to view angle, the motion of the Shuttle across the sensor, and the relative motion between the aircraft and the Shuttle. The nature of these distortions cannot be predetermined nor accurately defined in a mathematical



sense, and therefore, cannot be corrected in a preprogrammed automatic processing procedure. An interactive procedure is required to perform these corrections, and an iterative method used wherein an adjustment is made and the resultant image displayed. This necessitates a complex interrelated software and hardware system. The development of this system would require hardware and labor beyond the scope of this contract. However, the existent image processing facility at JPL has the capability to perform the geometric distortion corrections. Preliminary discussions with JPL have confirmed the feasibility of this approach.

The geometric correction requires two separate steps. The first is to remove the distortions and produce a geometrically accurate image. The second is to rotate the image to present a plan view of the Shuttle underside as required for further thermal analysis by Ames Research Center.

The importance of first removing the distortions increases as the Shuttle view angles decrease (where  $90^\circ$  is normal to the underside) resulting in a canted view. To correct the distortions, a three-dimensional line drawing of the Shuttle, as seen from the corresponding flight view angles, is required. We currently have the capability to produce this plot as part of the large Thermal Radiation Analysis System computer code. A more optimum plot capability is inherent in the Computer Aided Design/Manufacturing System (CAD/CAM) currently being assessed. This system will be used if available.

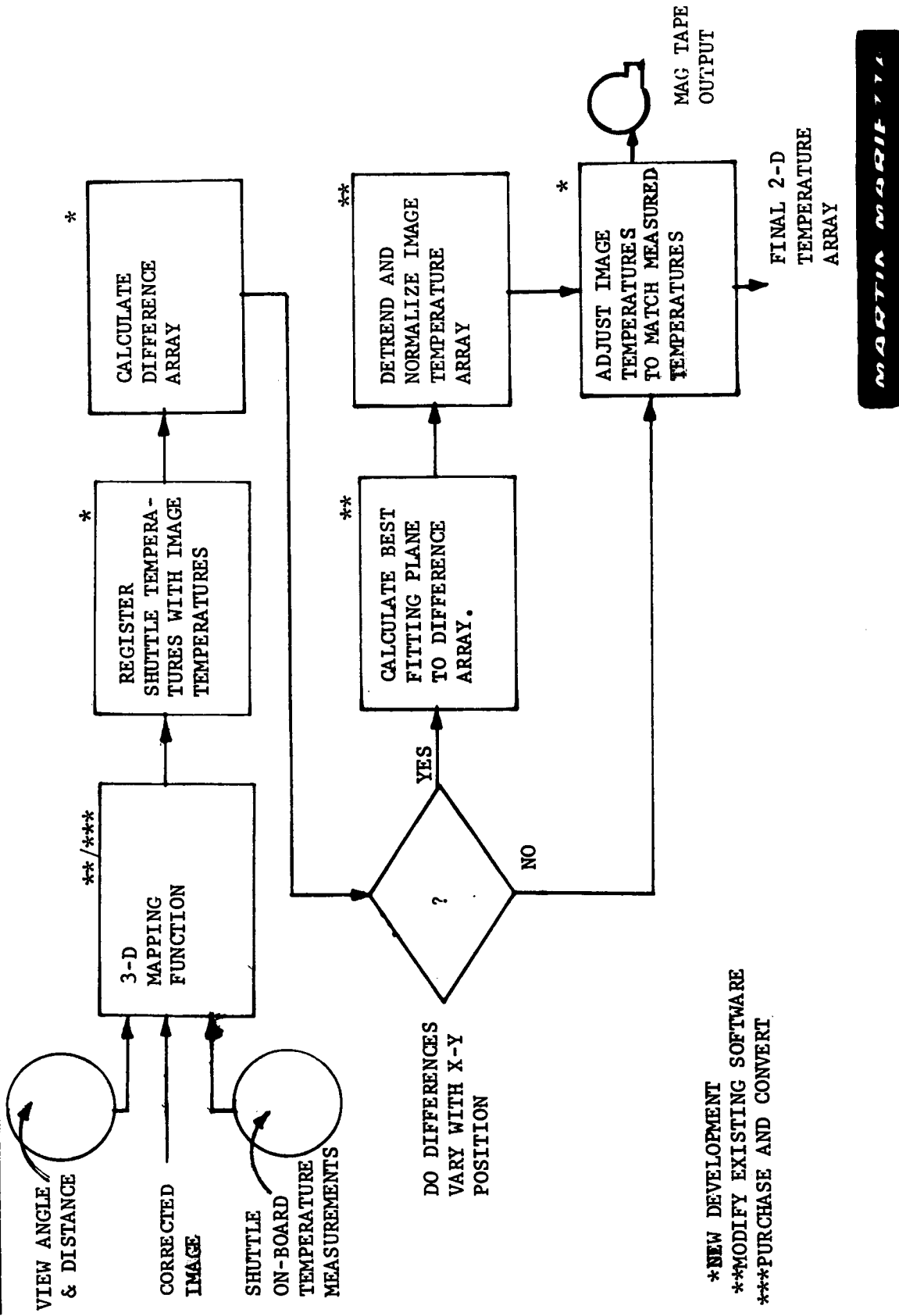
The second step of the geometric correction requires the 3-D line plot to be rotated to a plan view. The above mentioned systems can also perform this function. Both the canted and plan view 3-D plots will be provided to JPL along with the partially corrected temperature image data tape. Using these inputs JPL can produce a tape containing the geometrically corrected and rectified image data.

Calibration - The geometrically corrected temperature data tape can be additionally processed to adjust for the on-board Shuttle temperature measurements (see Fig. 69). These measurements will be provided by Ames after each Shuttle flight, probably on magnetic tape, and will consist of 10 to 20 centerline measurements along with X and Y addresses corresponding to a predefined Shuttle coordinate system. These measurements must be registered and compared with the temperature array data.

If the temperature array datum has been rotated to a plan view, registration of the Shuttle data is fairly straightforward. The array elements corresponding to the centerline Shuttle calibration values can be identified and compared. Some manual interaction will be required in this procedure. This may simply mean

# IMAGE PROCESSING/ CALIBRATION

FIG. 69



MARTIN MARIETTA

looking at a printout of the Shuttle temperature array and noting the required values to be further processed. However, if the CAD/CAM system is available, the appropriate points can interactively be selected from a plan view Shuttle line plot. The image values at those points can be displayed or compared to the appropriate on-board measurements.

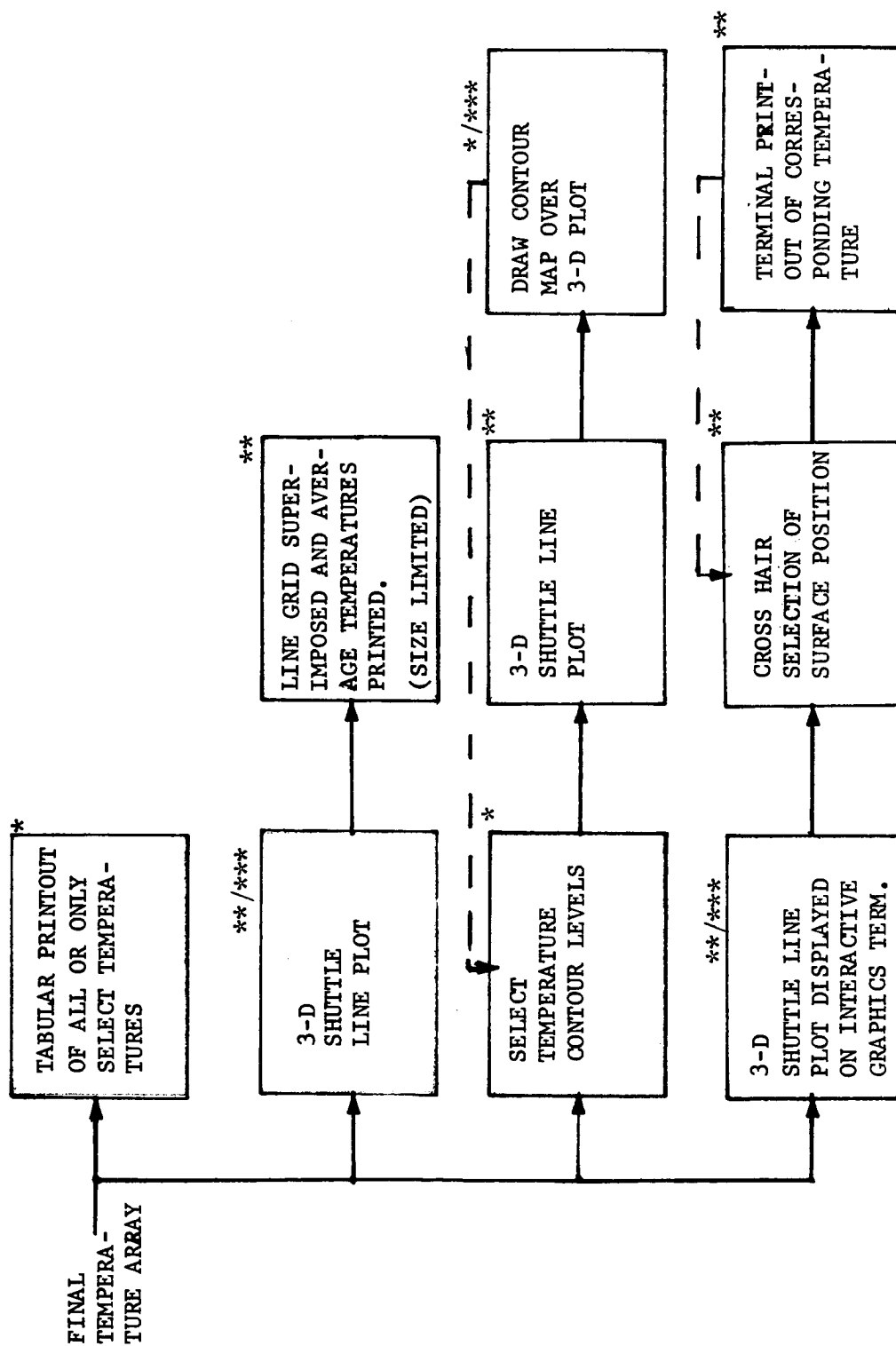
In fact, if the CAD/CAM system is used, the on-board calibration values can be related to the proper positions on the Shuttle image before it is rotated to the plan view. This can be done interactively by selecting the proper points on the canted 3-D Shuttle line drawing display. However, this operation cannot accurately compare the calibration values to the image unless all geometrical distortions have been corrected. Since the distortion correction and the rotation to a plan view are sequential operations, the plan view will normally be used for this registration procedure.

After the calibration values are registered with the temperature array values, a difference array should be calculated. This difference array will provide important information about the performance of both the temperature image array and on-board measurements. If both systems were performing well, the difference array should contain consistently small values. If there are anomalously high singular differences, a failure of the corresponding on-board measuring device may be indicated.

If the differences vary in an increasing or decreasing pattern with X-Y position, an erroneous trend is indicated. This might result if the Shuttle was tilted at an angle to the detectors so that the brightness varied measurably as the distance from sensor. Intensity variation of this nature would not be corrected in the rotation to a plan view operation, but can be corrected in the calibration procedure. The best fit straight line or plane, if these are also off-centerline values, can be computed and the entire image array normalized accordingly.

If the differences are of a random nature, the temperature array might be adjusted by an average difference or might be left unadjusted for further analysis by Ames.

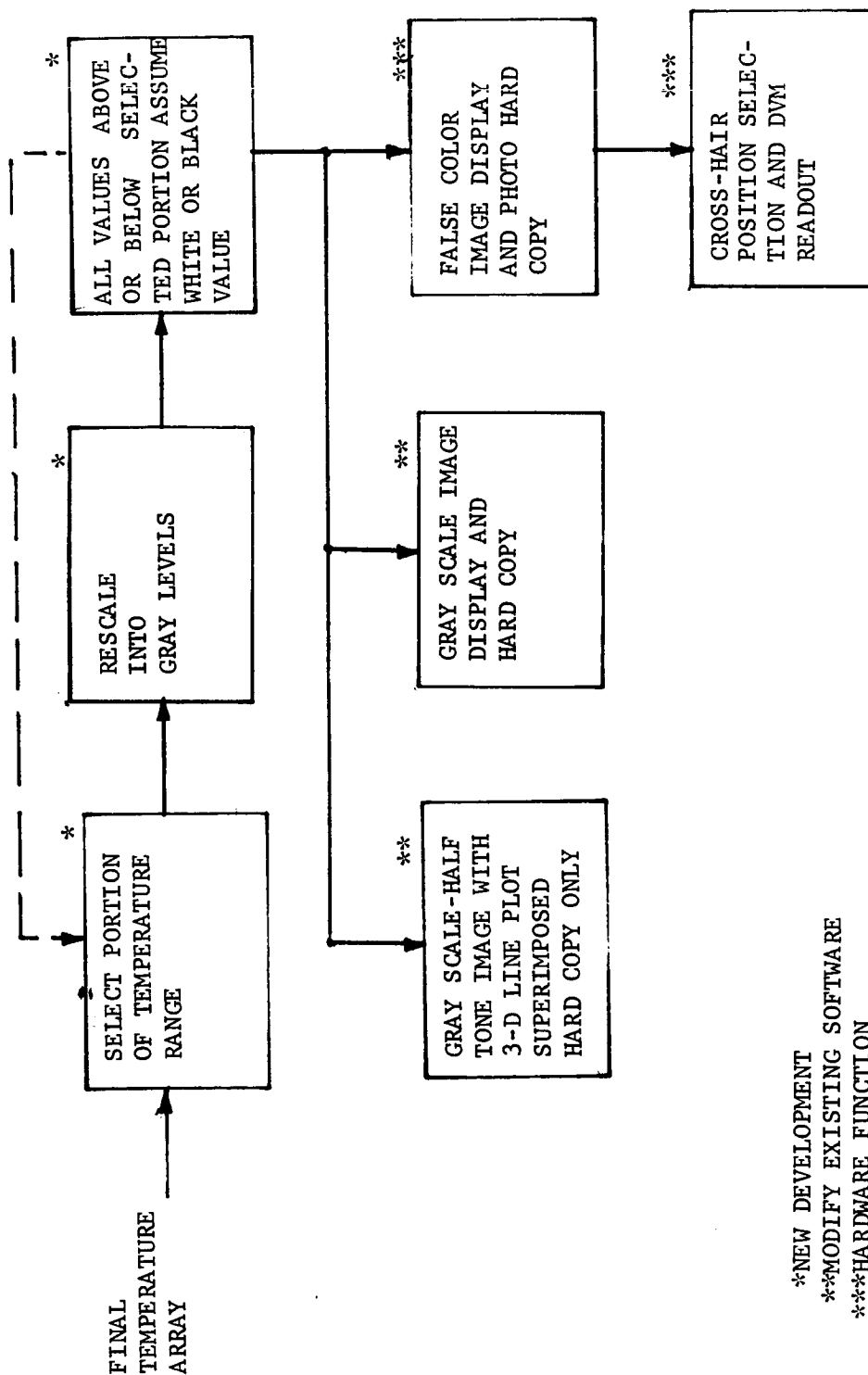
The final calibrated temperature array data would be output on magnetic tape and sent to Ames. This is the final output as requested, and future processing for display purposes will not be pursued. The display diagrams (Figs. 70, 71 and 72) showing these potential displays are included here and may be considered as additional future options. A quick-look display method will be used at various points in the processing for decision making or to assure accuracy of the procedures.



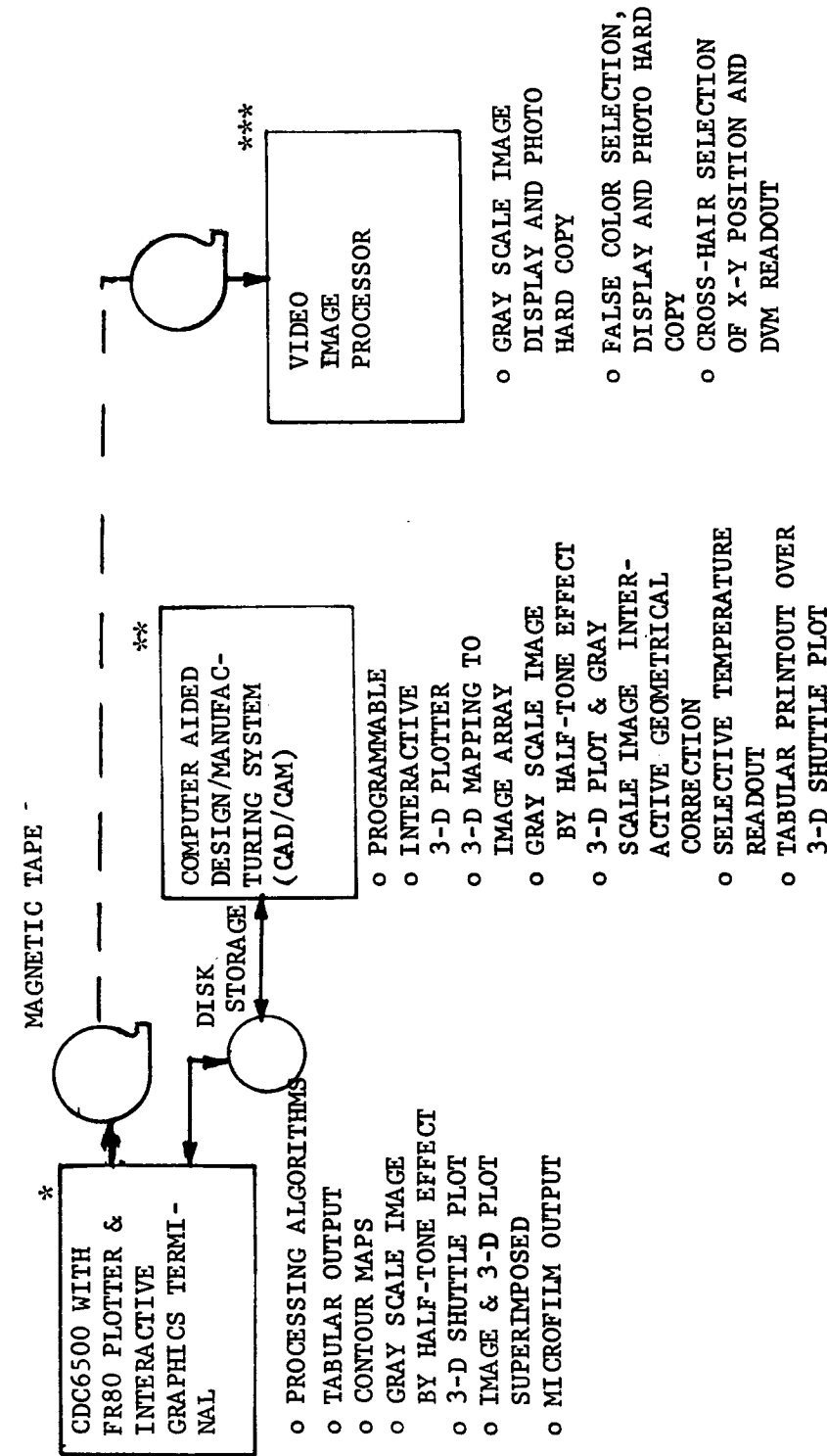
MARTIN MARIETTA

IMAGE PROCESSING/  
 DISPLAY-GRAY SCALE AND COLOR IMAGES

FIG. 71



\*NEW DEVELOPMENT  
 \*\*MODIFY EXISTING SOFTWARE  
 \*\*\*HARDWARE FUNCTION



\*STANDARD COMPUTER FACILITY

\*\*WILL BE AVAILABLE IN 1977

\*\*\*SOME HARDWARE FOR MAGNETIC TAPE INPUT REQUIRED

**MARTIN MARIETTA**

## COST AND SCHEDULE

---

The preliminary cost breakdown is shown in Figure 73. Detailed breakouts by work breakdown structure (WBS) task by month after go-ahead are shown in Figures 74 through 78. The schedules depict a start date in November 1977. However, if the program start is delayed several months, the cost per fiscal year can still be determined from the WBS breakouts. Final delivery of hardware would slip month for month of start delay thereby possibly missing the first Shuttle Orbiter flight anticipated in September 1979.

A WBS is included showing each subtask on which cost control will be maintained. Each WBS item, having a separate number, will be issued budget for that task. Reporting of charges against that WBS number will ensure proper cost control.

The schedule shown has been predicated on the first observed Shuttle flight occurring in September 1979, (see Figs. 79 to 89). This may or may not be OFT-1. Long lead-time procurement dictates a timely start in FY1978 to meet the September 1979 flight.

# PRELIMINARY PROGRAM COST BREAKDOWN

FIG. 73

	HOURS	PURCHASED PARTS	TRAVEL	COMPUTER
ENGINEERING DESIGN	7450		7K	
PROCUREMENT	1860	361.2K	6.3K	
ENGINEERING ASSEMBLY	2750		9K	
ENGINEERING TESTING	1800			
ENGINEERING SYSTEMS SUPPORT	2863		10K	
DENVER DATA SYSTEMS SUPPORT	2358		2K	7.5K
MFG/MODEL SHOP	1270			
QC SUPPORT	980			
PARTS ACCEPTANCE TESTS	450			
PROGRAM SUPPORT	<u>2200</u>			
	23981	<u>361.2K</u>	<u>34.3K</u>	<u>7.5K</u>

MARTIN MARIETTA



## ESTIMATING INPUT SHEETS

COMPUTER: CDC \$1900 Units IBM Units

---

Reason: Optical & Servo Analysis

---

---

---

---

TOTAL TRAVEL	- \$3,400
TOTAL PROC.	- \$29,700
TOTAL COMP.	- \$1,900

**LABOR RATIONALE:**

Design, fabrication, assembly and testing including specific test equipment for the Acquisition System. Major procurements for this subsystem are also included.

Parts/Material	-	\$25,000	Miscellaneous	\$1700
Test Equipment	-	\$3000		

## MAN MONTHS BY MONTH

[illegible]

## FOLDDOUT FRAME

115

**FIG. 74**

Name \_\_\_\_\_ IRIS \_\_\_\_\_  
Dept \_\_\_\_\_ Ext \_\_\_\_\_  
Section \_\_\_\_\_  
Date \_\_\_\_\_  
WBS 01100

PHASE I \_\_\_\_\_  
 II \_\_\_\_\_  
 III \_\_\_\_\_ X

## MAN MONTHS BY LABOR GRADE:

41. \_\_\_\_\_  
43. \_\_\_\_\_  
45. \_\_\_\_\_  
47. \_\_\_\_\_  
49. \_\_\_\_\_  
50. \_\_\_\_\_

FOLDOUT FRAME ?

## ESTIMATING INPUT SHEETS

TRAVEL: 6 Trips 2 Men 2 Days to Santa Barbara

Reason Subcontract \$4,000

Trips Men Days to

Reason

Trips Men Days to

Reason

Trips Men Days to

Reason

COMPUTER: CDC Units IBM Units

Reason:

Date

WBS 01200

NAME IRIS

Dept Ext

Section

PHASE I

II

III

TOTAL TRAVEL - \$4,000

TOTAL PROC. - \$218,700

## MAN MONTHS BY LABOR GRADE:

Design, fabrication, assembly and testing including specific test equipment and major procurements for the Image Plane System.

Part	Description	Quantity	Unit Price	Total Price
	<b>Parts/Material/Subcontract - \$214,000</b>			

Test Equipment	- \$3,000	Miscellaneous - \$1,7000
----------------	-----------	--------------------------

50\_\_\_\_\_

[illegible]

FIG. 76

DATA SYSTEMS

ESTIMATING INPUT SHEETS

TRAVEL: 2 Trips 2 Men 2 Days to East Coast  
Reason Vendor Interface \$1,500  
4 Trips 2 Men 2 Days to West Coast  
Reason Vendor Interface \$2,600  
Trips Men Days to  
Reason  
Trips Men Days to  
Reason  
COMPUTER: CDC Units IBM Units  
Reason:  
Date  
WBS 01300  
Name IRIS  
Dept Ext  
Section  
Phase I  
II  
III X

LABOR RATIONALE:

Design, fabrication assembly and testing including special test equipment and major procurements for the Data System.

Parts/Materials - \$84,000  
Test Equipment - \$4,000 Miscellaneous - \$1,600

MAN MONTHS BY LABOR GRADE:

41	38
43	36
45	34
47	
49	
50	

MAN MONTHS BY MONTH

	1	2	3	4	5	6	7	8	9	10	11	12	13	14	15	16	17	18	19	20	21	22	23	24	25	26	27	28	29	30	31	32	33	34	35	36	37	38	39	40	41	42	43	44	45	46	47	48	49	TOTAL
DESIGN	5	5	5	5	5	5	5	5																																								35		
FABRICATION								1	1	1																																							3	
ASSEMBLY								2	2	2	2	2	2	2																																		12		
TESTING						.1	.2	.2	.2	.1					.4	1	1	1	1	1	1	1	1	1	1	1	1	1	1	1	1	1	1	1	1	1	1	1	1	1	1	1	1	1	1	1	3.7			
TEST PROC.								.2	.2	.2	.2																																						.8	
TEST EQUIPMENT						.4	.4	.4	.4	.2																																						1.8		
Q.C.								.3	.4	.4	.3	.3	.2	.2																																	2.1			
																																																		58.4

FOLDOUT FRAME

FOLDOUT FRAME 2

## SYSTEM SUPPORT

Name IRIS  
Dept            Ext             
Section             
Date             
WBS 01400

PHASE I             
II             
III             
X           

COMPUTER:	CDC	\$5,600	Units	IBM	Units
-----------	-----	---------	-------	-----	-------

Reason: Software Dev. and Data Reduction

2	Trips	3	Men	10	Days to	NASA ARC
2	Trips	3	Men	10	Days to	NASA ARC

Reason	Installation	\$2,000

4	Trips	5	Men	5	Days to	NASA ARC
---	-------	---	-----	---	---------	----------

Reason	Calibration Flight	\$6,000
1. The flight was cancelled due to weather conditions.		
2. The flight was cancelled due to a technical issue with the aircraft.		
3. The flight was cancelled due to a medical emergency on board.		
4. The flight was cancelled due to a security threat.		
5. The flight was cancelled due to a change in the flight schedule.		
6. The flight was cancelled due to a change in the flight route.		
7. The flight was cancelled due to a change in the flight time.		
8. The flight was cancelled due to a change in the flight class.		
9. The flight was cancelled due to a change in the flight carrier.		
10. The flight was cancelled due to a change in the flight destination.		

1	Trips	5	Men	3	Days to	NASA ARC	\$2,000

Reason	Flight Support	\$2,000
--------	----------------	---------

3	Trips	2	Men	3	Days to	WEST COAST
---	-------	---	-----	---	---------	------------

Person	Data Reduction	\$2,000
--------	----------------	---------

**LABOR RATIONALE:**

Conduct thermal study. provide interface with NASA. develop and test software.

provide flight support for installation checkout calibration and first OET

Country	Year	Value	Unit	Source
Algeria	1980	1.0	1000	FAO
Algeria	1981	1.0	1000	FAO
Algeria	1982	1.0	1000	FAO
Algeria	1983	1.0	1000	FAO
Algeria	1984	1.0	1000	FAO
Algeria	1985	1.0	1000	FAO
Algeria	1986	1.0	1000	FAO
Algeria	1987	1.0	1000	FAO
Algeria	1988	1.0	1000	FAO
Algeria	1989	1.0	1000	FAO
Algeria	1990	1.0	1000	FAO
Algeria	1991	1.0	1000	FAO
Algeria	1992	1.0	1000	FAO
Algeria	1993	1.0	1000	FAO
Algeria	1994	1.0	1000	FAO
Algeria	1995	1.0	1000	FAO
Algeria	1996	1.0	1000	FAO
Algeria	1997	1.0	1000	FAO
Algeria	1998	1.0	1000	FAO
Algeria	1999	1.0	1000	FAO
Algeria	2000	1.0	1000	FAO
Algeria	2001	1.0	1000	FAO
Algeria	2002	1.0	1000	FAO
Algeria	2003	1.0	1000	FAO
Algeria	2004	1.0	1000	FAO
Algeria	2005	1.0	1000	FAO
Algeria	2006	1.0	1000	FAO
Algeria	2007	1.0	1000	FAO
Algeria	2008	1.0	1000	FAO
Algeria	2009	1.0	1000	FAO
Algeria	2010	1.0	1000	FAO
Algeria	2011	1.0	1000	FAO
Algeria	2012	1.0	1000	FAO
Algeria	2013	1.0	1000	FAO
Algeria	2014	1.0	1000	FAO
Algeria	2015	1.0	1000	FAO
Algeria	2016	1.0	1000	FAO
Algeria	2017	1.0	1000	FAO
Algeria	2018	1.0	1000	FAO
Algeria	2019	1.0	1000	FAO
Algeria	2020	1.0	1000	FAO
Algeria	2021	1.0	1000	FAO
Algeria	2022	1.0	1000	FAO
Algeria	2023	1.0	1000	FAO
Algeria	2024	1.0	1000	FAO
Algeria	2025	1.0	1000	FAO
Algeria	2026	1.0	1000	FAO
Algeria	2027	1.0	1000	FAO
Algeria	2028	1.0	1000	FAO
Algeria	2029	1.0	1000	FAO
Algeria	2030	1.0	1000	FAO
Algeria	2031	1.0	1000	FAO
Algeria	2032	1.0	1000	FAO
Algeria	2033	1.0	1000	FAO
Algeria	2034	1.0	1000	FAO
Algeria	2035	1.0	1000	FAO
Algeria	2036	1.0	1000	FAO
Algeria	2037	1.0	1000	FAO
Algeria	2038	1.0	1000	FAO
Algeria	2039	1.0	1000	FAO
Algeria	2040	1.0	1000	FAO
Algeria	2041	1.0	1000	FAO
Algeria	2042	1.0	1000	FAO
Algeria	2043	1.0	1000	FAO
Algeria	2044	1.0	1000	FAO
Algeria	2045	1.0	1000	FAO
Algeria	2046	1.0	1000	FAO
Algeria	2047	1.0	1000	FAO
Algeria	2048	1.0	1000	FAO
Algeria	2049	1.0	1000	FAO
Algeria	2050	1.0	1000	FAO
Algeria	2051	1.0	1000	FAO
Algeria	2052	1.0	1000	FAO
Algeria	2053	1.0	1000	FAO
Algeria	2054	1.0	1000	FAO
Algeria	2055	1.0	1000	FAO
Algeria				

100

Data Reduction Subcontract - \$20,000

General	\$1,200
---------	---------

MAN MONTHS BY LABOR GRADE:

41 \_\_\_\_\_

38 \_\_\_\_\_

43 36

2/

3/

43 \_\_\_\_\_

47\_\_\_\_\_

49\_\_\_\_\_

50\_\_\_\_\_

MAN MONTHS BY MONTH

[illegible]

## ESTIMATING INPUT SHEETS

## PROGRAM SUPPORT

TRAVEL: 5 Trips 2 Men 2 Days to West Coast

Reason Vendor Program Support \$3,000

3 Trips 2 Men 2 Days to East Coast

Reason Vendor Program Support \$1,800

Trips Men Days to

Reason

Trips Men Days to

Reason

COMPUTER: CDC \_\_\_\_\_ Units \_\_\_\_\_ IBM \_\_\_\_\_ Units \_\_\_\_\_

Reason: \_\_\_\_\_

\_\_\_\_\_

\_\_\_\_\_

\_\_\_\_\_

TOTAL TRAVEL -	\$4,800
TOTAL PROC. -	\$2,000
TOTAL COMP. -	0

**LABOR RATIONALE:**

Provide technical supervision, perform planning and cost control. Provide contract support, support procurement, reports, reproduction, and travel support. Program Support Task

**Draft and Reproduction Supplies - \$2,000**

## MAN MONTHS BY LABOR GRADE:

41 \_\_\_\_\_ 38 \_\_\_\_\_  
43 \_\_\_\_\_ 36 \_\_\_\_\_  
45 \_\_\_\_\_ 34 \_\_\_\_\_

PHASE I  
II  
II

MAN MONTHS BY MONTH

[illegible]

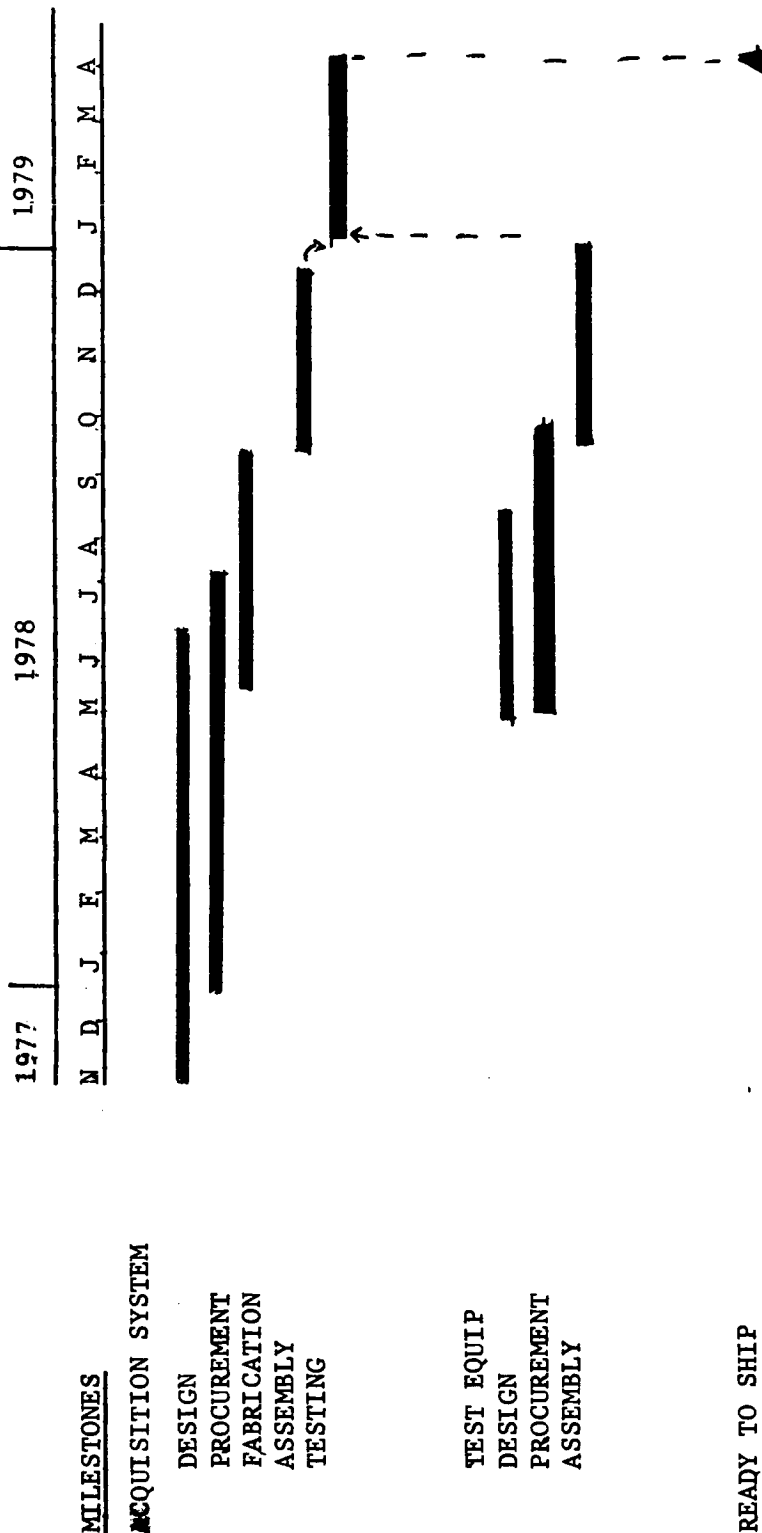
**FOLDOUT FRAME**

FOLDOUT FRAME 7 119

# SCHEDULE: INFRARED IMAGERY OF SHUTTLE

## BLACK BOX #1 - ACQUISITION SYSTEM

FIG. 79

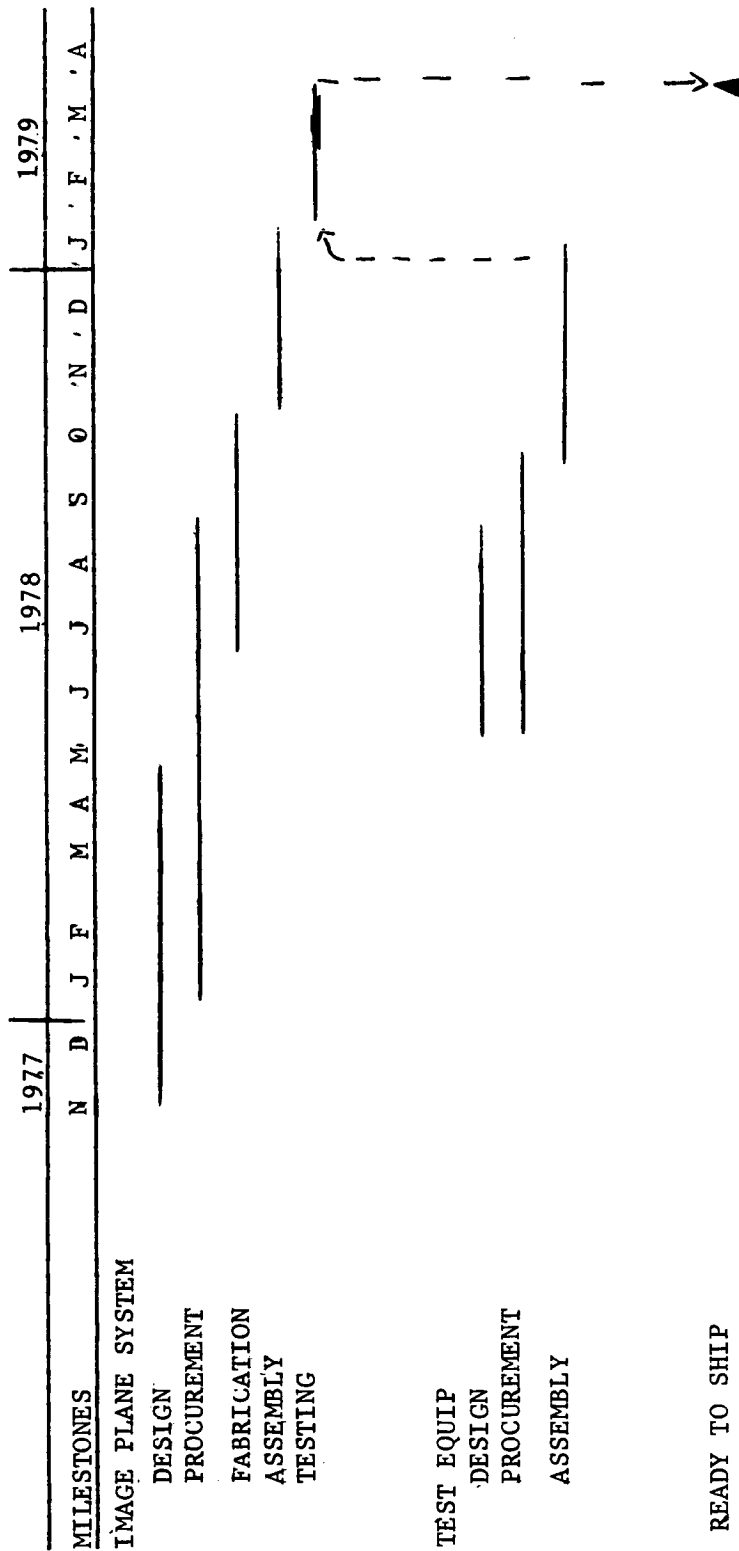


MARTIN MARIETTA

# SCHEDULE: INFRARED IMAGERY OF SHUTTLE

## BLACK BOX #2 - IMAGE PLANE SYSTEM

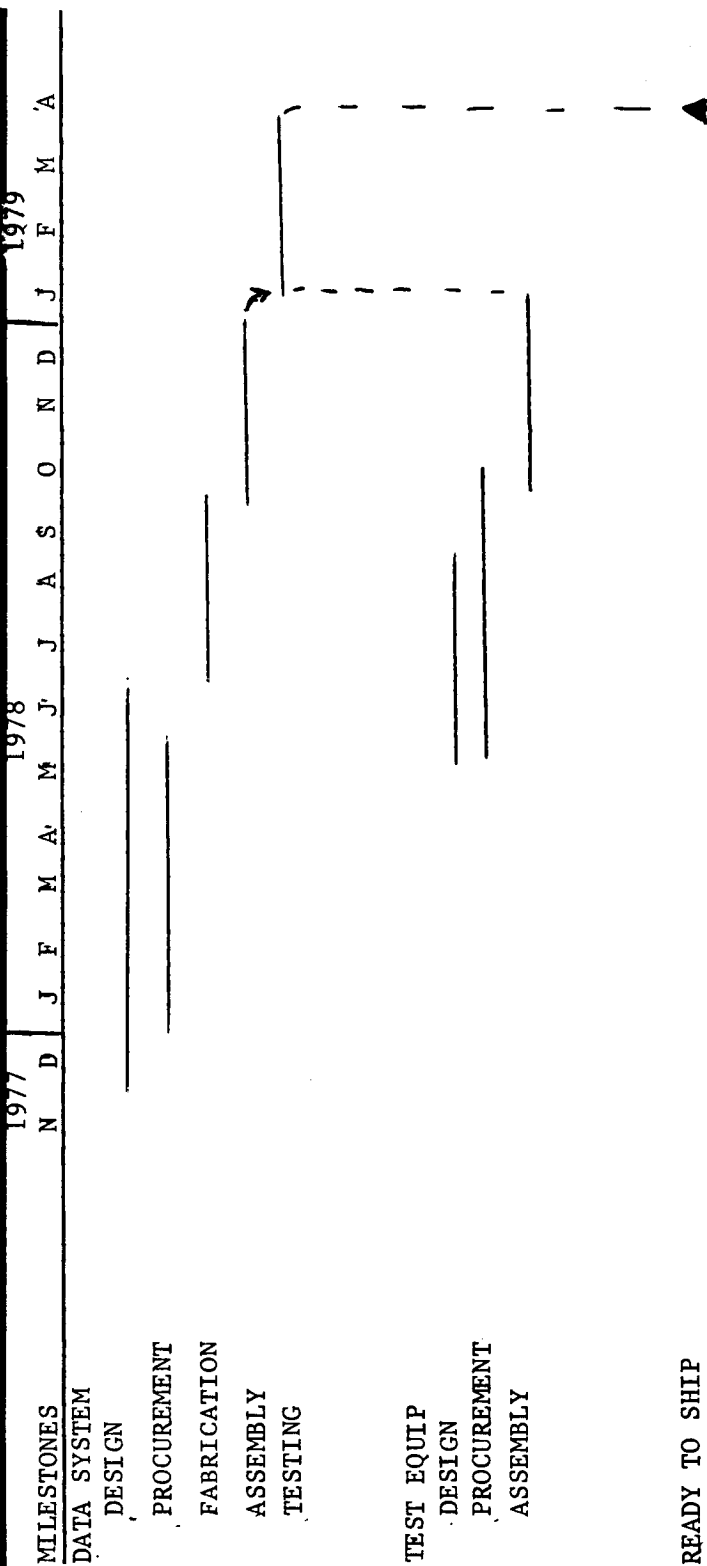
FIG. 80



# SCHEDULE: INFRARED IMAGERY OF SHUTTLE

FIG. 81

## BLACK BOX #3 - DATA SYSTEM



MARTIN MARIETTA



# SCHEDULE: INFRARED IMAGERY OF SHUTTLE

FIG. 82

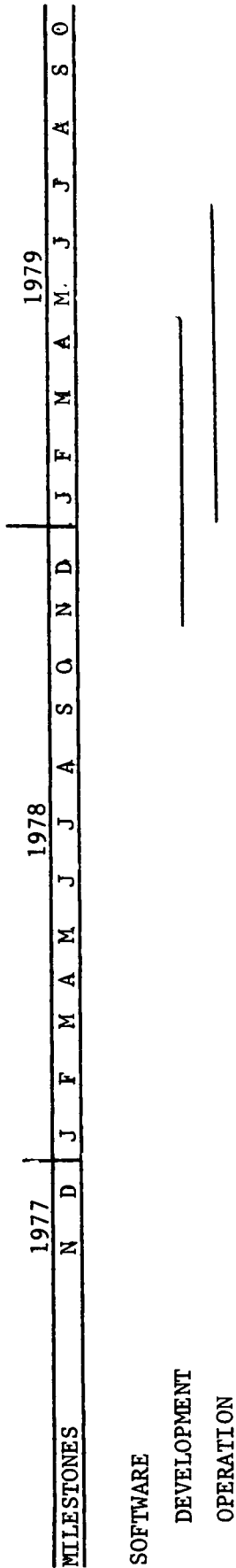
## SYSTEM SUPPORT

1977													1978												1979											
MILESTONES	N	D	J	F	M	A	M	J	J	A	S	O	N	D	J	F	M	A	M	J	J	A	S	O												
CONTRACT GO-AHEAD																																				
SHIP IR SYSTEM																																				
INSTALLATION/CHECKOUT																																				
CALIBRATION FLIGHT																																				
FIRST SHUTTLE FLIGHT																																				
DATA REDUCTION																																				
STATUS REPORTS																																				

MARTIN MARIETTA

# SCHEDULE: INFRARED IMAGERY OF SHUTTLE SOFTWARE

FIG. 83



MARTIN MARIETTA

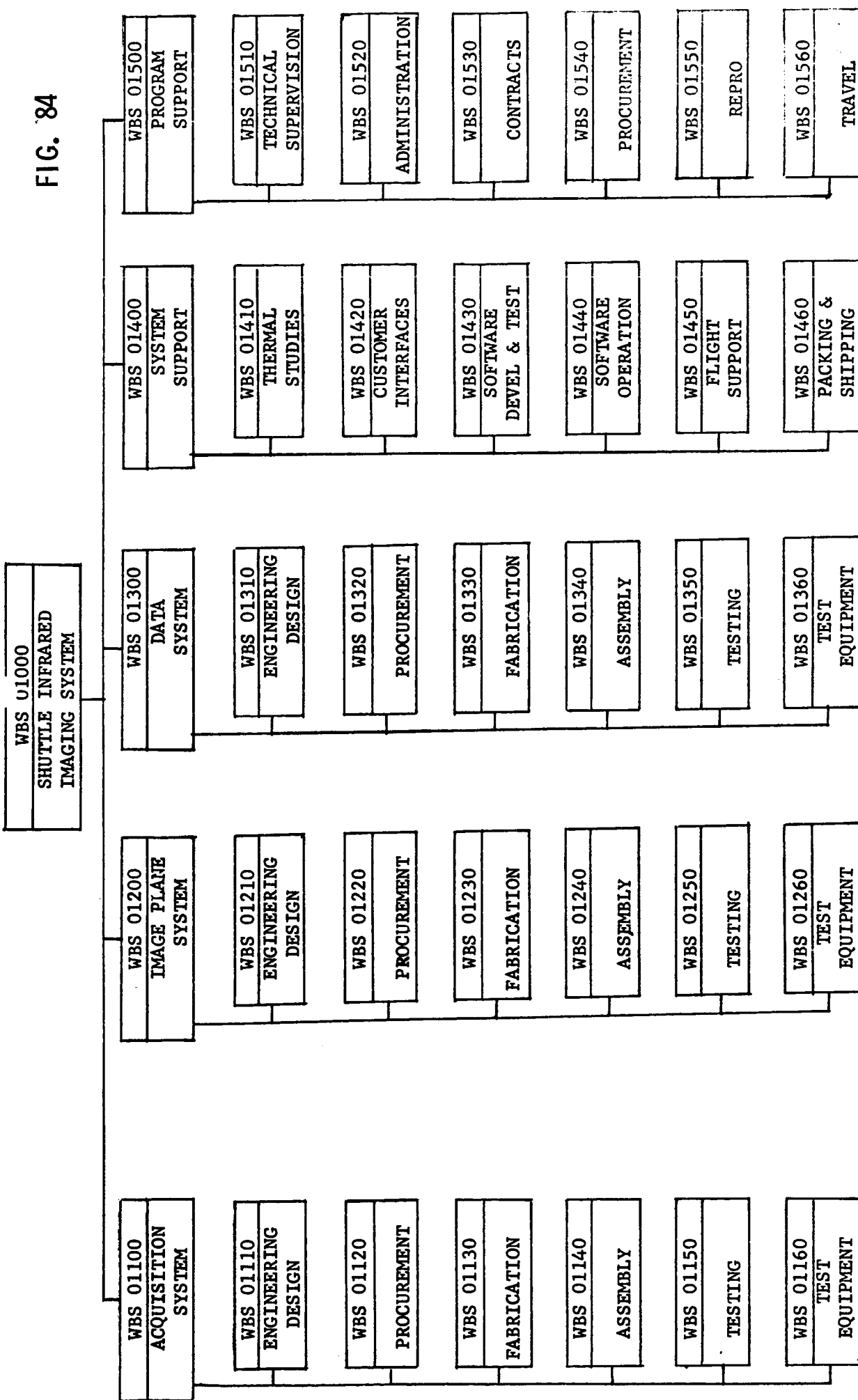


**FIG. 84**

**WORK BREAKDOWN STRUCTURE FOR SHUTTLE INFRARED IMAGING SYSTEM**

**2.0**
**WBS LEVEL**
**01100**
**WBS NUMBER**
**Acquisition System**
**WBS TITLE**
**DEFINITION**

This effort shall design, procure parts/materials, fabricate, assemble, and test the acquisition system for infrared imaging measurements of the shuttle.

**WORK CONTENT**
**SOW NO.\***

01110 - Design Acquisition System

01120 - Procure parts/materials for acquisition system

01130 - Fabricate piece parts for acquisition system

01140 - Assemble acquisition system

01150 - Test acquisition system

01160 - Provide test equipment for acquisition system

\*01 = ENGINEERING; 02 = TOOLING; 03 = MANUFACTURING; 05 = QUALITY  
06 = MFG TEST; 09 = OTHER TECHNICAL SERVICES,

**2.0**
**WBS LEVEL**
**01200**
**WBS NUMBER**
**Image Plane System**
**WBS TITLE**
**DEFINITION**

This effort shall design, procure parts/materials, fabricate, assemble, and test the Image Plane System for infrared imaging measurements of the shuttle.

**WORK CONTENT**
**SOW NO.\***

- 01210 - Design Image Plane System
- 01220 - Procure parts/materials for Image Plane System
- 01230 - Fabricate piece parts for Image Plane System
- 01240 - Assemble Image Plan System
- 01250 - Test Image Plane System
- 01260 - Provide test equipment for Image Plane System

\*01 = ENGINEERING; 02 = TOOLING; 03 = MANUFACTURING; 05 = QUALITY  
06 = MFG TEST; 09 = OTHER TECHNICAL SERVICES.

**2.0**
**WBS LEVEL**
**01300**
**WBS NUMBER**
**Data System**
**WBS TITLE**
**DEFINITION**

This effort shall design, procure parts/materials, fabricate; assemble, and test the Data System for infrared imaging measurements of the shuttle.

**WORK CONTENT**
**SOW NO.\***

01310 - Design Data System

01320 - Procure parts/materials for Data System

01330 - Fabricate piece parts for the Data System

01340 - Assemble Data System

01350 - Test Data System

01360 - Provide test equipment for Data System

\*01 = ENGINEERING; 02 = TOOLING; 03 = MANUFACTURING; 05 = QUALITY  
06 = MFG TEST; 09 = OTHER TECHNICAL SERVICES.

**2.0**
**01400**
**WBS LEVEL**
**WBS NUMBER**
**System Support**
**WBS TITLE**
**DEFINITION**

This effort shall consist of those functions that are applicable, the complete Shuttle Infrared Imaging System.

**WORK CONTENT**
**SOW NO.\***

01410 - Conduct Thermal Study

01420 - Provide interface with NASA, Ames Research Center,  
Moffett Field, CA 94035

01430 - Develop & Test Software

01440 - Operate Software and Reduce Data

01450 - Provide flight support consisting of installation, calibration, and checkout of system in C141 aircraft.

01460 - Pack and Ship System

\*01 = ENGINEERING; 02 = TOOLING; 03 = MANUFACTURING; 05 = QUALITY  
06 = MFG TEST; 09 = OTHER TECHNICAL SERVICES.

**2.0**
**WBS LEVEL**
**01500**
**WBS NUMBER**
**Program Support**
**WBS TITLE**
**DEFINITION**

This effort shall consist of those functions that are necessary to support the contract.

**WORK CONTENT**
**SOW NO.\***

01510 - Provide Technical Supervision and Direction

01520 - Perform Planning/Cost Control Support

01530 - Provide Contract Support

01540 - Procure supplies/materials that are not unique to system hardware.

01550 - Provide reproduction, printing and presentations support

01560 - Provide Travel Support

**\*01 = ENGINEERING; 02 = TOOLING; 03 = MANUFACTURING; 05 = QUALITY  
06 = MFG TEST; 09 = OTHER TECHNICAL SERVICES.**



## RECOMMENDATIONS FOR FUTURE WORK

---

Two items have been identified in the feasibility study for possible investigation to establish operating tolerances. The first is the accuracy obtainable by the Reticle/Demodulation System as part of the Acquisition System. Error sources for tracking have been identified but some assumptions as to Shuttle image size error and demodulation errors have been made. A breadboard of the subsystem would prove valuable in ascertaining tracking errors.

The second item is in the Data Handling System. The concept of tying three detectors to a common amplifier and then multiplexing 10 amplifiers to the sample and hold/A to D is sound but needs to be breadboarded to establish realizable data rates and amplifier noise. In addition, the dynamic range can be checked for available detector/amplifiers and an estimate made of minimum  $\Delta T$ . These two tasks are recommended for follow-on work to the feasibility study.

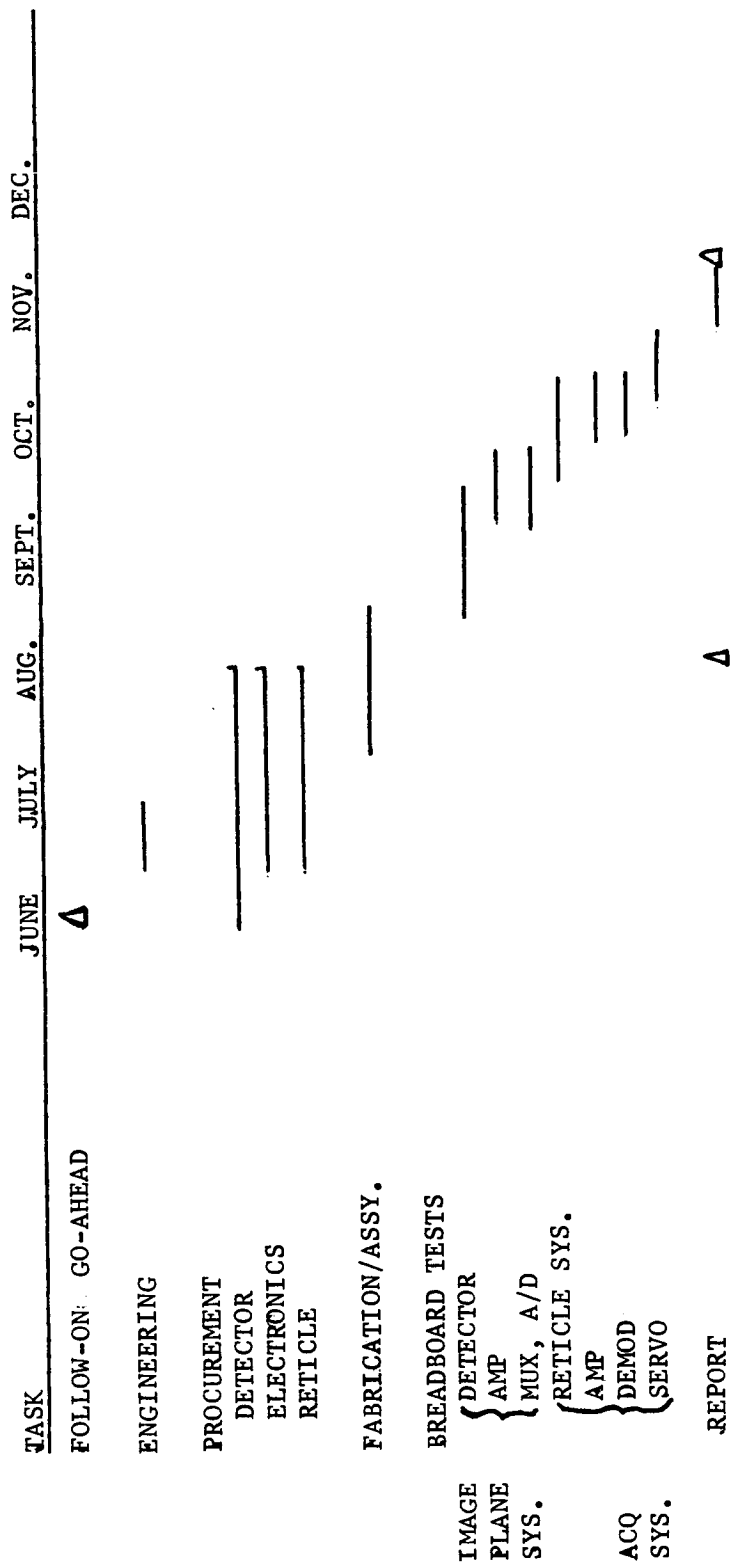
Figure 90 is an estimate of Engineering hours and purchased parts to complete these tasks and Figure 91 is a preliminary schedule for completion of the work.

TASK 1 - IMAGING SYSTEM	HOURS	PURCHASE PARTS
BREADBOARD AMPLIFIER/DETECTOR SAMPLE & HOLD/AD	360	\$12K
PERFORM DEVELOPMENT TESTS	290	
TASK 2 - ACQUISITION SYSTEM		
BUILD RETICLE/AMPLIFIER SYSTEM	240	\$3.1K
PERFORM DEVELOPMENT TESTS	100	
SIMULATE SOFTWARE/SERVO ERRORS	220	\$ .4K

**MARTIN MARIETTA**

FIG. 91

**INFRARED IMAGERY OF SHUTTLE - PRELIMINARY FOLLOW-ON CONTRACT SCHEDULE NAS2-9381**





## CONCLUSIONS

---

The feasibility of remote, high-resolution infrared imagery of the Shuttle Orbiter lower surface during entry to obtain accurate measurements of aerodynamic heat transfer has been demonstrated. In summary, the experiment is both feasible, within the current technology level, and requires minimum modification to the existing NASA C141 Airborne Infrared Observatory. The most important technical conclusions are as follows:

- 1) The four conditions of interest during the entry trajectory can be accommodated by an aircraft flying parallel to the Shuttle reentry ground track.
- 2) The temperature range that can be measured at an accuracy of 2.5% is from 700 to 1900 K depending on range. Temperatures below 700 K can be measured by relaxing the accuracy or re-scaling the Data System to limit the upper temperature to less than 1700 K.
- 3) The spatial resolution obtainable for the worst-case encounter with the Shuttle Orbiter (i.e., greatest range and maximum angle between LOS and Shuttle lower surface normal) is 1 meter at temperatures above 800 K. At higher temperatures and/or shorter ranges, this value can be as small as 0.4 meters.
- 4) An Acquisition System using a 6.25-cm aperture telescope and a single indium antimonide detector has been designed (preliminary) that will meet the acquisition requirements and will interface with the 91.5-cm telescope with minimum modification.
- 5) An Image Plane System using 600 indium antimonide detectors in two arrays has been designed (preliminary) that requires no modification to the existing telescope.
- 6) A Data Handling System built of components available currently has been designed (preliminary) that interfaces with the experimentors station and HP2100 computer (ADAMS) similar to any infrared experiment data system.
- 7) Thermal information from the sides of the Shuttle Orbiter can be obtained with degraded performance (i.e., temperatures below 800 K) by flying the C141 on the opposite side of the Shuttle ground track and in the direction opposite that which is optimum for lower surface viewing.



## REFERENCES

---

1. Byron L. Swenson and Larry E. Edsinger: *Preliminary Analysis of Remote Infrared Imagery of Shuttle During Entry, an Aerothermodynamic Flight Experiment*. NASA TM73, 251. Ames Research Center, Moffett Field, California 95035, 1977.
2. *Space Shuttle Orbiter Entry Aerodynamic Heating Data Book*. Contract NAS9-14000, WBS 1.2.2. Rockwell International, Feb. 1976.
3. *OFT-1 Preliminary Reference Flight Profile for Deorbit Through Landing*. JSC Internal Note No. 76-FM-68. Sept. 7, 1976. *Updated Conceptual Flight Profiles for OFT-4, OFT-5 and OFT-6*. JSC Internal Note No. 76-FM-35. NASA, Lyndon B. Johnson Space Center, Houston, Texas, June 2, 1976.
4. *AMOS Users Manual*. ARPA Order No. 2837. AVCO Everett Research Laboratory, Inc., Everett, Mass., June 1975.
5. *Experimenters Handbook*. NASA CV990. Airborne Laboratory. NASA Ames Research Center, Moffett Field, Calif. 94035
6. *Investigators Handbook*. NASA-TM X 62,389. Lear Jet Telescope System. NASA Lear Jet Airborne Observatory, NASA Ames Research Center, Moffett Field, Calif. 94035
7. *Investigators Handbook*. NASA C141 Airborne Infrared Observatory. NASA Ames Research Center, Moffett Field, Calif. 94035
8. Dr. Robert Hufnagel: "Random Wavefront Effects." Published in a *Symposium on Modulation Transfer Functions*. Perkin-Elmer, March 6, 1963.
9. Dr. Robert Hufnagel and N. Stanley: "Modulation Transfer Function Associated with Image Transmission Through Turbulent Media." *JOSA Vol. 54 No. 1*, January 1964.
10. N. Farhat and A. DeCou: "Relations Between Wave Structure Function Looking Up and Looking Down Through the Atmosphere." *JOSA*, Letters to the Editor, November 1969.
11. *Electro-Optical Telescope Study for Earth Observation*. Martin Marietta, Denver, Colorado 80201. December 1972.
12. J. Selby and R. McClatchey: *Atmospheric Transmittance from .25 to 28.5 Micrometers: Computer code LOWTRAN 3*. AFCRL-TR-75-0255. Air Force Cambridge Research Labs, Hanscom AFB, Mass. 01731, May 1975.

13. *Polypagos Users Manual*. The Aerospace Corp., SAMSO, Air Force Systems Command, Los Angeles Air Force Station, Los Angeles, California.
14. M. Robenau Jr.: "Image Motion Modulation Transfer Function." Production from a *Symposium on Modulation Transfer Functions*. Perkin-Elmer, March 6, 1963.
15. Khalil Seyrafi: *Electro-Optical Systems Analysis*. Electro-Optical Research Co.



## APPENDIX

---

The following set of tables (Figures 92 through 95) contain all of the geometric data pertaining to the four specified aerothermodynamic conditions for OFT-1. The 282-sec case represents peak heating near the nose of the vehicle; the 544-sec case represents peak heating further aft, the beginning of transition of boundary layer from laminar to turbulent and body flap heating; the 791-sec case represents the end of transition of the boundary layer and fully developed turbulent flow; and the 922-sec case represents lower surface turbulent boundary layer flow. The Shuttle altitude, velocity, roll and pitch are given along with the aircraft altitude for each case. The symbol definitions are as follows:

$\theta$	Telescope elevation
$R_p$	Data range in kilometers - Distance from aircraft-to-Shuttle at the time prime data is taken.
$A_Q$	Acquisition angle in degrees - Azimuth angle ahead of or behind athwartships position when acquisition can first occur.
$R_A$	Acquisition range in kilometers - Distance from aircraft to Shuttle at first point of acquisition
$\alpha$	Angle in degrees between 91.5-cm telescope line-of-sight and Shuttle underside normal when prime data are taken.
$\sigma$	Angle-in-degrees between acquisition telescope line-of-sight and Shuttle underside normal when acquisition first occurs.
Pix	Projected size of one pixel 50 x 50 micrometers on Shuttle surface given in meters.
MTF RES	Resolution based on MTF at a given modulation (%) in meters on the Shuttle surface.
Image <sub>D</sub>	Shuttle image size wing tip to wing tip at prime data point given in minutes of arc.
Image <sub>A</sub>	Shuttle image size nose to tail at first acquisition given in minutes of arc.
Time to Cross	Time in milliseconds Shuttle image takes to cross one detector array.

Across Track Data Array	Number of detectors that the Shuttle image will intercept at prime data point.
Along Track Sample Rate	Sampling rate of each detector to match along track resolution with cross track resolution.
C141 to Shuttle Ground Track Difference	The distance the C141 must fly displaced from the Shuttle ground track for best observation.

Figure 96 depicts the streak camera configuration that has been discussed in this report (see also Ref. 1).

# C141 DATA & ACQUISITION GEOMETRY - 282 SEC CASE

FIG. 92

Shuttle Alt 74.3 KM  
 C141 Alt 12.5 KM  
 Shuttle Velocity 7.16 KM/Sec  
 Shuttle Roll 74°  
 Shuttle Pitch 40°

$\theta$ (o)	R <sub>D</sub> (KM)	A <sub>Q</sub> (o)	R <sub>A</sub> (KM)	$\gamma$ (b)	$\sigma$ (o)	PIX (m)	MTF Res. @2% (m)	MTF Res. @5% (m)	Image <sup>D</sup> (min)	Image <sup>A</sup> (min)	Time To Cross (Milsec)	Across Track Data Array	Along Track Sample Rate
35	107.74	53.05	179.20	19.42	4.60	.46	.77	.92	.715	.626	4.57	51.48	15558
40	96.14	56.12	172.48	24.42	5.41	.42	.71	.85	.773	.650	4.57	55.70	16845
45	87.39	58.60	167.76	29.42	6.03	.40	.67	.81	.814	.667	4.57	58.61	17741
50	80.67	60.60	164.36	34.42	6.50	.39	.66	.79	.835	.681	4.57	60.14	18218
55	75.44	62.21	161.85	39.42	6.86	.39	.65	.78	.838	.691	4.57	60.22	18262
60	71.36	63.51	159.99	44.42	7.14	.40	.67	.80	.818	.698	4.57	58.06	17871
65	68.18	64.53	158.60	49.42	7.35	.42	.70	.84	.783	.704	4.57	56.37	17057
70	65.76	65.33	157.57	54.42	7.51	.45	.76	.91	.731	.708	4.57	52.41	15845

Optimum  $\theta$

282 sec case  $\theta = 55^\circ$

C141 to shuttle ground track difference

43.27 KM

MARTIN MARIETTA

# C141 DATA & ACQUISITION GEOMETRY - 544 SEC CASE

FIG. 93

142

Shuttle Alt. 63.7 KM  
C141 12.5 KM  
Shuttle Velocity 5.64 KM/SEC  
Shuttle Roll 63°  
Shuttle Pitch 40°

$\theta$ (o)	$R_D$ (KM)	$A_Q$ (o)	$R_A$ (KM)	$\gamma$ (o)	$\sigma$ (o)	PIX (m)	MTF Res @2% (m)	MTF Res @5% (m)	Image <sup>D</sup> (min)	Image <sup>A</sup> (min)	Time to Cross (milsec)	Across Track Data Array	Along Track Sample Rate
35	89.26	51.64	143.84	9.89	2.68	.36	.61	.73	.907	.782	5.81	65.25	15496
40	79.65	54.77	138.08	14.89	1.77	.33	.55	.66	1.000	.815	5.81	71.95	17087
45	72.40	57.30	134.03	19.89	1.07	.31	.51	.62	1.07	.810	5.81	77.25	18347
50	66.83	59.35	131.11	24.89	.54	.29	.49	.59	1.12	.859	5.81	81.00	19238
55	62.50	61.00	128.95	29.89	.14	.29	.48	.58	1.15	.873	5.81	83.08	19733
60	59.12	62.34	127.35	34.89	.17	.29	.48	.58	1.16	.884	5.81	83.43	19816
65	56.49	63.39	126.15	39.89	.41	.29	.49	.59	1.14	.893	5.81	82.04	19485
70	54.48	64.21	125.56	44.89	.59	.31	.51	.62	1.09	.899	5.81	78.95	18750

Optimum  $\theta$

544 sec case  $\theta = 50^\circ$

C141 to shuttle ground track difference

52.96 KM

MARTIN MARIETTA

# CI41 DATA & ACQUISITION GEOMETRY - 791 SEC CASE

FIG. 94

Shuttle Alt 54.2 KM  
 CI41 Alt 12.5 KM  
 Shuttle Velocity 3.49 KM/SEC  
 Shuttle Roll 50°  
 Shuttle Pitch 39°

$\theta_o$	$R_D(KM)$	$A_A(o)$	$R_A(KM)$	$\gamma(o)$	$\sigma(o)$	PIX (m)	MTF Res. @2% (m)	MTF Res. @5% (m)	Image D (min)	Image A (min)	Cross Time To (milsec)	Across Track Data Array	Along Track Sample Rate
35	72.70	43.83	100.78	23	10.32	.29	.43	.58	1.12	1.099	9.38	80.59	11835
40	64.87	47.09	95.29	5.23	8.81	.26	.43	.48	1.26	1.168	9.38	90.66	13314
45	58.97	49.80	91.37	10.23	7.23	.24	.40	.48	1.38	1.222	9.38	99.35	14591
50	54.43	52.05	88.51	15.23	6.65	.22	.37	.45	1.47	1.264	9.38	106.41	15626
55	50.90	53.89	86.39	20.23	5.90	.21	.36	.43	1.55	1.297	9.38	111.60	16389
60	48.15	55.40	84.79	25.23	5.30	.21	.35	.43	1.59	1.322	9.38	114.78	16856
65	46.01	56.60	83.60	30.23	4.84	.21	.35	.43	1.61	1.342	9.38	115.85	17014
70	44.37	57.55	82.71	35.23	4.48	.21	.36	.43	1.59	1.357	9.38	114.78	16856

Optimum  $\theta$  CI41 to shuttle ground track difference

791 sec case  $\theta = 45^\circ$

41.70 KM

MARTIN MARIETTA

# C141 DATA & ACQUISITION GEOMETRY - 922 SEC CASE

FIG. 95

144

Shuttle Alt 43.9 KM  
 C141 Alt 12.5 KM  
 Shuttle Velocity 2.37 KM/SEC  
 Shuttle Roll 45°  
 Shuttle Pitch 28°

$\theta_o$	$R_b(KM)$	$A_{Q(o)}$	$R_A(KM)$	$\gamma_{(o)}$	$\sigma_{(o)}$	Pix (m)	MTF Res. @2% (m)	MTF Res. @5% (m)	Image D (min)	Image A (min)	Time To Cross (milsec)	Across Track Data Array	Along Track Sample Rate
35	54.74	40.88	72.41	6.44	15.74	.22	.37	.44	1.47	1.497	13.82	105.81	10546
40	48.84	44.13	68.06	1.44	13.97	.19	.32	.39	1.66	1.606	13.82	119.94	11955
45	44.40	46.85	64.95	3.55	12.53	.17	.29	.35	1.84	1.693	13.82	132.45	13202
50	40.99	49.14	62.66	8.55	11.37	.16	.27	.33	1.98	1.762	13.82	142.95	14240
55	38.33	51.03	60.96	13.55	10.43	.15	.26	.31	2.10	1.817	13.82	151.11	15061
60	36.25	52.58	59.67	18.55	9.69	.15	.25	.30	2.17	1.861	13.82	156.69	15618
65	34.64	53.83	58.71	23.55	9.11	.15	.25	.30	2.21	1.894	13.82	159.53	15901
70	33.41	54.81	57.99	28.55	8.66	.15	.25	.30	2.21	1.920	13.82	159.53	15901

Optimum  $\theta$

922 sec case  $\theta = 35^\circ$

C141 to shuttle ground track difference

44.84 KM

MARTIN MARIETTA

